iScience

CellPress
OPEN ACCESS

Article

Altered neuronal lactate dehydrogenase A expression affects cognition in a sex- and age-dependent manner

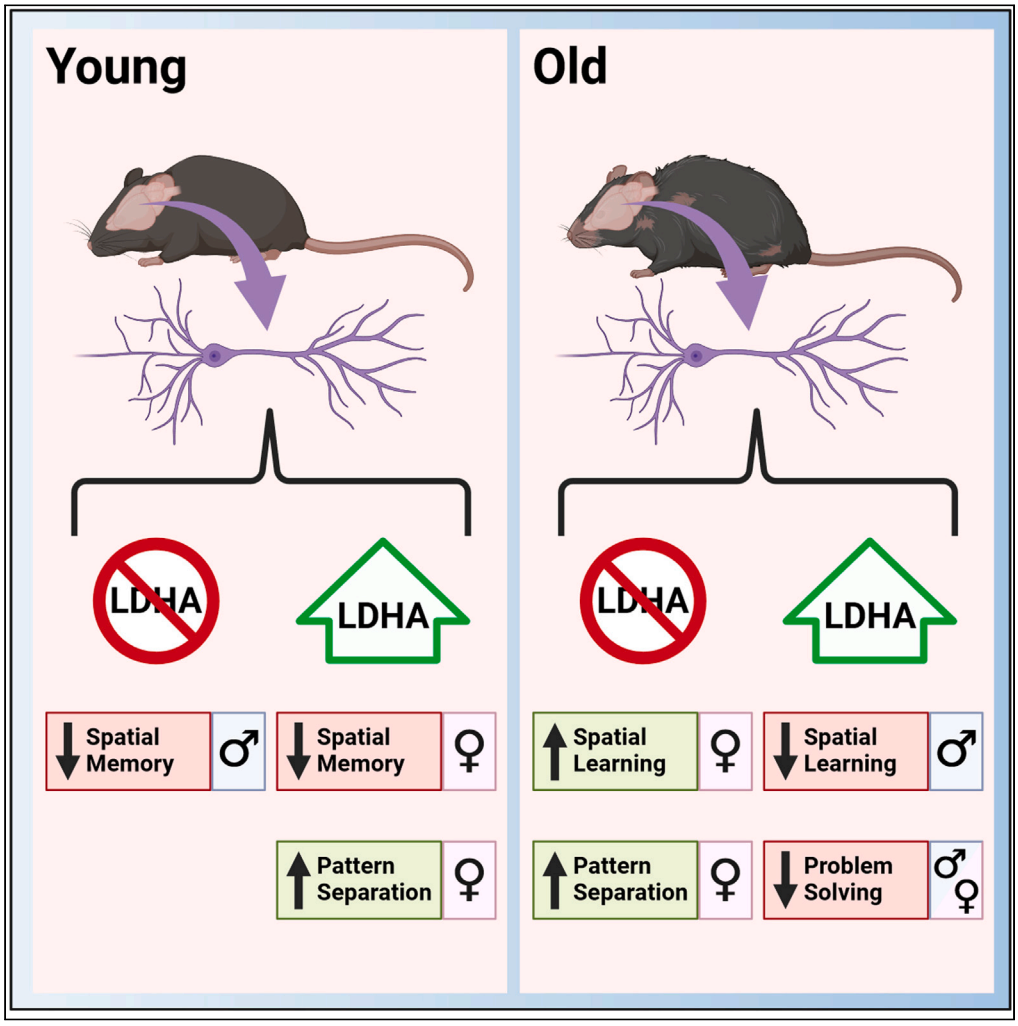

Ariel K. Frame, Jessica L. Sinka, Marc Courchesne, ..., Mark A. Bernards, Robert Bartha, Robert C. Cumming

aframe@uwo.ca (A.K.F.)
rcummin5@uwo.ca (R.C.C.)

Highlights

Altered neuronal *Ldha* expression elicits cognitive changes depending on sex and age

Induced neuronal *Ldha* causes cognitive deficits in old mice

Knockout of neuronal *Ldha* causes cognitive improvements in old mice

Neuronal lactate production may help or hinder cognition depending on the context

Frame et al., iScience *27*, 110342
July 19, 2024
https://doi.org/10.1016/j.isci.2024.110342

iScience

CellPress
OPEN ACCESS

Article

Altered neuronal lactate dehydrogenase A expression affects cognition in a sex- and age-dependent manner

Ariel K. Frame,[1,*] Jessica L. Sinka,[1] Marc Courchesne,[1] Rashad A. Muhammad,[1] Sandra Grahovac-Nemeth,[1] Mark A. Bernards,[1] Robert Bartha,[2] and Robert C. Cumming[1,3,*]

SUMMARY

The astrocyte-neuron lactate shuttle (ANLS) model posits that astrocyte-generated lactate is transported to neurons to fuel memory processes. However, neurons express high levels of lactate dehydrogenase A (LDHA), the rate-limiting enzyme of lactate production, suggesting a cognitive role for neuronally generated lactate. It was hypothesized that lactate metabolism in neurons is critical for learning and memory. Here transgenic mice were generated to conditionally induce or knockout (KO) the *Ldha* gene in CNS neurons of adult mice. High pattern separation memory was enhanced by neuronal *Ldha* induction in young females, and by neuronal *Ldha* KO in aged females. In older mice, *Ldha* induction caused cognitive deficits whereas *Ldha* KO caused cognitive improvements. Genotype-associated cognitive changes were often only observed in one sex or oppositely in males and females. Thus, neuronal-generated lactate has sex-specific cognitive effects, is largely indispensable at young age, and may be detrimental to learning and memory with aging.

INTRODUCTION

Mammalian brains require a disproportionate amount of energy compared to the rest of the body.[1–5] These energetic needs are met mainly through carbohydrate metabolism[6–8] that differs between neurons and astrocytes, the two principle brain cell types. Astrocytes predominately break down sugars into lactate using glycolysis or glycogenolysis.[9–11] Neurons can also utilize glycolysis, but generally favor oxidative metabolism involving further break down of glycolytic end-products through the tricarboxylic acid (TCA) cycle and mitochondrial oxidative phosphorylation.[12–14] Astrocytes support neuronal metabolism by releasing lactate that can be taken up by neurons and used for oxidative metabolism through a process known as the astrocyte-neuron lactate shuttle (ANLS).[15,16] While numerous studies have shown that the ANLS plays a key role in learning and memory,[17–53] these findings were based on experiments in which lactate transport or glycogenolysis were inhibited using a pharmaceutical approach with potentially non-cell-type specific actions or using a genetic approach targeting either astrocytes or non-specific cell types. However, the effect of directly manipulating lactate production within certain CNS cell types on cognition has not been examined before.

There are two predominant lactate dehydrogenase (LDH) isoforms in the mammalian brain, LDHA and LDHB, which form a tetramer in either a homo- or heteromeric fashion resulting in five possible combinations. The number of LDHA or LDHB isoforms that make up an LDH tetramer influences its activity; LDHB predominantly converts lactate to pyruvate whereas LDHA predominantly converts pyruvate to lactate.[54–65] Thus neurons are predicted to express high levels of LDHB in order to oxidatively metabolize lactate to pyruvate, whereas astrocytes are predicted to express high levels of LDHA to reduce pyruvate to lactate.[66–68] However, recent studies using cell-type distinction methods have revealed that LDHA is readily detectable in neurons.[69–75] Furthermore, neurons can take up glucose directly[76,77] and, under certain contexts, exhibit increased glycolysis and lactate release.[52,78–81] Therefore, neurons have the capacity to either break down astrocyte-derived lactate, in accordance with the ANLS, or produce lactate glycolytically in a cell autonomous manner, and this choice may be biased in one direction depending on the levels or activity of LDHA. The question arises as to why neurons express high levels of LDHA and what role neuronal produced lactate plays in cognition? In addition, how neuronal lactate metabolism changes with age or between sexes is unknown.

To address these questions, two separate neuronal transgenic mice were generated with *Ldha* either induced or knocked out in neurons of the brain. Different cognitive domains were tested in neuronal *Ldha* transgenic mice using a variety of behavioral assays. In most paradigms used, altered neuronal *Ldha* expression resulted in either cognitive improvements or deficits that were also age- and sex-dependent.

[1]Department of Biology, Western University, London, ON N6A 5B7, Canada
[2]Department of Medical Biophysics, Schulich School of Medicine and Dentistry, Western University, London, ON N6A 3K7, Canada
[3]Lead contact
*Correspondence: aframe@uwo.ca (A.K.F.), rcummin5@uwo.ca (R.C.C.)
https://doi.org/10.1016/j.isci.2024.110342

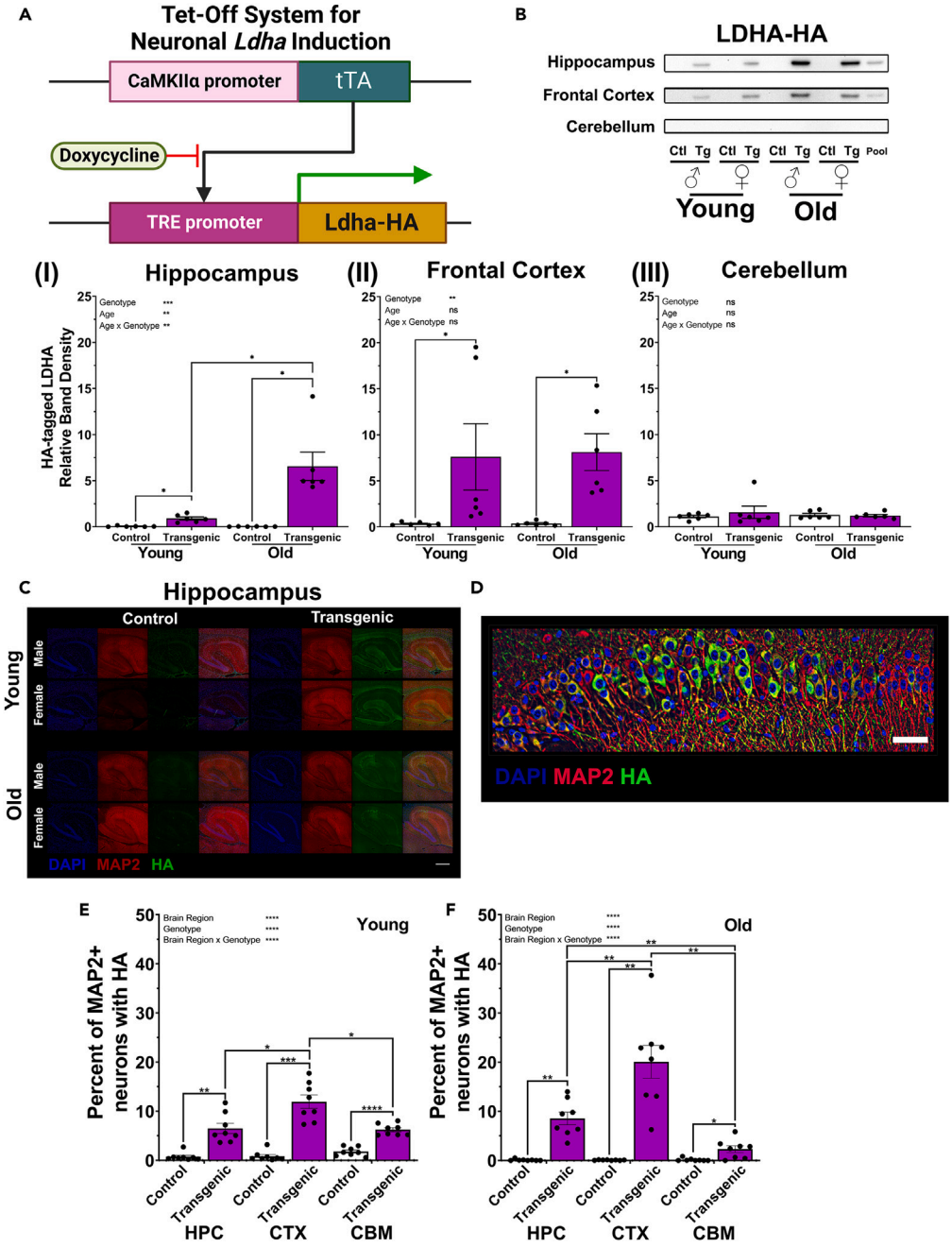

Figure 1. Neuronal *Ldha* induction transgenic mice express HA-tagged LDHA in the brain

(A) Schematic outlining Tet-Off system used to induce expression of Ldha in neurons. Neuronal *Ldha* induction mice contain both the genetic constructs encoding the tetracycline-controlled transactivator (tTA) and the tetracycline-responsive promoter element (TRE). Control mice lack either one or both constructs. The tTA induces expression of *Ldha* downstream of TRE following removal of doxycycline from the diet.

(B) Western blot analysis demonstrating HA-tagged LDHA expression in the hippocampus (I) and frontal cortex (II), but not cerebellum (II), of neuronal Ldha induction mice at young (7 months) and old (18 months) age. HA-tagged LDHA increased with age in neuronal *Ldha* induction mice (I; genotype × age effect: $F(1, 20) = 13.54$, $p = 0.0015$). $n = 6$. Comparisons made by two-way ANOVA, fixed effects presented in each graph, with Šídák multiple comparisons between genotype for each age or, if there was an effect including age, Holm-Šídák multiple comparisons between genotype for each age and between age for each genotype. See also Figure S1.

(C) Representative immunofluorescence images revealed increased levels of HA-tagged LDHA in the hippocampus of neuronal *Ldha* induction mice at young (7 months) and old (18.5 months) age compared with age-matched control. Scale bar: 500 μm. See also Figures S2 and S5.

(D) Magnified view of immunofluorescence image from hippocampal Cornu Ammonis 2 (CA2) region of 18.5 month old female neuronal *Ldha* induction mouse revealing neuronal localization of HA-tagged LDHA. Scale bar: 50 μm.

Figure 1. *Continued*

(E and F) Quantification of immunofluorescence staining showing the region-dependent increased percentage of MAP2 and HA-tagged LDHA positive neurons in neuronal *Ldha* induction mice compared to control mice. Increases were detected in hippocampus (HPC), frontal cortex (CTX), and cerebellum (CBM) at young age (E; brain region effect: $F(1.816, 21.80) = 17.26$, $p < 0.0001$; genotype effect: $F(1, 12) = 63.20$, $p < 0.0001$; brain region × genotype effect: $F(2, 24) = 23.75$, $p < 0.0001$) and old age (F; brain region effect: $F(1.167, 16.34) = 28.98$, $p < 0.0001$; genotype effect: $F(1, 14) = 40.28$, $p < 0.0001$; brain region × genotype effect: $F(2, 28) = 29.47$, $p < 0.0001$). $n = 8$. See also Figures S2–S7. Comparisons made using a mixed-effects model with Geisser-Greenhouse correction, fixed effects presented in each graph, and Holm-Šídák multiple comparisons between genotypes for each brain region and between each brain region for transgenic. Data presented as mean ± SEM.

Importantly, in older mice, all cognitive changes affected by neuronal *Ldha* induction were detrimental, whereas cognition was improved by neuronal *Ldha* knockout (KO). These results highlight that elevated neuronal lactate metabolism elicits sex-dependent effects that may have detrimental consequences on cognition with age.

RESULTS

LDHA is increased in the brains of neuronal *Ldha* induction mice

To manipulate LDHA in the brains of mice across age, two separate systems were employed to either induce or KO the *Ldha* gene in central nervous system (CNS) neurons. A novel transgenic mouse line was generated containing a tetracycline-responsive promoter element (TRE) upstream of the mouse *Ldha* gene fused to a hemagglutinin (HA) tag combined with the Tet-Off system[82,83] to selectively induce HA-tagged LDHA in neurons (Figure 1A). HA-tagged *Ldha* expression was restricted to excitatory neurons in adulthood by employing the calcium-calmodulin-dependent kinase II (CaMKIIα) driver upstream of the tetracycline transactivator gene to turn off TRE-*Ldha* expression during embryonic and post-natal development using dietary doxycycline (Figure 1A). The CaMKIIα driver was selected because it strongly induces neuronal expression in the hippocampus and frontal cortex with only minor expression in the cerebellum.[84,85] In neuronal *Ldha* induction mice of both sexes, HA-tagged LDHA was detectable across age in the hippocampus (Figures 1BI and S1), frontal cortex (Figures 1BII and S1), but not cerebellum (Figures 1BIII and S1) by western blotting, and localized to microtubule-associated protein 2 (MAP2) positive neurons by immunofluorescence analysis (Figures 1C–1F and S2–S7). Interestingly, hippocampal HA-tagged LDHA levels, measured by western blotting, in neuronal *Ldha* induction mice were higher in 14-month-old mice compared to 7-month-old mice (Figures 1BI and S1).

LDHA is reduced in the brains of neuronal *Ldha* knockout mice

The ligand-activated site-specific Cre-lox system[86,87] was used to generate neuronal *Ldha* KO mice using the same neuronal driver, CaMKIIα, as in the neuronal *Ldha* induction mice (Figure 2A). *Ldha* KO was restricted to adulthood by administering tamoxifen at 4–5 months of age. In neuronal *Ldha* KO mice at young and old ages, western blotting revealed a decrease in LDHA protein levels in the hippocampus (Figures 2BI and S8) and frontal cortex (Figures 2BII and S8), with no effect in the cerebellum (Figures 2BIII and S8). In contrast, LDHB protein levels were unaltered (Figure 2C). Immunofluorescence staining also showed reduced LDHA in the brains of neuronal *Ldha* KO mice (Figures 2D, 2E, and S9–S11).

Neuronal *Ldha* induction raises hippocampal lactate levels

To assess whether altered LDHA in neurons causes a change in hippocampal lactate, neuronal *Ldha* induction and KO mice were analyzed using *in vivo* ^{1}H-magnetic resonance spectroscopy (^{1}H-MRS). Young female neuronal *Ldha* induction mice exhibited increased hippocampal lactate levels compared to age-matched control mice (Figure 3AI), whereas old neuronal *Ldha* induction mice did not (Figure 3AII). Neuronal *Ldha* KO mice did not have any detectable changes in hippocampal lactate at young (Figure 3BI) or old (Figure 3BII) age compared to age-matched control mice when measured by ^{1}H-MRS. In addition, metabolite levels in the hippocampus of neuronal *Ldha* induction and KO mice were analyzed using gas chromatography-mass spectrometry (GC-MS). Notably, perfusion during extraction of the hippocampus for GC-MS analysis allows for measurement of intracellular lactate without confounding cerebrovascular lactate present in the brain during *in vivo* ^{1}H-MRS. GC-MS analysis revealed increased hippocampal lactate levels in both young and old age neuronal induction mice compared with control mice (Figure 3C). In contrast, increased hippocampal lactate was detected with age, regardless of genotype, in the hippocampus of neuronal *Ldha* KO and age-matched control mice (Figure 3D). Including all features detected by GC-MS, a principal component analysis (PCA) was conducted to identify outliers (Figures S12 and S13) and partial least squares-discriminant analysis (PLSDA) to identify the metabolites with the highest variable importance in projection (VIP) scores (Figures 3E and 3F).

Ascorbic acid was elevated in young female neuronal *Ldha* induction mice relative to age-matched control mice. In contrast, L-aspartic acid and L-glutamic acid were slightly elevated in neuronal *Ldha* KO mice relative to age-matched control mice.

Neuronal *Ldha* transgenic mice do not have locomotor abnormalities

Locomotor abnormalities can be a confounding factor when assessing cognitive behavioral tasks in mice. To ensure that *Ldha* transgenic mice had normal motor function, locomotor ability was assessed on the rotarod (Figure 4A). Neither neuronal *Ldha* induction (Figure 4B) nor *Ldha* KO (Figure 4C) mice had deficits in locomotor learning or maximum ability on the rotarod at old age. In fact, old neuronal *Ldha* KO mice were better able to familiarize themselves to the rotarod (Figure 4CI). Locomotor function was also assessed by measuring swimming speed using

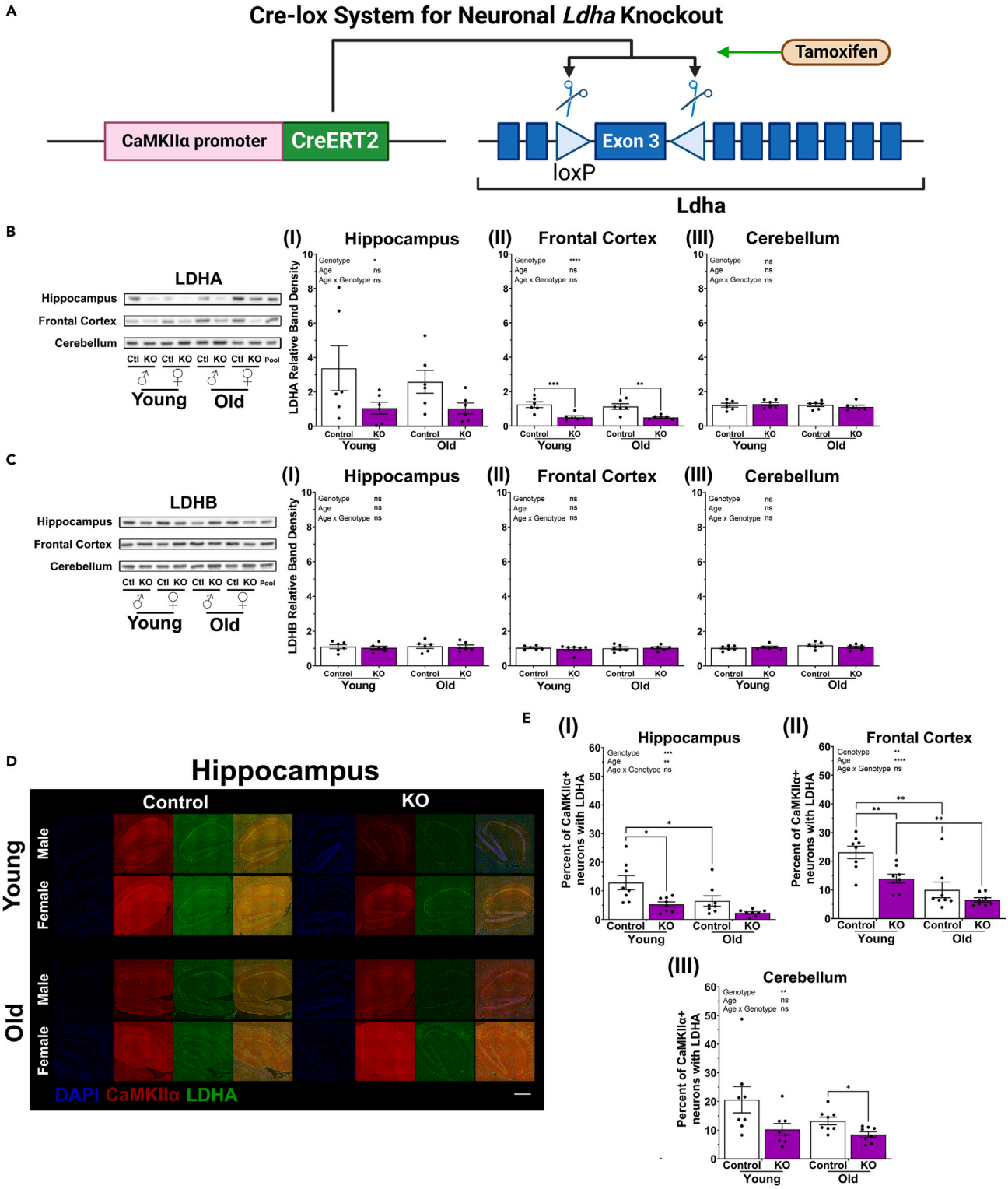

Figure 2. Neuronal *Ldha* knockout mice exhibit reduced LDHA in the brain

(A) Schematic outlining Cre-lox system used for knocking out *Ldha* in neurons. Neuronal *Ldha* KO mice contain both a genetic construct encoding the tamoxifen-dependent cyclization recombination (Cre) recombinase and mutant human estrogen receptor ligand-binding domain chimera (CreERT2) and two locus of crossing-over of bacteriophage *P*1 (*loxP*) recognition sites flanking exon 3 of the *Ldha* gene. Control mice lack CreERT2. CreERT2 permits the excision of exon 3 of *Ldha* in the presence of tamoxifen.

Figure 2. *Continued*

(B) Western blot analysis demonstrating LDHA protein levels are reduced in the hippocampus (I; genotype effect: $F(1, 20) = 6.353$, $p = 0.0203$) and frontal cortex (II; genotype effect: $F(1, 20) = 30.24$, $p < 0.0001$), but not cerebellum (II), of neuronal *Ldha* KO mice at young (6 months) and old (18 months) age. $n = 6$. See also Figure S8.

(C) Western blot analysis demonstrating LDHB protein levels are not reduced in hippocampus (I), frontal cortex (I), or cerebellum (II) of neuronal *Ldha* KO mice at young (6 months) and old (18 months) age. $n = 6$. Comparisons made by two-way ANOVA, fixed effects presented in each graph, with Šídák multiple comparisons between genotype for each age or, if there was an effect including age, Holm-Šídák multiple comparisons between genotype for each age and between age for each genotype. See also Figure S8.

(D) Representative immunofluorescence images showing reduced LDHA in the hippocampus of neuronal *Ldha* KO mice at young (8 months) and old (18.5 months) age compared with age-matched control. Scale bar: 500 μm. See also Figure S9.

(E) Quantification of immunofluorescence staining showing a decrease in CaMKIIα positive neurons containing LDHA in neuronal *Ldha* KO mice compared to control mice in the hippocampus (I; genotype effect: $F(1, 28) = 13.52$, $p = 0.0010$), frontal cortex (II; genotype effect: $F(1, 28) = 10.56$, $p = 0.0030$), and cerebellum (III; genotype effect: $F(1, 28) = 9.508$, $p = 0.0046$) at young (8 months) and old (18.5 months) of age. The percent of CaMKIIα and LDHA positive neurons decreased with age in the hippocampus (age effect: $F(1, 28) = 8.532$, $p = 0.0068$) and frontal cortex (age effect: $F(1, 28) = 27.76$, $p < 0.0001$) in neuronal *Ldha* KO and control mice. $n = 8$. See also Figures S9–S11. Comparisons made using a three-way ANOVA, fixed effects presented in each graph, and Holm-Šídák multiple comparisons between genotype within each age and between ages for each genotype. Data presented as mean ± SEM.

the Morris water maze (MWM) (Figure 4D). Relative to control mice, neuronal *Ldha* induction (Figures 4E–4H) and *Ldha* KO (Figures 4I–4L) mice did not exhibit any changes in swimming ability at young or old age during training days or probe trials.

Neuronal *Ldha* transgenic mice have altered anxiety-like behavior

Emotional state and temperament can influence cognitive ability.[88,89] To gauge the extent to which temperament is influenced by modifying neuronal *Ldha* expression, anxiety-like behavior was evaluated using two different paradigms, thigmotaxis (Figure 5A) and the light-dark box (Figure 5D). Thigmotaxis is an anxiety-like behavior defined by the centrophobic tendency to stay near the walls of a novel open space.[90,91] Among young and old neuronal *Ldha* induction mice, only old induction males exhibited an increase in thigmotaxis anxiety-like behavior compared with age-matched controls (Figure 5B). Thigmotaxis anxiety-like behavior in neuronal *Ldha* KO mice was significantly lower in young mice but unchanged at old age compared with age-matched controls (Figure 5C). Light-dark box anxiety-like behavior is the propensity to avoid brightly lit spaces. A longer latency to enter the dark side, or decreased time spent in the dark side, is reflective of reduced anxiety. Light-dark box and thigmotaxis in white light both measure mouse behavior analogous to human state anxiety,[92,93] yet testing with anxiogenic and anxiolytic drugs indicate that thigmotaxis is more sensitive to anxiety increases compared to anxiety decreases.[90] In the light-dark box, young male neuronal *Ldha* induction mice exhibited significantly reduced anxiety-like behavior compared to age-matched control mice (Figure 5EII). In contrast, young male neuronal *Ldha* KO mice in the light-dark box exhibited increased anxiety-like behavior compared to control mice (Figure 5FII).

Neuronal *Ldha* transgenic mice do not exhibit changes in long-term recognition memory

Recognition memory is a type of declarative memory[94] that is most reliant on the perirhinal cortex.[95] The spontaneous object recognition (SOR) test in rodents increasingly depends on the perirhinal cortex dependent recognition memory when conducted in a Y-shaped maze.[96] SOR testing with a Y-shaped maze was used to measure 24 h long-term recognition memory in young and old neuronal *Ldha* induction and KO transgenic mice (Figure 6A). Neuronal *Ldha* induction (Figures 6B and 6C) and *Ldha* KO mice (Figures 6D and 6E) did not exhibit changes in recognition memory compared to age-matched controls at young or old age. Moreover, in both transgenic lines and their controls, recognition memory was not lost at the older ages (Figures 6C and 6E).

Neuronal *Ldha* transgenic mice have age- and sex-dependent changes in short-term spatial memory

Spatial memory assessed using spontaneous location recognition (SLR) depends on spontaneously elicited exploration of objects and tests pattern separation ability.[97] One advantage of the SLR test of spatial memory is the ability to systematically alter the difficulty of the task and the amount of pattern separation required. Spatial memory in young and old aged neuronal *Ldha* induction and *Ldha* KO transgenic mice was measured using two configurations of SLR with either low (dSLR) or high (sSLR) pattern separation load (Figure 6F). In young neuronal *Ldha* induction transgenic mice, spatial memory tested with dSLR did not differ compared to age-matched control mice (Figure 6G). However, spatial memory tested with sSLR was significantly enhanced in young neuronal *Ldha* induction females compared to female control mice (Figure 6H). Old neuronal *Ldha* induction mice compared to age-matched control mice did not differ in spatial memory tested with dSLR (Figure 6I) and sSLR (Figure 6J). Notably, both neuronal *Ldha* induction and age-matched control mice did not retain spatial memory tested with sSLR at old age (Figure 6J). Neuronal *Ldha* KO mice compared to age-matched controls did not differ in spatial memory tested at young age with dSLR (Figure 6K) and sSLR (Figure 6L) as well as when tested at old age with dSLR (Figure 6M). Interestingly, while spatial memory tested with sSLR did not differ between old neuronal *Ldha* KO male mice compared to age-matched control males, memory was significantly improved in old female *Ldha* KO mice compared to age-matched control female mice (Figure 6N).

Neuronal *Ldha* transgenic mice have age- and sex-dependent changes in spatial learning and long-term memory

The MWM is one of the most well-established spatial learning and memory tests for rodents. This task allows for assessment of both acquisition (learning) and retrieval of memory and produces strong enough memory traces for assessment of long-term memory and memory

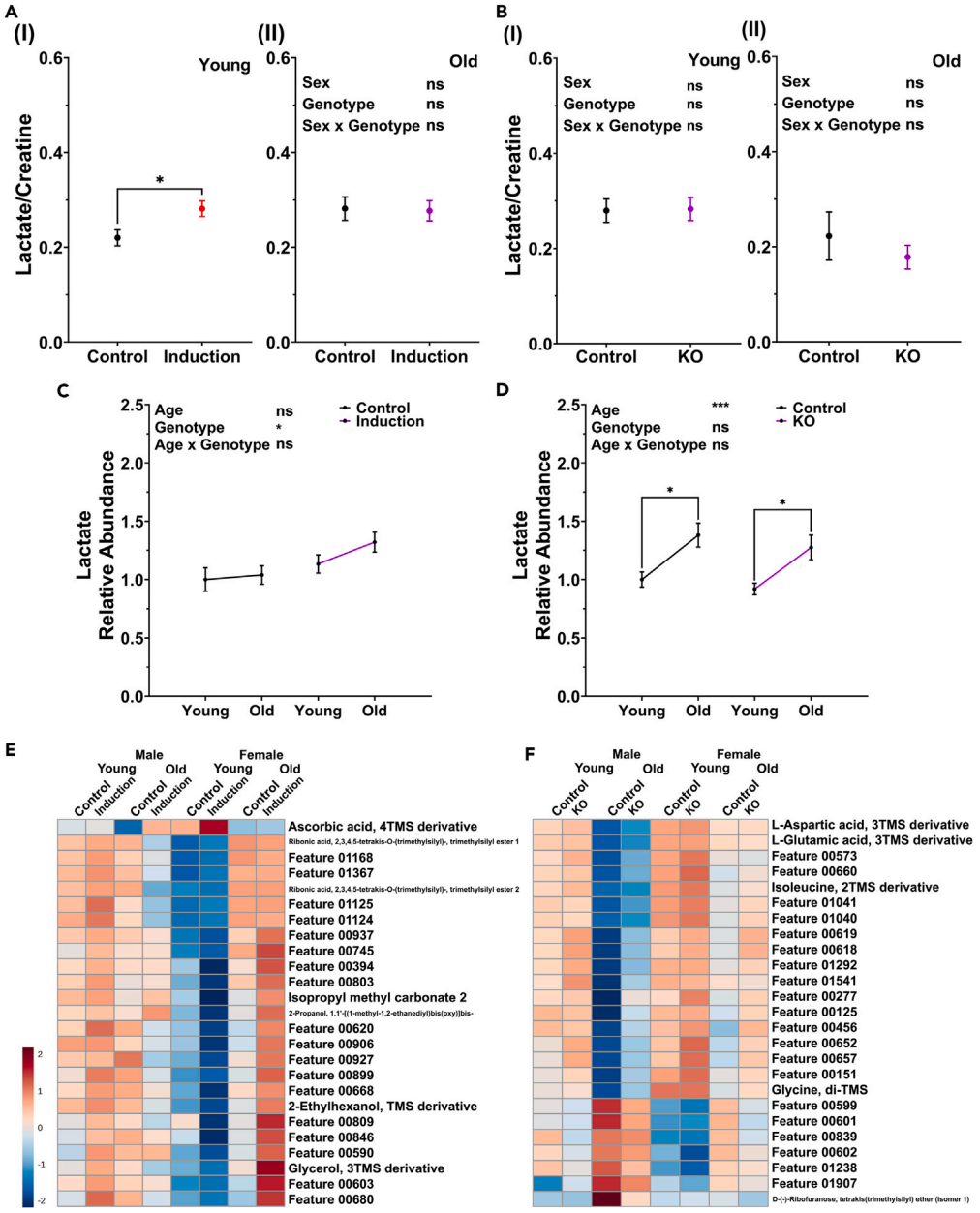

Figure 3. Hippocampal lactate levels are elevated in neuronal *Ldha* induction mice

(A) *In vivo* ^{1}H-MRS analysis revealed elevated hippocampal lactate levels in young (8 months) neuronal *Ldha* induction female mice compared to age-matched control mice (I; $n = 8$; $t(14) = 2.611$, $p = 0.0205$) whereas no genotype effects on lactate levels were detected in old (15 months) mice (II; $n = 8$).

(B) *In vivo* ^{1}H-MRS analysis of lactate levels revealed similar hippocampal lactate levels when comparing neuronal *Ldha* KO to age-matched control mice at both young age (I; $n = 7$; 9.5 months) and old age (15 months). Comparisons for ^{1}H-MRS analysis were made using unpaired t test if only one sex measured and using two-way ANOVA, fixed effects presented in each graph, with unpaired t test between genotypes.

(C) GC-MS analysis revealed elevated hippocampal lactate levels in neuronal *Ldha* induction mice across both young and old (genotype effect: $F(1, 37) = 5.628$, $p = 0.0230$) compared to young and old control.

(D) GC-MS analysis revealed in neuronal *Ldha* KO mice only elevation of hippocampal lactate with age across both genotypes (age effect: $F(1, 37) = 18.61$, $p = 0.0001$; control: $t(18) = 3.139$, $p = 0.022521$; KO: $t(19) = 2.963$, $p = 0.023766$) with no difference between genotypes. Comparisons for GC-MS analysis were made using two-way ANOVA, fixed effects presented in each graph, with Holm-Šídák multiple comparisons. *p* values for partial correlation analysis were Bonferonni corrected.

(E and F) Heatmaps depicting relative abundance of the 25 metabolites with the top variable importance in projection (VIP) scores identified by partial least squares-discriminant analysis (PLSDA) of metabolomes generated by GC-MS analysis of the hippocampus in neuronal *Ldha* induction and age-matched control mice (E) or neuronal *Ldha* KO and age-matched control mice (F). Metabolites that could not be identified in the NIST database are listed as a number based on their mean retention time. See also Figures S12 and S13. Data presented as mean ± SEM.

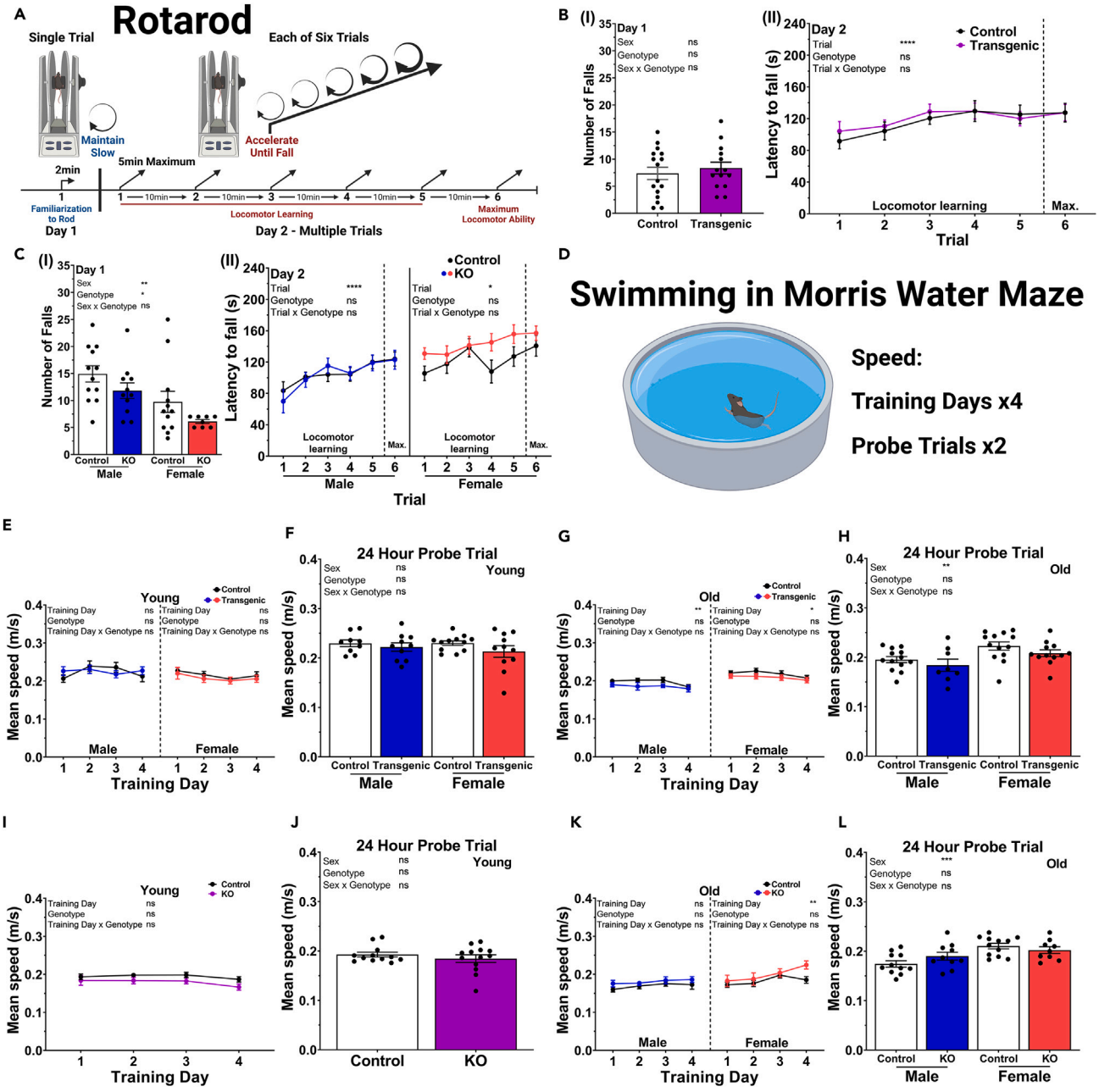

Figure 4. Locomotor ability is not impacted by neuronal *Ldha* induction or knockout

(A) In the rotarod paradigm mouse locomotor ability was determined by assessing familiarization to a spinning rod on day 1, followed by learning to remain on a spinning rod as it progressively accelerates across each of five consecutive trials on day 2 and with maximum performance assessed on day 2 trial 6.

(B) Locomotor ability on the rotarod for 14.5 month old neuronal *Ldha* induction and age-matched control mice for either sex did not differ on day 1 (I) or day 2 (II). Transgenic mice did not differ from age-matched control mice for day 1 number of falls (I), day 2 latency to fall (II) or day 2 at maximum ability (II). $n = 5–9$.

(C) Locomotor ability on rotarod for 14.5 month old *Ldha* KO and age-matched controls on day 1 familiarization to the rod differed by sex and genotype (I; $n = 8–12$; sex effect: $F(1, 39) = 11.56$, $p = 0.0016$; genotype effect: $F(1, 39) = 4.432$, $p = 0.0418$) and on day 2 differed by sex (II; $n = 9–12$; sex effect trial 1–5: $F(1, 40) = 10.61$, $p = 0.0023$; sex effect trial 6: $F(1, 40) = 4.988$, $p = 0.0312$). KO and control mice did not differ on day 2 (II). Comparisons of rotarod performance on day 1 and day 2 trial 6 were made using a two-way ANOVA across sex and genotype, fixed effects presented in each graph, and unpaired t test between genotypes. Comparisons for rotarod day 2 trial 1–5 were made using a mixed-effects model with Geisser-Greenhouse correction, fixed effects presented in each graph, and Šídák's multiple comparisons test between genotype for each trial, within each sex if there was an effect of sex.

(D) Locomotor activity assessed by measuring average swimming speed during training day trials and probe trials in the Morris water maze as depicted in Figure 7A.

(E) Locomotor ability on training days was retained equally in 6 month old neuronal *Ldha* induction and age-matched control mice for both sexes. $n = 9–12$.

Figure 4. *Continued*

(F) Locomotor ability in young aged (6 months) was retained equally in neuronal *Ldha* induction compared to age-matched control mice of both sexes for mean swimming speed in the 24 h probe trial. $n = 9–12$.

(G) Locomotor ability on training days was retained equally in old aged (12.5 months) neuronal *Ldha* induction and control mice for both sexes. $n = 8–13$.

(H) Locomotor ability in old aged (12.5 months) neuronal *Ldha* induction and age-matched control mice of both sexes was retained equally in the 24 h probe trial. $n = 8–13$.

(I) Locomotor ability on training days in young aged (7 months) neuronal *Ldha* KO compared to age-matched control mice was retained equally. $n = 12–13$.

(J) Locomotor ability in young aged (7 months) neuronal *Ldha* KO compared to age-matched control mice was retained equally in the 24 h probe trial. $n = 12–13$.

(K) Locomotor ability on training days in young aged (13 months) neuronal *Ldha* KO and age-matched control mice of both sexes were retained equally. $n = 9–12$.

(L) Locomotor ability in old aged (13 months) neuronal *Ldha* KO and age-matched control mice of both sexes were retained equally in the 24 h probe trial. $n = 9–12$. For training days mean speed swimming, comparisons were made using a mixed-effects model with Geisser-Greenhouse correction, fixed effects presented in each graph, and further comparisons between genotype for each day were made using unpaired t tests for conditions with an effect including genotype. For probe trials, comparisons were made using a two-way ANOVA, fixed effects presented in each graph, and further comparisons between genotype made using unpaired t tests, within each sex for conditions with an effect including sex for training days or probe trials. Data presented as mean ± SEM.

decay over multiple days. The MWM was used to test spatial learning in addition to 24 h and 7 days long-term spatial memory in young and old aged neuronal *Ldha* induction and KO mice (Figure 7A). Neuronal *Ldha* induction compared to age-matched control mice did not differ in spatial learning at young age (Figure 7B), but neuronal *Ldha* induction mice exhibited reduced spatial learning in males only at old age (Figure 7C). Neuronal *Ldha* KO mice compared to age-matched control mice also had no difference in spatial learning at young age (Figure 7D), but at old age female KO mice exhibited improved spatial learning compared to control mice (Figure 7E). Young neuronal *Ldha* induction mice had sex-dependent changes in long-term spatial memory compared to age-matched controls (Figures 7F and 7H). Female neuronal *Ldha* induction mice had 24 h (Figure 7FI) and 7 days (Figure 7HII) memory deficits compared to controls, whereas males had an improvement that was only detectable at 24 h (Figure 7FII). Neuronal *Ldha* induction compared to age-matched control mice did not differ in 24 h (Figure 7G) or 7 days (Figure 7I) long-term spatial memory at old age. Young neuronal *Ldha* KO mice also had sex-dependent changes in long-term spatial memory compared to age-matched controls (Figures 7J and 7L). Males had a memory deficit evident only at 7 days (Figure 7L) and not at 24 h (Figure 7J), while females did not differ from controls at either time points (Figures 7J and 7L). Neuronal *Ldha* KO compared to age-matched control mice did not differ in 24 h (Figure 7K) or 7 days (Figure 7M) long-term spatial memory at old age.

Neuronal *Ldha* transgenic mice have age- and sex-dependent changes in cognitive behavior tested in the puzzle box

The last test used to assess the cognition of neuronal *Ldha* induction and *Ldha* KO mice was the puzzle box. The puzzle box allows for screening of changes in general cognition by testing mice with consecutive trials requiring they escape from the light to the dark side of the box through increasingly difficult novel obstructions (problem solving) or through an obstruction they have passed through before (memory) (Figure 8A). This task allows for screening of deficits in medial prefrontal cortex (mPFC) changes that may alter executive function[98] and cognitive changes that may only be evident at particular levels of difficulty. No changes in habituation phase were detected in neuronal *Ldha* induction (Figures S15A and S15B) or neuronal *Ldha* KO (Figures S15C and S15D) compared with control mice. Young neuronal *Ldha* induction mice compared to age-matched control mice had no change in problem solving (Figure 8B) and 3 min memory (Figure 8C), but did exhibit a sex-dependent change in 24 h memory with only female transgenic mice exhibiting a deficit (Figure 8D). Conversely, old aged neuronal *Ldha* induction compared to age-matched control mice showed deficits in problem solving (Figure 8E) and 3 min memory (Figure 8F) but no change in 24 h memory (Figure 8G). Problem solving in young aged neuronal *Ldha* KO mice compared to age-matched control mice differed in the opposite direction; better for males and worse for females (Figure 8H). Young aged neuronal *Ldha* KO mice compared to age-matched control mice also showed a deficit in 3 min memory (Figure 8I) and a sex-dependent improvement in 24 h memory; unchanged in males and increased in females (Figure 8J). No changes in problem solving (Figure 8K), 3 min memory (Figure 8L), or 24 h memory (Figure 8M) were observed in old aged neuronal *Ldha* KO mice compared to age-matched controls.

DISCUSSION

Neuronal lactate production can affect certain types of cognition in an age- and sex-specific manner

Here it is shown that neuronal lactate metabolism is involved in different types of cognitive processing in mice depending on sex and age (Table 1). These results provide insight into the potential role of neuronal lactate metabolism on cognition in the context of age and sex, factors mostly unexplored in previous ANLS studies. Moreover, these findings indicate that neurons are capable of generating lactate independently of astrocytes. The question arises as to the fate of lactate produced within neurons. Cytosolic lactate can either be exported via MCTs or oxidized back to pyruvate to be used as a mitochondrial fuel source. Whether lactate is converted back to pyruvate in the cytosol or within mitochondria has been a controversial issue. Almost 50 years ago it was demonstrated that both LDHA and LDHB isoforms are present in neuronal mitochondria.[99] In 1999, George Brooks demonstrated that mitochondrial localized LDH in rat liver, cardiac, and skeletal muscle can oxidize lactate to pyruvate to fuel the TCA cycle and respiration.[100] These observations have led to the intracellular lactate shuttle hypothesis, which posits that cytosolic lactate, formed during glycolysis, can be transported into mitochondria where it is converted to pyruvate by the mitochondrial oxidation complex (mLOC), in part composed of isomers of LDHA and LDHB.[101] Thus, elevated neuronal *Ldha* expression could drive high levels of lactate production and subsequent lactate oxidation in mitochondria to fuel mitochondrial respiration and ATP synthesis to enable synaptic processes. Alternatively, cytosolic lactate can be exported and either used by adjacent cells as a fuel source or as a

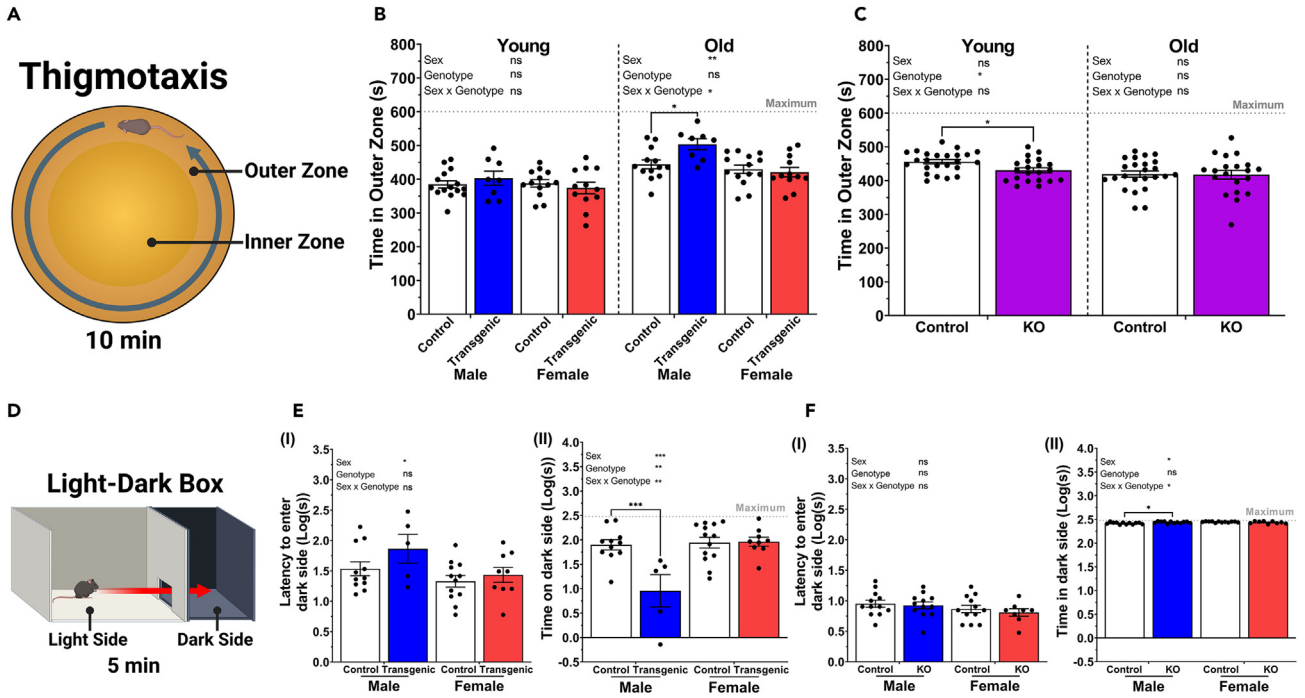

Figure 5. Thigmotaxis and light-dark box anxiety-like behavior are differentially impacted by neuronal *Ldha* induction or knockout depending on age and sex

(A) Thigmotaxis is a type of anxiety-like behavior that was measured as time spent in outer zone during the first day of habituation to the circular arena during the spontaneous location recognition paradigm (Figure 6F).

(B) Thigmotaxis anxiety-like behavior in neuronal *Ldha* induction mice compared to age-matched control mice was unchanged at young age (5 months) and higher at old age (12 months) for males ($t(43) = 2.819$, $p = 0.0144$; sex × genotype effect: $F(1, 43) = 5.943$, $p = 0.0190$) but not females. $n = 8–15$.

(C) Thigmotaxis anxiety-like behavior in neuronal *Ldha* KO mice compared to age-matched control mice was lower at young age (6 months; $t(43) = 2.641$, $p = 0.0115$; genotype effect: $F(1, 41) = 6.746$, $p = 0.013$) and unchanged at old age (12.5 months). $N = 20–24$. For thigmotaxis, comparisons made by two-way ANOVA within each age group, fixed effects presented in each graph, with Šídák's multiple comparisons between genotypes.

(D) Anxiety-like behavior was assessed in the light-dark box as time spent on dark side and latency to enter dark side.

(E) Light-dark box anxiety-like behavior of young age (6.5 months) neuronal *Ldha* induction mice and age-matched control differed by sex for latency to enter dark side (I; $F(1, 33) = 5.601$, $p = 0.024$), and time on dark side (II; $F(1, 34) = 13.31$, $p = 0.0009$). Transgenic males had decreased anxiety-like behavior for time on dark side (II; sex × genotype effect: $F(1, 34) = 11.10$, $p = 0.0021$; $t(34) = 4.186$, $p = 0.0004$). $n = 5–13$.

(F) Light-dark box anxiety-like behavior of young aged (7 months) neuronal *Ldha* KO mice and age-matched control differed by sex for time on dark side (II; $F(1, 41) = 5.180$, $p = 0.0281$). KO males had increased anxiety-like behavior for time on dark side (II; sex × genotype effect: $F(1, 41) = 6.612$, $p = 0.0139$; $t(41) = 2.47$, $p = 0.0352$). $n = 8–12$. Comparisons for light-dark box made using two-way ANOVA, fixed effects presented in each graph, and Šídák's multiple comparisons between genotype for each sex. Data presented as mean ± SEM.

signaling molecule.[102–104] Within the brain, elevated extracellular lactate can affect nearly all cell types, including neurons, neural stem cells, neural progenitor cells, and pericytes.[105–110] Thus, the changes in cognition resulting from either elevated or repressed neuronal *Ldha* expression may arise from altered lactate levels affecting metabolism or signaling in either a cell autonomous manner or through the action of secreted lactate affecting adjacent cells.

One important finding of this study is that modifying expression of *Ldha* in neurons has a female-specific impact on sSLR memory that differs with age; memory was improved by neuronal *Ldha* induction in young mice and by neuronal *Ldha* KO in old mice. The higher level of pattern separation required for memory encoding in the sSLR over the dSLR test variant is a reflection of the sSLR being particularly sensitive to changes in brain-derived neurotrophic factor (BDNF) and adult hippocampal neurogenesis.[111–116] All steps of adult hippocampal neurogenesis progression promote various forms of cognition,[113,115,117–127] including pattern separation, through production of new neurons at different maturation stages.[128–132] BDNF can support sSLR memory through enhanced synaptic plasticity via activation of receptors on mature neurons[133–135] or highly excitable immature neurons,[136–140] and through promotion of adult hippocampal neurogenesis.[141–143]

Lactate has been shown to promote *Bdnf* expression through neuronal silent information regulator 1 (sirtuin 1/SIRT1) signaling,[38,144] N-methyl-D-aspartate (NMDA) receptor potentiation,[17,109,145] or hydroxycarboxylic acid receptor 1 (HCAR1/GPCR81) receptor activation.[146–153] Alternatively, lactate may trigger neural stem, precursor, or progenitor cell proliferation in the hippocampus directly through pentose phosphate pathway metabolic reprogramming[110] or zinc-dependent anaphase promotion.[154] Therefore, neuronal-generated

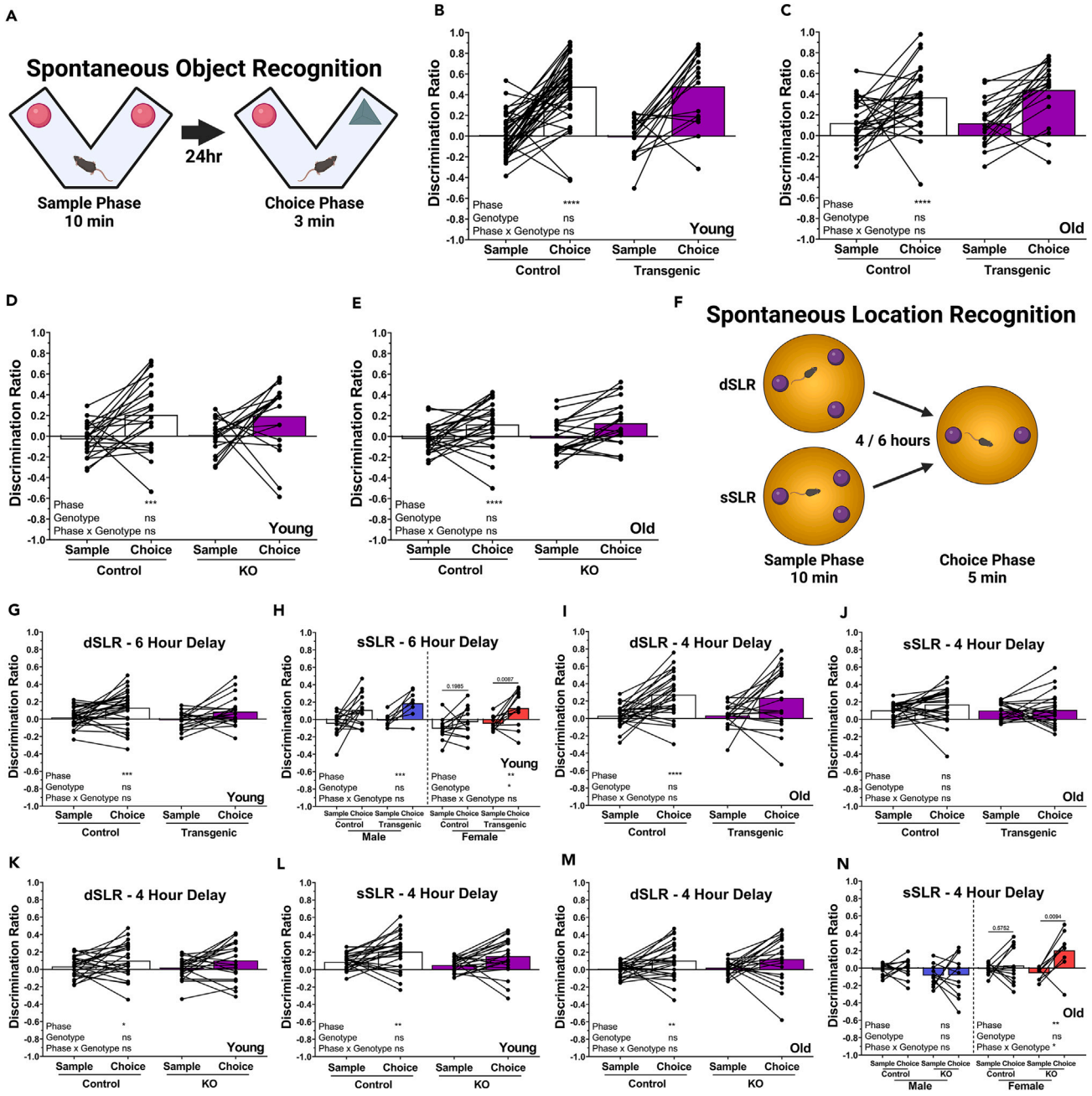

Figure 6. Short-term spatial memory with high pattern separation is increased by neuronal *Ldha* induction in young and by neuronal *Ldha* knockout in old female mice whereas long-term recognition memory is unaffected by neuronal *Ldha* modification at both ages

(A) Spontaneous Object Recognition (SOR) paradigm for testing recognition memory with a 24 h delay between sample and choice phase. See also Figure S14A.

(B and C) 24 h recognition memory in SOR was retained in both neuronal *Ldha* induction and age-matched control mice at young (B; 4.5 months; $n = 18–44$; phase effect: $F(1, 120) = 86.24$, $p < 0.0001$) and old (C; 11 months; $n = 20–27$; phase effect: $F(1, 45) = 27.96$, $p < 0.0001$) age.

(D and E) 24 h recognition memory in SOR was retained in both neuronal *Ldha* KO and age-matched control mice at young (D; 5.5 months; $n = 18–23$; phase effect: $F(1, 78) = 13.32$, $p = 0.0005$) and old (E; 11 months; $n = 21–24$; phase effect: $F(1, 43) = 18.90$, $p < 0.0001$) age.

(F) Spontaneous Location Recognition (SLR) paradigm for testing spatial memory with low (dSLR) or high (sSLR) pattern separation with a 4 or 6 h delay between sample and choice phase. See also Figure S14B.

(G) 6 h spatial memory in dSLR was retained at young age (5 months) in both neuronal *Ldha* induction and age-matched control mice ($n = 20–28$; phase effect: $F(1, 46) = 2.62$, $p = 0.0009$).

Figure 6. *Continued*

(H) 6 h spatial memory in sSLR at differed with sex ($F(1, 44) = 4.902$, $p = 0.0321$) in young aged (5 months) neuronal *Ldha* induction and age-matched control mice. Memory was retained in male *Ldha* induction and control mice (n = 8–15; phase effect: $F(1, 21) = 15.37$, $p = 0.0008$) but was enhanced in *Ldha* induction female ($t(11) = 3.181$, $p = 0.0087$) mice compared to controls ($t(12) = 1.361$, $p = 0.1985$) (n = 12–13; genotype effect: $F(1, 23) = 5.829$, $p = 0.0241$).

(I) 4 h spatial memory in dSLR was retained at old age (12 months) in both neuronal *Ldha* induction and age-matched control mice (n = 20–27; phase effect: $F(1, 43) = 24.38$, $p < 0.0001$).

(J) 4 h spatial memory in sSLR was lost at old age (12 months) in both neuronal *Ldha* induction and age-matched control mice (n = 20–27; phase effect: $F(1, 45) = 1.477$, $p = 0.2305$).

(K) 4 h spatial memory in dSLR was retained at young age (6 months) in both neuronal *Ldha* KO and age-matched control mice (n = 21–24; phase effect: $F(1, 43) = 5.679$, $p = 0.0217$).

(L) 4 h spatial memory in sSLR was retained at young age (6 months) in both neuronal *Ldha* KO and age-matched control mice (n = 21–24; phase effect: $F(1, 43) = 10.58$, $p = 0.0022$).

(M) 4 h spatial memory in dSLR was retained at old age (12.5 months) in both neuronal *Ldha KO* and age-matched control mice (n = 21–24; phase effect: $F(1, 84) = 6.953$, $p = 0.01$).

(N) 4 h spatial memory in sSLR at old age (12.5 months) differed with sex ($F(1, 80) = 7.209$, $p = 0.0088$) in neuronal *Ldha* KO and age-matched control mice. Memory in KO and control was lost in males (n = 11–12; phase effect: $F(1, 42) = 0.04346$, $p = 0.8359$) but differed in females (n = 9–12; phase × genotype effect: $F(1, 38) = 4.718$, $p = 0.0362$), with memory enhanced in KO ($t(8) = 3.394$, $p = 0.0094$) and lost in control mice ($t(11) = 0.5775$, $p = 0.5752$). Comparisons across all conditions in SOR and SLR were made using a mixed-effects model with matching by phase and fixed effects presented in each graph. For comparisons with a fixed effect of genotype or phase × genotype, further comparisons between phase for each genotype were made using paired t tests with the p value reported above each comparison. Bars in each graph represent the mean.

lactate may be exported to promote an increase in BDNF levels and adult hippocampal neurogenesis thereby contributing to an increase in sSLR memory in young female neuronal *Ldha* induction mice. Moreover, enhanced sSLR memory in young females but not males may be due to higher basal or estrogen-induced[155–157] expression of hippocampal BDNF[158] and NMDA receptors.[159] Further investigation is required to determine if elevated neuronal lactate production in females contributes to increased BDNF production and altered neurogenesis to facilitate pattern separation memory.

Neuronal *Ldha* is detrimental to cognition in aged mice

Although neuronal *Ldha* induction enhanced sSLR memory in young females, elevated neuronal lactate production had no effect on sSLR memory at old age in both sexes. In contrast, neuronal *Ldha* KO resulted in improved sSLR memory and MWM learning in old female mice. BDNF levels,[160–162] adult hippocampal neurogenesis,[115,163–167] and cognition[115,163,168] typically decline with age. In addition, stem cell exhaustion has been identified as a hallmark of aging.[169,170] Elevated *Ldha* expression is associated with proliferation of various adult somatic stem cells throughout the body.[171–173] *In vitro* studies have shown that proliferative neural stem cells express high levels of glycolytic enzymes, including *Ldha*, and secrete elevated levels of lactate.[174] Furthermore, addition of lactate to the media of cultured neural progenitor cells triggers increased proliferation.[110] As described previously, high pattern separation tasks such as sSLR memory in young female neuronal *Ldha* induction mice may have benefited from a lactate-dependent increase in adult hippocampal neurogenesis. In contrast, enhancement of sSLR memory at old age in female neuronal *Ldha* KO mice may have occurred by preventing lactate induced proliferation and exhaustion of the pool of hippocampal stem cells. Alternatively, chronically increased hippocampal lactate may impede non-neurogenesis specific cognition with age. For example, hippocampal KO of the pyruvate dehydrogenase E1 component alpha subunit (*Pdha1*) causes lactate accumulation, altered monocarboxylate transporter levels, and severe impairment of spatial learning and memory in the MWM, but not recognition memory.[37] In addition, chronic systemic chemical inhibition of glycogen breakdown, and subsequent lactate production, impairs memory in young mice[17,21,22,28,29,52] but improves long-term potentiation in hippocampal slices[175] and short-term object recognition and location memory in old mice.[50] Interestingly, here it was observed that protein levels of ectopically expressed *Ldha* increased with age with a concomitant increase in intracellular lactate, as assessed by GC-MS. A recent study revealed that elevated brain lactate levels are linked to poorer working memory performance in multiple mouse models of neuropsychiatric disorders.[176] Thus, elevated neuronal lactate production with age may contribute to cognitive impairment in older mice.

Memory enhancement in old female neuronal *Ldha* KO mice could also be attributed to non-BDNF dependent mechanisms, such as increased LDHB-catalyzed lactate oxidization-dependent alterations in expression of immediate-early genes and synaptic plasticity genes.[109,177] There could be a shift with age toward neuronal LDHB dependent ANLS support within the hippocampus for cognitive processing. In fact, a recent finding saw global KO of *Ldhb* resulted in Y-maze spontaneous alternation and MWM learning and memory deficits along with apoptosis, neurodegeneration, and mitochondrial dysfunction typically associated with age-related cognitive decline.[23] Hypothetically, a metabolic shift toward ANLS supported neuronal metabolism with age may normally be enabled without changes in expression of either LDH isoform but rather the redistribution of LDHA or LDHB between neuronal processes and the soma, as neurons have been shown to localize specific metabolic enzymes to different subcellular compartments. For instance, *Caenorhabditis elegans* neurons under energetic stress conditions localize glycolytic enzymes toward the synapse[178] and hippocampal neurons in aged mice localize LDHA away from the soma.[179]

LDHA was recently found to be enriched on axonal vesicles and is required to provide ATP for fast axonal vesicular transport.[180] In addition, the preferential conversion of pyruvate to lactate enabled by LDHA allowed for the concomitant recycling of the reduced form of nicotinamide adenine dinucleotide (NADH) into the oxidized form (NAD+) on vesicles.[180] With age, excess lactate produced by neurons, or imported from

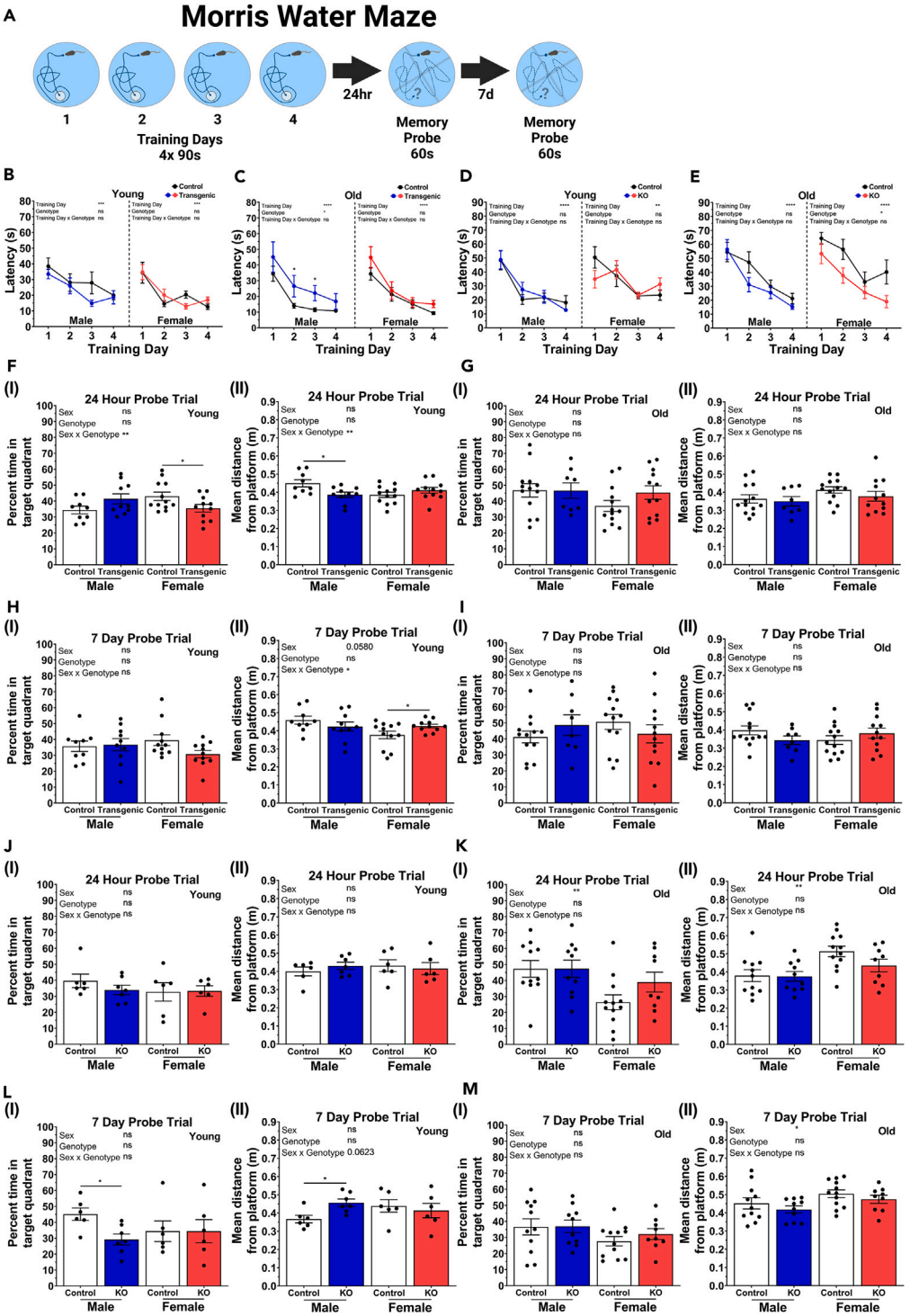

Figure 7. Spatial learning and long-term memory are both differentially impacted by neuronal *Ldha* induction and knockout depending on age and sex

(A) Morris water maze paradigm for testing spatial learning during training days and long-term spatial memory at 24 h and 7 days probe trials.

(B) Spatial learning in young (6 months) neuronal *Ldha* induction was retained equally in transgenic and age-matched control mice for both sexes. n = 9–12.

(C) Spatial learning in old (12.5 months) neuronal *Ldha* induction compared with age-matched control mice was worse in males only (genotype effect: $F(1, 19) = 5.939$, $p = 0.0248$). n = 8–13.

(D) Spatial learning in young (7 months) neuronal *Ldha* KO compared with age-matched control mice was retained equally for both sexes. N = 5–7.

Figure 7. *Continued*

(E) Spatial learning in old (13 months) neuronal *Ldha* KO compared with age-matched control mice was improved in females only (genotype effect: $F(1, 19) = 5.850$, $p = 0.0258$). $n = 9–12$.

(F) 24 h long-term spatial memory in young (6 months) neuronal *Ldha* induction compared to age-matched control mice was decreased in females for percent time in target quadrant (I; sex × genotype effect: $F(1, 38) = 7.430$, $p = 0.0096$; $t(21) = 2.125$, $p = 0.0457$) and increased in males for mean distance from platform (II; sex × genotype effect: $F(1, 38) = 7.424$, $p = 0.0097$; $t(17) = 2.594$, $p = 0.0189$). $n = 9–12$.

(G) 24 h long-term spatial memory in old (12.5 months) neuronal *Ldha* induction compared to age-matched control was retained equally for percent time in target quadrant and mean distance from platform (I + II) for both sexes. $n = 8–13$.

(H) 7 days long-term spatial memory in young (6 months) neuronal *Ldha* induction compared with age-matched control mice was retained equally for percent time in target quadrant (I) and decreased in females only for mean distance from platform (II; sex × genotype effect: $F(1, 38) = 4.459$; $t(21) = 2.084$, $p = 0.0496$). $n = 9–12$.

(I) 7 days long-term spatial memory in old (12.5 months) neuronal *Ldha* induction compared with age-matched control mice was retained equally for percent time in target quadrant and mean distance from platform (I + II) for both sexes. $n = 8–13$.

(J) 24 h long-term spatial memory in young (7 months) neuronal *Ldha* KO compared to age-matched control mice is retained equally for percent time in target quadrant and mean distance from platform (I + II) for both sexes. $n = 6–7$.

(K) 24 h long-term spatial memory in old (13 months) was retained equally for percent time in target quadrant and mean distance from platform (I + II) for both sexes. $n = 9–12$.

(L) 7 days long-term spatial memory in young (7 months) neuronal *Ldha* KO compared to age-matched control was decreased in males only for percent time in target quadrant (I; $t(11) = 3.069$, $p = 0.0107$) and mean distance from platform (II; $t(11) = 3.076$, $p = 0.0106$). $n = 6–7$.

(M) 7 days long-term spatial memory in old (13 months) was retained equally for percent time in target quadrant and mean distance from platform (I + II) for both sexes. $n = 9–12$. For training days, comparisons were made using a mixed-effects model with Geisser-Greenhouse correction, fixed effects presented in each graph, and further comparisons between genotype for each day were made using unpaired t tests for conditions with an effect including genotype. For probe trials, comparisons were made using a two-way ANOVA, fixed effects presented in each graph, and further comparisons between genotype for each sex were made using unpaired t tests for conditions with an effect including sex for memory, learning, or locomotor ability (Figure 4). Data presented as mean ± SEM.

astrocytes, might block glycolytic reactions from taking place on vesicular membranes, as high lactate levels would inhibit LDHA and potentially interfere with axonal vesicular transport and synaptic function.

Numerous studies support opposing effects on the age-related dependence on ANLS and neuronal LDHB-dependent lactate oxidization. In a previous study LDHA and LDHB expression were found to decrease within the frontal cortex of mice with age.[69] Moreover, LDHA protein was detected in neurons in the brain and elevated LDHA levels correlated positively with memory in aged mice.[69] Others have found that the glycogenolysis enzyme glycogen phosphorylase increasingly localizes to hippocampal neurons with age[179] and KO of glycogen synthase in neurons or neural precursor cells in young mice lowers the capacity for learning in an operant conditioning test.[181,182] The discovery that glycogenolysis is not astrocyte-specific necessitates reinterpretation of previous studies suggesting that the ANLS supports cellular processing underlying cognition by showing that lactate rescues cognitive deficits caused by non-cell-type specific chemical inhibition of glycogenolysis in young animals.[17,19,21,22,24,28,29,39,45,52] Similarly, the possibility that neuronal glycogenolysis modulates cognition makes it difficult to decipher which cell type to attribute the improvement in memory recently found in old mice treated systemically with the glycogen phosphorylase inhibitor, BAY U6751.[50] Active neuronal glycogen metabolism also suggests that glycogen may sometimes fuel synaptic functions that require glycolysis, such as presynaptic action potentials,[183] vesicle cycling,[184] and neurite outgrowth.[81] Furthermore, chemical or genetic inhibition of glucose transport in the dorsal hippocampus reduces contextual fear conditioning learning and memory in young mice,[18] while neuronal KO of a glucose transporter, *Glut3*, or a pyruvate-producing glycolytic enzyme, pyruvate kinase (*Pkm1*), causes active place avoidance learning deficits with age.[77] Of note, age-related cognitive deficits found in neuronal *Pkm1* KO mice were restricted to females, much like the female-only cognitive benefits observed here in old neuronal *Ldha* KO mice. Hence, neuronal glycolysis or glycogenolysis, independently or in addition to the ANLS, may also be important for retention of certain cognitive abilities depending on age. The findings presented here strongly warrant further study on the connection between cognition and age-related changes in cell-type and subcellular localization of lactate metabolism and ANLS-related processes. Overall, it would appear that cognition with age becomes sensitive to changes in expression of the lactate-producing enzyme LDHA in neurons whereby increases are detrimental and decreases are beneficial.

Potential sex differences in ANLS involvement in cognition

In the present study, multiple sex differences in cognition were identified following altered neuronal *Ldha* expression. This observation is important because previous studies that implicate the ANLS in cognitive processes used exclusively males or failed to report whether sex differences were investigated. Numerous studies have provided experimental evidence in young vertebrates to support the involvement of ANLS in cognition, yet only five of those include females.[37,47,51–53] Therefore, the extent to which sex differences affect ANLS-mediated cognition is quite unclear.

When assessing MWM long-term memory in young mice, it was observed that neuronal *Ldha* induction enhanced memory up to 24 h in males and decreased memory up to 7 days in females, whereas neuronal *Ldha* KO reduced memory in males after 7 days and did not impact female memory. Unlike other cognitive behavior paradigms employed in this study, the MWM is an inherently stressful assay. Levels of stress response hormones,[185] proteins such as the murine glucocorticoid corticosterone[186,187] and α-amino-3-hydroxy-5-methyl-4-isoxazolepropionic acid (AMPA) glutamate receptors, respectively, are higher in females compared to males in the basolateral amygdala, a fear- and stress-mediating brain region.[186] Moreover, stressors tend to have opposite effects on male and female hippocampal-dependent cognition, negative and positive, respectively.[185,187,188] Therefore, if neuronal expression of *Ldha* within the hippocampus mediates stress-related sex

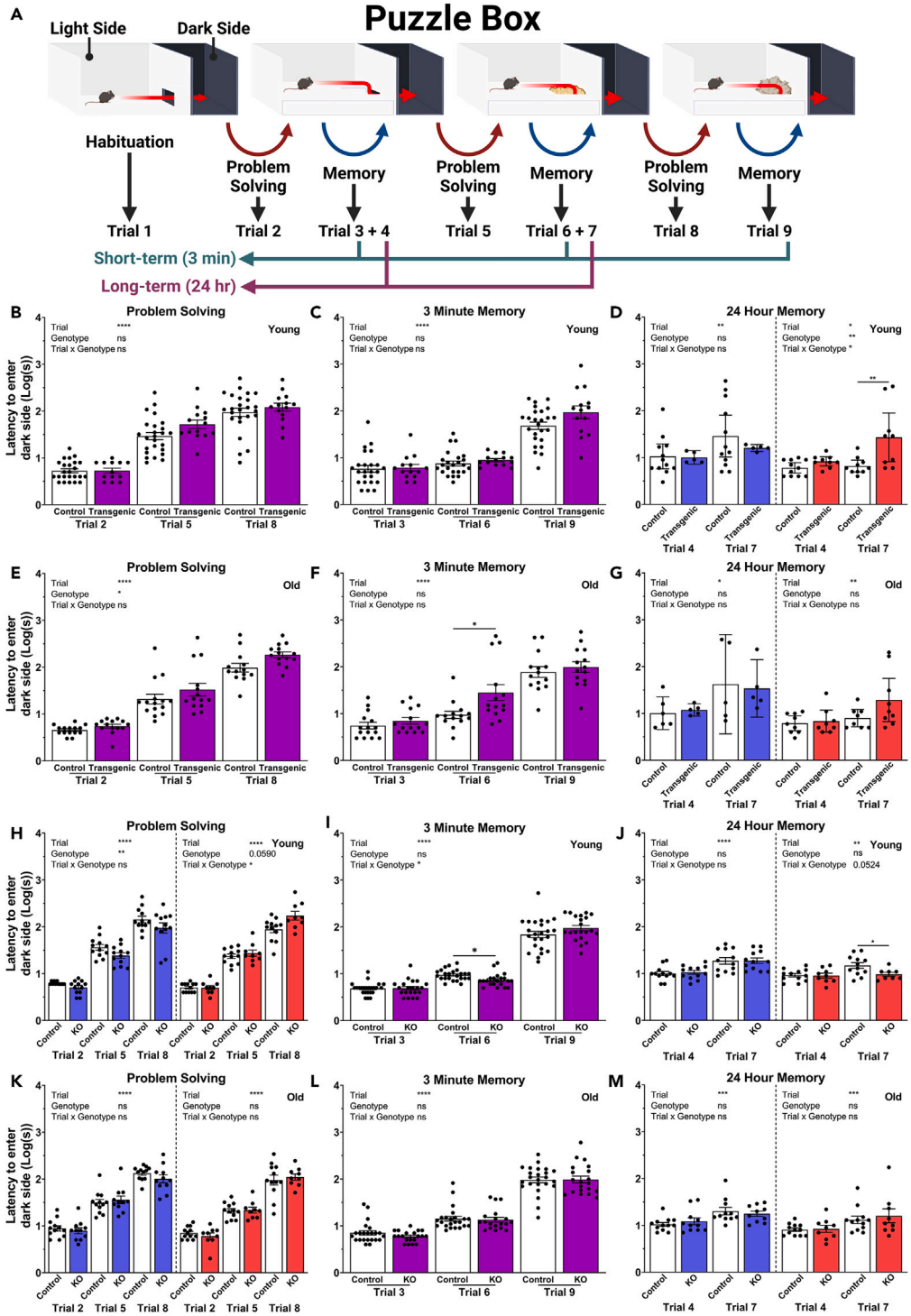

Figure 8. Cognitive behavior in puzzle box is differentially impacted by neuronal *Ldha* induction and knockout depending on age and sex

(A) In the puzzle box mice must pass from the light to dark side of a light-dark box with various barriers of increasing difficulty put in place during nine trials that were spread across three successive days with three trials per day. For each trial, higher latency to enter the dark side is indicative of worse performance. Habituation is exhibited during the first trial that has no barrier. Problem solving ability is exhibited during trials 2, 5, and 8 when the task difficulty is increased from the previous one on the same day. 3 min memory is exhibited during trials 3, 6, and 9 when the task is of equal difficulty to the previous one on the same day. 24 h memory is exhibited during trials 4 and 7 when the task is of equal difficulty to the previous one on the day prior. See also Figure S15.

(B) Problem solving ability was retained equally in young (7 months) neuronal *Ldha* induction compared to age-matched control mice. *n* = 13–25.

Figure 8. *Continued*

(C) 3 min memory was retained equally in young (7 months) neuronal *Ldha* induction compared to age-matched control mice. n = 14–24.

(D) 24 h memory in young (7 months) neuronal *Ldha* induction and age-matched control mice differed by sex (sex × genotype effect: $F(1, 33) = 4.003$, $p = 0.0537$; trial × sex × genotype effect: $F(1, 32) = 5.143$, $p = 0.0302$). 24 h memory in induction compared with control mice was retained equally in males, worse in females across both trial 4 and 7 (genotype effect: $F(1, 18) = 10.18$, $p = 0.0051$; trial × genotype effect: $F(1, 17) = 4.713$, $p = 0.0444$), and worse in females particularly for higher difficulty trial 7 ($t(35) = 3.776$, $p = 0.0012$). n = 5–12.

(E) Problem solving ability was worse in old (14 months) neuronal *Ldha* induction compared to age-matched control across trials 2, 5, and 8 (genotype effect: $F(1, 27) = 4.276$, $p = 0.0483$). n = 13–15.

(F) 3 min memory in old (14 months) neuronal *Ldha* induction mice was worse particularly for the intermediate difficulty trial 6 ($t(79) = 2.899$, $p = 0.0145$). n = 14–15.

(G) 24 h memory in old (14 months) neuronal *Ldha* induction and age-matched control differed by sex (sex effect: $F(1, 25) = 5.497$, $p = 0.0273$). 24 h memory was retained equally in induction and control mice. n = 5–9.

(H) Problem solving ability in young (7.5 months) neuronal *Ldha* KO and age-matched control mice differed by sex (sex effect: $F(1, 41) = 11.30$, $p = 0.0017$). Problem solving ability in KO compared with control mice was better across trials 2, 5, and 8 for males (genotype effect: $F(1, 65) = 7.654$, $p = 0.0074$) and for females (genotype effect: $F(1, 19) = 4.036$, $p = 0.059$; trial × genotype effect: $F(2, 38) = 4.252$, $p = 0.0215$). n = 9–12.

(I) 3 min memory in young (7.5 months) neuronal *Ldha* KO compared with age-matched control mice was better (trial × genotype effect: $F(2, 86) = 4.771$, $p = 0.0108$) particularly for the intermediate difficulty trial 6 ($t(38.93) = 2.783$, $p = 0.0246$). n = 21–24.

(J) 24 h memory in young (7.5 months) neuronal *Ldha* KO and age-matched control mice differed by sex (sex effect: $F(1, 41) = 8.327$, $p = 0.0062$; trial × sex: $F(1, 40) = 4.371$, $p = 0.0429$). 24 h memory in KO compared with control mice was retained equally in males and better in females (trial × genotype effect: $F(1, 18) = 4.314$, $p = 0.0524$) particularly in the higher difficulty trial 7 ($t(37) = 2.455$, $p = 0.0375$). n = 8–12.

(K) Problem solving ability in old (14 months) neuronal *Ldha* KO and age-matched control mice differed by sex (sex effect: $F(1, 40) = 5.490$, $p = 0.0242$). Problem solving ability was retained equally in KO and control mice. n = 9–12.

(L) 3 min memory was retained equally in old (14 months) neuronal *Ldha* KO compared with age-matched control mice. n = 19–24.

(M) 24 h memory in old (14 months) neuronal *Ldha* KO and age-matched control mice differed by sex (sex effect: $F(1, 40) = 4.154$, $p = 0.0482$). 24 h memory was retained equally in KO compared with control mice. n = 9–12. For habituation trials, comparisons made by two-way ANOVA, fixed effects presented in each graph, and unpaired t test between genotypes. For problem solving, 3 min memory and 24 h memory trials, comparisons made using a mixed-effects model, fixed effects presented in each graph, with Geisser-Greenhouse correction for problem solving and 3 min memory and Šídák's multiple comparisons tests between genotype for each trial. Data presented as mean ± SEM.

differences in memory, then this could explain the sex differences detected in MWM long-term memory. Increased neuronal *Ldha* may have alleviated handling and swimming-induced stress in male MWM memory while preventing the same stressors from enhancing MWM memory in females. In support of this hypothesis, decreased anxiety-like behavior, time on dark side of the light-dark box, was observed only in male neuronal *Ldha* induction mice. Neuronal *Ldha* KO may have exacerbated stress-related lowering of male MWM memory, as increased anxiety-like behavior was observed in male neuronal *Ldha* KO mice.

In contrast to sSLR memory, which has been closely tied to adult hippocampal neurogenesis, MWM long-term spatial memory involves hippocampal cellular processes without necessarily depending on adult hippocampal neurogenesis unless the task is altered to require increased pattern separation, cognitive flexibility, or difficulty.[118,119,122,124,129,189,190] Dendritic spine formation is one such cellular process that occurs in the hippocampus. Although the ANLS has been implicated in learning-induced increases in hippocampal[28] and cortical[35] dendritic spine density, these studies were conducted using males only. Moreover, CA1 region dendritic large spine density[159] is higher in females compared to males. The overlap between lactate- and estrogen-related metabolic and signaling pathways involved in learning-dependent formation and maintenance of dendritic spines may explain why in females, compared to males, lactate has an opposite effect on some memory related neuronal processes. Both lactate and estrogen can influence dendritic spine formation through modification of mitochondrial activity and biogenesis. Lactate provides fuel for mitochondrial activity, through oxidative conversion into pyruvate by LDHB,[73,191–193] and promotes mitochondrial biogenesis by increasing peroxisome proliferator activated receptor gamma coactivator α (PGC-1α) expression, through raising BDNF and cyclic adenosine monophosphate (cAMP) response element binding protein (CREB).[38,194] Estrogen can modulate mitochondrial activity by binding to intracellular estrogen receptors that, in turn, bind estrogen response elements within the promoter regions of mitochondrial genes.[195–202] Estrogen also promotes mitochondrial biogenesis through nuclear estrogen- and estrogen-related receptors that induce expression of *Bdnf*[156,157,203] and PGC-1α.[204–206] Moreover, estrogen-related receptors colocalize with estrogen receptors in the hippocampus,[207] and have been found to upregulate *Ldhb* and neuronal mitochondrial oxidative metabolism required for long-term potentiation and cognition.[208] Therefore, hippocampal dendritic spine regulation required for MWM long-term memory in young female mice may depend on estrogen-mediated neuronal mitochondrial functions that are facilitated by the ANLS. In contrast to females, hippocampal neurons in young male mice may have the metabolic flexibility to utilize neuronal generated lactate to promote dendritic spine formation and improve MWM long-term memory. Future studies are required to determine whether altered neuronal *Ldha* expression affects MWM memory in young mice differently between sexes due to overlapping roles of estrogen and the ANLS in modulating synaptic plasticity via mitochondria or opposing effects of stress on the hippocampus in males and females.

Metabolic alterations arising from altered neuronal *Ldha* expression

GC-MS analysis of hippocampal tissue extracts revealed several metabolites that varied between experimental conditions and sex. Ascorbic acid was elevated in old male neuronal *Ldha* induction mice and young female *Ldha* induction mice relative to age-matched control mice. Intracellular ascorbic acid inhibits glucose consumption and stimulates lactate uptake in neurons.[209] In addition, glutamate (glutamic acid)

Table 1. Summary of cognitive test results for neuronal *Ldha* induction and knockout mice

		Induction		Knockout	
Test type	Measurement	Young	Old	Young	Old
SOR	24 h recognition memory	–	–	–	–
SLR	4/6 h spatial memory – easier – dSLR	–	–	–	–
	4/6 h spatial memory – harder – sSLR	-♂,↑♀	–	–	-♂,↑♀
MWM	Spatial learning	–	↓♂,-♀	–	-♂,↑♀
	24 h spatial memory – percent target	-♂,↓♀	–	–	–
	24 h spatial memory – mean platform distance	↑♂,-♀	–	–	–
	7 days spatial memory – percent target	–	–	↓♂,-♀	–
	7 days spatial memory – mean platform distance	-♂,↓♀	–	↓♂,-♀	–
Puzzle box	Problem solving	–	↓	↑♂,↓♀	–
	3 min memory	–	↓	↑	–
	24 h memory	-♂,↓♀	–	-♂,↑♀	–

stimulates ascorbic acid release from astrocytes, which is subsequently transported into neurons. Both glutamic and aspartic acid decreased with age in control male mice, and to a lesser extent female control mice. However, the decline in glutamic and aspartic acid with age was less pronounced in male *Ldha* KO mice. Aspartic and glutamic acid are also important metabolites in the brain that are involved in the malate-aspartate shuttle (MAS) connecting glycolysis to the TCA cycle.[210] Due to the impermeability of the inner mitochondrial membrane to NAD+ and NADH, NADH generated during glycolysis depends on the indirect transfer of reducing equivalents into the mitochondria via the MAS. Lactate transported into the mitochondrial inner membrane space may be converted to pyruvate by mitochondrial localized LDHA with the concurrent reduction of NAD+ to NADH. The regeneration of NAD+ within the inner membrane space to maintain LDHA activity is achieved by the coordinated action of the MAS and the glutamate/aspartate carrier.[211] Thus, it is possible that perturbations to neuronal lactate metabolism promote compensatory changes in other metabolites to maintain mitochondrial activity required for synaptic processes. In keeping with the sex differences observed in other measures, the top candidates identified by GC-MS often seem to differ greatly by sex. Further studies are required to determine how these metabolites connect with lactate metabolism and contribute to age-related cognitive decline in both sexes. Overall, our results suggest that sex is an important mitigating factor in neuronal lactate metabolism involved in spatial memory.

Various types of cognition differ in their dependence on neuronal lactate metabolism

In this study, SOR long-term memory was assessed using a Y-maze apparatus, instead of an open field, to restrict mice from using spatial cues for object discrimination, thereby lowering the spatial complexity of the task, reducing requirement for hippocampal spatial processing, and increasing the specificity for need of protein synthesis dependent activity in the perirhinal cortex.[94,96,212–215] Altered expression of neuronal *Ldha* had no impact on SOR memory regardless of age and sex. These results suggest a limited role for neuronal lactate metabolism in the perirhinal cortex. Moreover, to the extent that hippocampal function still plays a role in SOR memory when tested in a Y-maze, the results presented here are in line with a recent study that showed hippocampal injection of oxamate, a potent LDH inhibitor, had no effect on novel object recognition memory tested in an open field.[31] In contrast to SOR tested in a Y-maze, the puzzle box cognitive task necessitates mice navigate through a larger arena with more surrounding visual input toward a barrier that requires various levels of physical exertion to overcome. The complexity of this task makes the puzzle box a crude measure of mouse executive function. Puzzle box 3 min memory and problem solving are not analogous to behavioral outcomes in the other cognitive tasks. However, the female-specific long-term memory deficit of young neuronal *Ldha* induction mice in the puzzle box mirrors the findings in the MWM. The results from the puzzle box suggest neuronal lactate metabolism may be involved in executive function, but deeper examination using tasks designed specifically for testing cognitive flexibility and more strictly evaluate problem solving ability are required to make more robust conclusions about the ANLS involvement in this type of cognition.

The results presented in this study demonstrate that genetic alteration of neuronal *Ldha* expression in mice promotes cognitive changes that differed by age and sex. Using a variant of spatial memory testing requiring high pattern separation, female-specific cognitive enhancements were identified in young mice with raised neuronal *Ldha* expression and in old mice with ablated neuronal *Ldha* expression. Across multiple measures of cognition at old age, induced neuronal *Ldha* expression caused deficits whereas neuronal *Ldha* KO caused improvements. These findings provide evidence supporting a potential age- and sex-related shift in the ability of neurons to utilize lactate for the purpose of supporting cognition. This study bolsters past findings showing the importance of lactate metabolism for enabling cognitive processes and highlights the need for future investigation to include females and older animals.

Limitations of the study

The genetic manipulations made in this study (Figure 9) were restricted to CaMKIIα expressing neurons, which represent a broad category of neurons throughout the brain. There may be non-CaMKIIα expressing neurons that were unaffected by the conditional induction and KO of

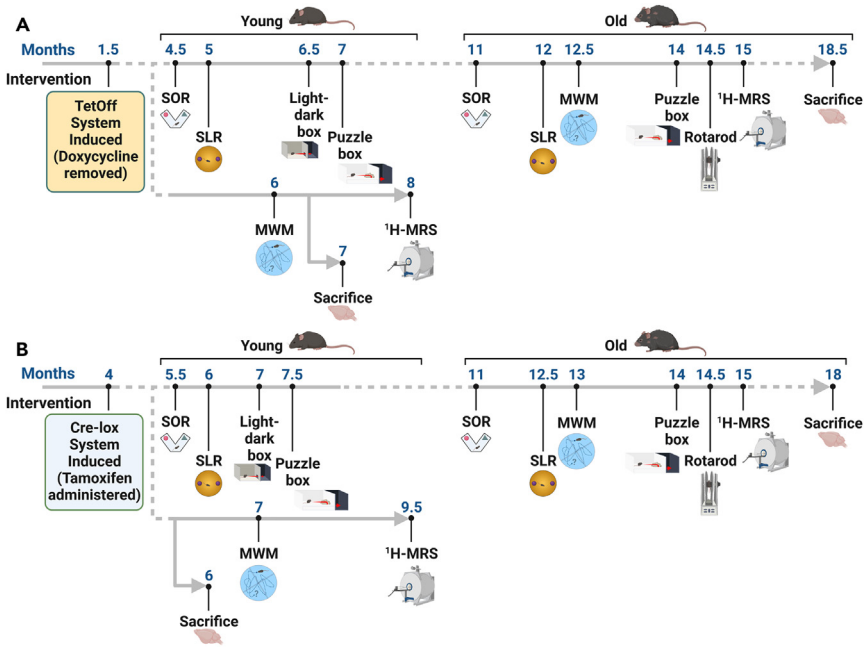

Figure 9. Neuronal *Ldha* induction and KO mouse experimental timelines

Experimental timeline for neuronal *Ldha* induction mice (A) and KO mice (B). Branches in each timeline indicate utilization of separate cohorts with different trajectories.

Ldha yet rely on cognition-relevant lactate metabolism. Moreover, genetic manipulations were not restricted to any single brain region and occurred chronically after *Ldha* induction or ablation was induced. Acute manipulation of neuronal lactate metabolism in different brain regions using viral vectors may allow for less compensation and yield different behavioral outcomes. Lastly, there are several forms of post-translational modifications, including phosphorylation,[216–219] acetylation,[220–222] succinylation,[223] methylation,[224,225] and lactylation[226,227] that can affect the activity of LDHA but were not assessed in this study. Moreover, other factors that can also affect LDHA activity include: post-transcriptional regulation of messenger ribonucleic acid (mRNA) stability[228–230]; direct binding to long non-coding RNA (lncRNA)[231,232]; and protein-metabolite interaction with various keto acids related to pyruvate and lactate, nucleotides and dinucleotides, adenosine nucleotide derivatives, and coenzyme A (CoA) derivatives.[233]

STAR★METHODS

Detailed methods are provided in the online version of this paper and include the following:

- KEY RESOURCES TABLE
- RESOURCE AVAILABILITY
  - Lead contact
  - Materials availability
  - Data and code availability
- EXPERIMENTAL MODEL AND STUDY PARTICIPANT DETAILS
  - Mice
- METHOD DETAILS
  - Western blotting
  - Immunofluorescence microscopy
  - ^{1}H magnetic resonance spectroscopy
  - Gas chromatography-mass spectrometry
  - Rotarod
  - Light-dark box
  - Spontaneously elicited object-based cognitive behaviours
  - Morris Water Maze
  - Puzzle box
- QUANTIFICATION AND STATISTICAL ANALYSIS

SUPPLEMENTAL INFORMATION

Supplemental information can be found online at https://doi.org/10.1016/j.isci.2024.110342.

ACKNOWLEDGMENTS

We thank Auntic Ahamad, Subhan Shaikh, Jenan Altoum, and Ikjot Mann for assisting in manual scoring of mouse behavioral videos for SOR and SLR; Dr. Richard Harris for help designing and generating the TRE-LDHA mice; and the Biotron integrated microscopy facility at Western university for equipment/software use and support. This work was supported by the Natural Sciences and Engineering Research Council of Canada (NSERC) (RGPIN-2019-355803, R.C.C.; RGPIN-2020-05290, R.B.; RGPIN-2023-03407, M.A.B.; and PGSD 547949–2020, A.K.F.), the government of Ontario graduate scholarships (OGS) (M.C. and A.K.F.), and the Canadian Consortium on Neurodegeneration in Aging (CCNA) (137794, R.C.C. and R.B; 163902, R.C.C and R.B.).

AUTHOR CONTRIBUTIONS

Conceptualization, A.K.F., and R.C.C.; methodology, A.K.F., J.L.S., M.C., M.A.B., R.B., and R.C.C.; formal analysis, A.K.F. and J.L.S.; investigation, A.K.F., J.L.S., M.C., R.A.M., and S.G.-N.; resources, M.A.B., R.B., and R.C.C.; data curation, A.K.F. and J.L.S.; writing – original draft, A.K.F. and R.C.C.; writing – review & editing, A.K.F, J.L.S., M.C., S.G.-N., M.A.B., R.B., and R.C.C.; visualization, A.K.F.; supervision, M.A.B., R.B., and R.C.C.; project administration, A.K.F. and R.C.C.; funding acquisition, M.A.B., R.B., and R.C.C.

DECLARATION OF INTERESTS

The authors declare no competing interests.

Received: November 24, 2023
Revised: May 15, 2024
Accepted: June 19, 2024
Published: June 21, 2024

REFERENCES

1. Mink, J.W., Blumenschine, R.J., and Adams, D.B. (1981). Ratio of central nervous system to body metabolism in vertebrates: Its constancy and functional basis. Am. J. Physiol. Regul. Integr. Comp. Physiol. *241*, 203–212. https://doi.org/10.1152/ajpregu.1981.241.3.r203.
2. Attwell, D., and Laughlin, S.B. (2001). An Energy Budget for Signaling in the Grey Matter of the Brain. J. Cereb. Blood Flow Metab. *21*, 1133–1145. https://doi.org/10.1097/00004647-200110000-00001.
3. Aiello, L.C., and Wheeler, P. (1995). The Expensive-Tissue Hypothesis: The Brain and the Digestive System in Human and Primate Evolution. Curr. Anthropol. *36*, 199–221. https://doi.org/10.1086/204350.
4. Rolfe, D.F., and Brown, G.C. (1997). Cellular energy utilization and molecular origin of standard metabolic rate in mammals. Physiol. Rev. *77*, 731–758. https://doi.org/10.1152/physrev.1997.77.3.731.
5. Clarke, D.D., and Sokoloff, L. (1999). Circulation and energy metabolism in the brain. In Basic Neurochemistry: Molecular, Cellular and Medical Aspects, pp. 637–669.
6. Himwich, H.E., and Nahum, L.H. (1932). The Respiratory Quotient of the Brain. Am. J. Physiol. Content *101*, 446–453. https://doi.org/10.1152/ajplegacy.1932.101.3.446.
7. Gibbs, E.L., Lennox, W.G., Nims, L.F., and Gibbs, F.A. (1942). Arterial and Cerebral Venous Blood. J. Biol. Chem. *144*, 325–332. https://doi.org/10.1016/S0021-9258(18)72512-X.
8. Kerr, S.E., and Ghantus, M. (1936). The Carbohydrate Metabolism of Brain. J. Biol. Chem. *116*, 9–20. https://doi.org/10.1016/S0021-9258(18)74656-5.
9. Bonvento, G., and Bolaños, J.P. (2021). Astrocyte-neuron metabolic cooperation shapes brain activity. Cell Metab. *33*, 1546–1564. https://doi.org/10.1016/j.cmet.2021.07.006.
10. Almeida, A., Delgado-Esteban, M., Bolaños, J.P., and Medina, J.M. (2002). Oxygen and glucose deprivation induces mitochondrial dysfunction and oxidative stress in neurones but not in astrocytes in primary culture. J. Neurochem. *81*, 207–217. https://doi.org/10.1046/j.1471-4159.2002.00827.x.
11. Walz, W., and Mukerji, S. (1988). Lactate release from cultured astrocytes and neurons: A comparison. Glia *1*, 366–370. https://doi.org/10.1002/glia.440010603.
12. Bolaños, J.P., Heales, S.J.R., Land, J.M., and Clark, J.B. (2002). Effect of Peroxynitrite on the Mitochondrial Respiratory Chain: Differential Susceptibility of Neurones and Astrocytes in Primary Culture. J. Neurochem. *64*, 1965–1972. https://doi.org/10.1046/j.1471-4159.1995.64051965.x.
13. Dringen, R., Gebhardt, R., and Hamprecht, B. (1993). Glycogen in astrocytes: possible function as lactate supply for neighboring cells. Brain Res. *623*, 208–214. https://doi.org/10.1016/0006-8993(93)91429-V.
14. Bolaños, J.P., Almeida, A., and Moncada, S. (2010). Glycolysis: a bioenergetic or a survival pathway? Trends Biochem. Sci. *35*, 145–149. https://doi.org/10.1016/j.tibs.2009.10.006.
15. Pellerin, L., and Magistretti, P.J. (2012). Sweet sixteen for ANLS. J. Cereb. Blood Flow Metab. *32*, 1152–1166. https://doi.org/10.1038/jcbfm.2011.149.
16. Pellerin, L., and Magistretti, P.J. (1994). Glutamate uptake into astrocytes stimulates aerobic glycolysis: a mechanism coupling neuronal activity to glucose utilization. Proc. Natl. Acad. Sci. USA *91*, 10625–10629.
17. Tan, X., Liu, X., Liu, E., Liu, M., Mu, S., Hang, Z., Han, W., Wang, T., Zhang, Y., Zhang, J., et al. (2022). Astrocyte-derived lactate/NADH alters methamphetamine-induced memory consolidation and retrieval by regulating neuronal synaptic plasticity in the dorsal hippocampus. Brain Struct. Funct. *227*, 2681–2699. https://doi.org/10.1007/s00429-022-02563-1.
18. Kong, L., Zhao, Y., Zhou, W.J., Yu, H., Teng, S.W., Guo, Q., Chen, Z., and Wang, Y. (2017). Direct neuronal glucose uptake is required for contextual fear acquisition in the dorsal hippocampus. Front. Mol. Neurosci. *10*, 388. https://doi.org/10.3389/fnmol.2017.00388.
19. Gibbs, M.E., Anderson, D.G., and Hertz, L. (2006). Inhibition of glycogenolysis in astrocytes interrupts memory consolidation in young chickens. Glia *54*, 214–222. https://doi.org/10.1002/glia.20377.
20. Gibbs, M.E., and Hertz, L. (2008). Inhibition of astrocytic energy metabolism by d-lactate exposure impairs memory. Neurochem. Int. *52*, 1012–1018. https://doi.org/10.1016/j.neuint.2007.10.014.
21. Suzuki, A., Stern, S.A., Bozdagi, O., Huntley, G.W., Walker, R.H., Magistretti, P.J., and Alberini, C.M. (2011). Astrocyte-Neuron Lactate Transport Is Required for Long-Term Memory Formation. Cell *144*, 810–823. https://doi.org/10.1016/j.cell.2011.02.018.
22. Newman, L.A., Korol, D.L., and Gold, P.E. (2011). Lactate Produced by Glycogenolysis in Astrocytes Regulates Memory Processing. PLoS One *6*, e28427. https://doi.org/10.1371/journal.pone.0028427.
23. Park, J.S., Saeed, K., Jo, M.H., Kim, M.W., Lee, H.J., Park, C.-B., Lee, G., and Kim, M.O.

(2022). LDHB Deficiency Promotes Mitochondrial Dysfunction Mediated Oxidative Stress and Neurodegeneration in Adult Mouse Brain. Antioxidants *11*, 261. https://doi.org/10.3390/antiox11020261.

24. Boury-Jamot, B., Carrard, A., Martin, J.L., Halfon, O., Magistretti, P.J., and Boutrel, B. (2016). Disrupting astrocyte-neuron lactate transfer persistently reduces conditioned responses to cocaine. Mol. Psychiatry *21*, 1070–1076. https://doi.org/10.1038/mp.2015.157.
25. Zhang, Y., Xue, Y., Meng, S., Luo, Y., Liang, J., Li, J., Ai, S., Sun, C., Shen, H., Zhu, W., et al. (2016). Inhibition of Lactate Transport Erases Drug Memory and Prevents Drug Relapse. Biol. Psychiatry *79*, 928–939. https://doi.org/10.1016/j.biopsych.2015.07.007.
26. Chen, S.M., Li, M., Xie, J., Li, S., Xiang, S.S., Liu, H.Y., Chen, Z., Zhang, P., Kuang, X., and Tang, X.Q. (2020). Hydrogen sulfide attenuates postoperative cognitive dysfunction through promoting the pathway of Warburg effect-synaptic plasticity in hippocampus. Toxicol. Appl. Pharmacol. *409*, 115286. https://doi.org/10.1016/j.taap.2020.115286.
27. Tadi, M., Allaman, I., Lengacher, S., Grenningloh, G., and Magistretti, P.J. (2015). Learning-Induced Gene Expression in the Hippocampus Reveals a Role of Neuron -Astrocyte Metabolic Coupling in Long Term Memory. PLoS One *10*, e0141568. https://doi.org/10.1371/journal.pone.0141568.
28. Vezzoli, E., Calì, C., De Roo, M., Ponzoni, L., Sogne, E., Gagnon, N., Francolini, M., Braida, D., Sala, M., Muller, D., et al. (2020). Ultrastructural Evidence for a Role of Astrocytes and Glycogen-Derived Lactate in Learning-Dependent Synaptic Stabilization. Cereb. Cortex *30*, 2114–2127. https://doi.org/10.1093/cercor/bhz226.
29. Descalzi, G., Gao, V., Steinman, M.Q., Suzuki, A., and Alberini, C.M. (2019). Lactate from astrocytes fuels learning-induced mRNA translation in excitatory and inhibitory neurons. Commun. Biol. *2*, 247. https://doi.org/10.1038/s42003-019-0495-2.
30. Korol, D.L., Gardner, R.S., Tunur, T., and Gold, P.E. (2019). Involvement of lactate transport in two object recognition tasks that require either the hippocampus or striatum. Behav. Neurosci. *133*, 176–187. https://doi.org/10.1037/bne0000304.
31. Dembitskaya, Y., Piette, C., Perez, S., Berry, H., Magistretti, P.J., and Venance, L. (2022). Lactate supply overtakes glucose when neural computational and cognitive loads scale up. Proc. Natl. Acad. Sci. USA *119*, e2212004119. https://doi.org/10.1073/pnas.2212004119.
32. Zhou, Z., Okamoto, K., Onodera, J., Hiragi, T., Andoh, M., Ikawa, M., Tanaka, K.F., Ikegaya, Y., and Koyama, R. (2021). Astrocytic cAMP modulates memory via synaptic plasticity. Proc. Natl. Acad. Sci. USA *118*, e2016584118. https://doi.org/10.1073/pnas.2016584118.
33. Kambe, Y., Yamauchi, Y., Thanh Nguyen, T., Thi Nguyen, T., Ago, Y., Shintani, N., Hashimoto, H., Yoshitake, S., Yoshitake, T., Kehr, J., et al. (2021). The pivotal role of pituitary adenylate cyclase-activating polypeptide for lactate production and secretion in astrocytes during fear memory. Pharmacol. Rep. *73*, 1109–1121. https://doi.org/10.1007/s43440-021-00222-6.
34. Gao, V., Suzuki, A., Magistretti, P.J., Lengacher, S., Pollonini, G., Steinman, M.Q., and Alberini, C.M. (2016). Astrocytic β 2 -adrenergic receptors mediate hippocampal long-term memory consolidation. Proc. Natl. Acad. Sci. USA *113*, 8526–8531. https://doi.org/10.1073/pnas.1605063113.
35. Lundquist, A.J., Llewellyn, G.N., Kishi, S.H., Jakowec, N.A., Cannon, P.M., Petzinger, G.M., and Jakowec, M.W. (2022). Knockdown of Astrocytic Monocarboxylate Transporter 4 in the Motor Cortex Leads to Loss of Dendritic Spines and a Deficit in Motor Learning. Mol. Neurobiol. *59*, 1002–1017. https://doi.org/10.1007/s12035-021-02651-z.
36. Frame, A.K., Robinson, J.W., Mahmoudzadeh, N.H., Tennessen, J.M., Simon, A.F., and Cumming, R.C. (2023). Aging and memory are altered by genetically manipulating lactate dehydrogenase in the neurons or glia of flies. Aging (Albany NY) *15*, 947–981. https://doi.org/10.18632/aging.204565.
37. Chen, W., Sun, X., Zhan, L., Zhou, W., and Bi, T. (2021). Conditional Knockout of *Pdha1* in Mouse Hippocampus Impairs Cognitive Function: The Possible Involvement of Lactate. Front. Neurosci. *15*, 767560. https://doi.org/10.3389/fnins.2021.767560.
38. El Hayek, L., Khalifeh, M., Zibara, V., Abi Assaad, R., Emmanuel, N., Karnib, N., El-Ghandour, R., Nasrallah, P., Bilen, M., Ibrahim, P., et al. (2019). Lactate mediates the effects of exercise on learning and memory through SIRT1-dependent activation of hippocampal brain-derived neurotrophic factor (BDNF). J. Neurosci. *39*, 1661–1718. https://doi.org/10.1523/JNEUROSCI.1661-18.2019.
39. Iqbal, Z., Liu, S., Lei, Z., Ramkrishnan, A.S., Akter, M., and Li, Y. (2022). Astrocyte L-Lactate Signaling in the ACC Regulates Visceral Pain Aversive Memory in Rats. Cells *12*, 26. https://doi.org/10.3390/cells12010026.
40. Ikeda, H., Yamamoto, S., and Kamei, J. (2021). Increase in brain l-lactate enhances fear memory in diabetic mice: Involvement of glutamate neurons. Brain Res. *1767*, 147560. https://doi.org/10.1016/j.brainres.2021.147560.
41. Gibbs, M.E., O'Dowd, B.S., Hertz, E., and Hertz, L. (2006). Astrocytic energy metabolism consolidates memory in young chicks. Neuroscience *141*, 9–13. https://doi.org/10.1016/j.neuroscience.2006.04.038.
42. Song, Y., Liu, Z., Zhu, X., Hao, C., Hao, W., Wu, S., Yang, J., Lu, X., and Jin, C. (2022). Metformin alleviates the cognitive impairment caused by aluminum by improving energy metabolism disorders in mice. Biochem. Pharmacol. *202*, 115140. https://doi.org/10.1016/j.bcp.2022.115140.
43. Netzahualcoyotzi, C., and Pellerin, L. (2020). Neuronal and astroglial monocarboxylate transporters play key but distinct roles in hippocampus-dependent learning and memory formation. Prog. Neurobiol. *194*, 101888. https://doi.org/10.1016/j.pneurobio.2020.101888.
44. Newman, L.A., Scavuzzo, C.J., Gold, P.E., and Korol, D.L. (2017). Training-induced elevations in extracellular lactate in hippocampus and striatum: Dissociations by cognitive strategy and type of reward. Neurobiol. Learn. Mem. *137*, 142–153. https://doi.org/10.1016/j.nlm.2016.12.001.
45. Wang, J., Tu, J., Cao, B., Mu, L., Yang, X., Cong, M., Ramkrishnan, A.S., Chan, R.H.M., Wang, L., and Li, Y. (2017). Astrocytic l -Lactate Signaling Facilitates Amygdala-Anterior Cingulate Cortex Synchrony and Decision Making in Rats. Cell Rep. *21*, 2407–2418. https://doi.org/10.1016/j.celrep.2017.11.012.
46. Scavuzzo, C.J., Newman, L.A., Gold, P.E., and Korol, D.L. (2021). Time-dependent changes in hippocampal and striatal glycogen long after maze training in male rats. Neurobiol. Learn. Mem. *185*, 107537. https://doi.org/10.1016/j.nlm.2021.107537.
47. Zhang, H., Zheng, Q., Guo, T., Zhang, S., Zheng, S., Wang, R., Deng, Q., Yang, G., Zhang, S., Tang, L., et al. (2022). Metabolic reprogramming in astrocytes results in neuronal dysfunction in intellectual disability. Mol. Psychiatry *25*, 1–14. https://doi.org/10.1038/s41380-022-01521-x.
48. Skupio, U., Tertil, M., Bilecki, W., Barut, J., Korostynski, M., Golda, S., Kudla, L., Wiktorowska, L., Sowa, J.E., Siwiec, M., et al. (2020). Astrocytes determine conditioned response to morphine via glucocorticoid receptor-dependent regulation of lactate release. Neuropsychopharmacology *45*, 404–415. https://doi.org/10.1038/s41386-019-0450-4.
49. Harris, R.A., Lone, A., Lim, H., Martinez, F., Frame, A.K., Scholl, T.J., and Cumming, R.C. (2019). Aerobic Glycolysis Is Required for Spatial Memory Acquisition But Not Memory Retrieval in Mice. eNeuro *6*, ENEURO.0389-18.2019. https://doi.org/10.1523/ENEURO.0389-18.2019.
50. Drulis-Fajdasz, D., Krzystyniak, A., Puścian, A., Pytyś, A., Gostomska-Pampuch, K., Pudełko-Malik, N., Wiśniewski, J.Ł., Młynarz, P., Miazek, A., Wójtowicz, T., et al. (2023). Glycogen phosphorylase inhibition improves cognitive function of aged mice. Aging Cell *22*, 1–18. https://doi.org/10.1111/acel.13928.
51. Vaccari Cardoso, B., Shevelkin, A.V., Terrillion, C., Mychko, O., Mosienko, V., Kasparov, S., Pletnikov, M.V., and Teschemacher, A.G. (2021). Reducing l-lactate release from hippocampal astrocytes by intracellular oxidation increases novelty induced activity in mice. Glia *69*, 1241–1250. https://doi.org/10.1002/glia.23960.
52. Cruz, E., Bessières, B., Magistretti, P., and Alberini, C.M. (2022). Differential role of neuronal glucose and PFKFB3 in memory formation during development. Glia *3*, 1–25. https://doi.org/10.1002/glia.24248.
53. Becker-Krail, D.D., Ketchesin, K.D., Burns, J.N., Zong, W., Hildebrand, M.A., DePoy, L.M., Vadnie, C.A., Tseng, G.C., Logan, R.W., Huang, Y.H., and McClung, C.A. (2022). Astrocyte Molecular Clock Function in the Nucleus Accumbens Is Important for Reward-Related Behavior. Biol. Psychiatry *92*, 68–80. https://doi.org/10.1016/j.biopsych.2022.02.007.
54. Gerhardt-Hansen, W. (1968). Lactate Dehydrogenase Isoenzymes in the Central Nervous System: Theoretical Aspects and Practical Application in Diagnosis of Brain Tumors (Costers Bogtrykkeri, Virumgardsvej 12).
55. Kaplan, N.O., Ciotti, M.M., and Stolzenbach, F.E. (1956). Reaction of Pyridine Nucleotide Analogues With Dehydrogenases. J. Biol. Chem. *221*,

833–844. https://doi.org/10.1016/S0021-9258(18)65197-X.
56. Quistorff, B., and Grunnet, N. (2011). The isoenzyme pattern of LDH does not play a physiological role; except perhaps during fast transitions in energy metabolism. Aging (Albany NY) *3*, 457–460. https://doi.org/10.18632/aging.100329.
57. Latner, A.L., Siddiqui, S.A., and Skillen, A.W. (1966). Pyruvate Inhibition of Lactate Dehydrogenase Activity in Human Tissue Extracts. Science *154*, 527–529. https://doi.org/10.1126/science.154.3748.527.
58. Markert, C.L., and Ursprung, H. (1962). The ontogeny of isozyme patterns of lactate dehydrogenase in the mouse. Dev. Biol. *5*, 363–381. https://doi.org/10.1016/0012-1606(62)90019-2.
59. Vesell, E.S. (1965). Lactate Dehydrogenase Isozymes: Substrate Inhibition in Various Human Tissues. Science *150*, 1590–1593. https://doi.org/10.1126/science.150.3703.1590.
60. Pesce, A., Fondy, T.P., Stolzenbach, F., Castillo, F., and Kaplan, N.O. (1967). The comparative enzymology of lactic dehydrogenases. 3. Properties of the H4 and M4 enzymes from a number of vertebrates. J. Biol. Chem. *242*, 2151–2167. https://doi.org/10.1016/S0021-9258(18)96030-8.
61. Kaplan, N.O., Everse, J., and Admiraal, J. (1968). Significance of Substrate Inhibition of Dehydrogenases. Ann. N. Y. Acad. Sci. *151*, 400–412. https://doi.org/10.1111/j.1749-6632.1968.tb11903.x.
62. Bishop, M.J., Everse, J., and Kaplan, N.O. (1972). Identification of Lactate Dehydrogenase Isoenzymes by Rapid Kinetics. Proc. Natl. Acad. Sci. USA *69*, 1761–1765. https://doi.org/10.1073/pnas.69.7.1761.
63. Kaplan, N.O., and Everse, J. (1972). Regulatory characteristics of lactate dehydrogenases. Adv. Enzyme Regul. *10*, 323–336. https://doi.org/10.1016/0065-2571(72)90021-0.
64. Dawson, D.M., Goodfriend, T.L., and Kaplan, N.O. (1964). Lactic Dehydrogenases : Functions of the Two Types. Science *143*, 929–933. https://doi.org/10.1126/science.143.3609.929.
65. Cahn, R.D., Zwilling, E., Kaplan, N.O., and Levine, L. (1962). Nature and Development of Lactic Dehydrogenases: The two major types of this enzyme form molecular hybrids which change in makeup during development. Science *136*, 962–969. https://doi.org/10.1126/science.136.3520.962.
66. Laughton, J.D., Bittar, P., Charnay, Y., Pellerin, L., Kovari, E., Magistretti, P.J., and Bouras, C. (2007). Metabolic compartmentalization in the human cortex and hippocampus: evidence for a cell- and region-specific localization of lactate dehydrogenase 5 and pyruvate dehydrogenase. BMC Neurosci. *8*, 35. https://doi.org/10.1186/1471-2202-8-35.
67. Bittar, P.G., Charnay, Y., Pellerin, L., Bouras, C., and Magistretti, P.J. (1996). Selective distribution of lactate dehydrogenase isoenzymes in neurons and astrocytes of human brain. J. Cereb. Blood Flow Metab. *16*, 1079–1089. https://doi.org/10.1097/00004647-199611000-00001.
68. Laughton, J.D., Charnay, Y., Belloir, B., Pellerin, L., Magistretti, P.J., and Bouras, C. (2000). Differential messenger RNA distribution of lactate dehydrogenase LDH-1 and LDH-5 isoforms in the rat brain. Neuroscience *96*, 619–625. https://doi.org/10.1016/S0306-4522(99)00580-1.
69. Harris, R.A., Tindale, L., Lone, A., Singh, O., Macauley, S.L., Stanley, M., Holtzman, D.M., Bartha, R., and Cumming, R.C. (2016). Aerobic Glycolysis in the Frontal Cortex Correlates with Memory Performance in Wild-Type Mice But Not the APP/PS1 Mouse Model of Cerebral Amyloidosis. J. Neurosci. *36*, 1871–1878. https://doi.org/10.1523/JNEUROSCI.3131-15.2016.
70. Zhang, Y., Chen, K., Sloan, S.A., Bennett, M.L., Scholze, A.R., O'Keeffe, S., Phatnani, H.P., Guarnieri, P., Caneda, C., Ruderisch, N., et al. (2014). An RNA-Sequencing Transcriptome and Splicing Database of Glia, Neurons, and Vascular Cells of the Cerebral Cortex. J. Neurosci. *34*, 11929–11947. https://doi.org/10.1523/JNEUROSCI.1860-14.2014.
71. O'Brien, J., Kla, K.M., Hopkins, I.B., Malecki, E.A., and McKenna, M.C. (2007). Kinetic Parameters and Lactate Dehydrogenase Isozyme Activities Support Possible Lactate Utilization by Neurons. Neurochem. Res. *32*, 597–607. https://doi.org/10.1007/s11064-006-9132-9.
72. Yao, S., Xu, M.-D., Wang, Y., Zhao, S.-T., Wang, J., Chen, G.-F., Chen, W.-B., Liu, J., Huang, G.-B., Sun, W.-J., et al. (2023). Astrocytic lactate dehydrogenase A regulates neuronal excitability and depressive-like behaviors through lactate homeostasis in mice. Nat. Commun. *14*, 729. https://doi.org/10.1038/s41467-023-36209-5.
73. Karagiannis, A., Gallopin, T., Lacroix, A., Plaisier, F., Piquet, J., Geoffroy, H., Hepp, R., Naudé, J., Le Gac, B., Egger, R., et al. (2021). Lactate is an energy substrate for rodent cortical neurons and enhances their firing activity. Elife *10*, e71424. https://doi.org/10.7554/eLife.71424.
74. Ximerakis, M., Lipnick, S.L., Innes, B.T., Simmons, S.K., Adiconis, X., Dionne, D., Mayweather, B.A., Nguyen, L., Niziolek, Z., Ozek, C., et al. (2019). Single-cell transcriptomic profiling of the aging mouse brain. Nat. Neurosci. *22*, 1696–1708. https://doi.org/10.1038/s41593-019-0491-3.
75. Zhang, Y., Sloan, S.A., Clarke, L.E., Caneda, C., Plaza, C.A., Blumenthal, P.D., Vogel, H., Steinberg, G.K., Edwards, M.S.B., Li, G., et al. (2016). Purification and Characterization of Progenitor and Mature Human Astrocytes Reveals Transcriptional and Functional Differences with Mouse. Neuron *89*, 37–53. https://doi.org/10.1016/j.neuron.2015.11.013.
76. Lundgaard, I., Li, B., Xie, L., Kang, H., Sanggaard, S., Haswell, J.D.R., Sun, W., Goldman, S., Blekot, S., Nielsen, M., et al. (2015). Direct neuronal glucose uptake heralds activity-dependent increases in cerebral metabolism. Nat. Commun. *6*, 6807. https://doi.org/10.1038/ncomms7807.
77. Li, H., Guglielmetti, C., Sei, Y.J., Zilberter, M., Le Page, L.M., Shields, L., Yang, J., Nguyen, K., Tiret, B., Gao, X., et al. (2023). Neurons require glucose uptake and glycolysis *in vivo*. Cell Rep. *42*, 112335. https://doi.org/10.1016/j.celrep.2023.112335.
78. Díaz-García, C.M., Mongeon, R., Lahmann, C., Koveal, D., Zucker, H., and Yellen, G. (2017). Neuronal Stimulation Triggers Neuronal Glycolysis and Not Lactate Uptake. Cell Metab. *26*, 361–374.e4. https://doi.org/10.1016/j.cmet.2017.06.021.
79. Ivanov, A.I., Malkov, A.E., Waseem, T., Mukhtarov, M., Buldakova, S., Gubkina, O., Zilberter, M., and Zilberter, Y. (2014). Glycolysis and Oxidative Phosphorylation in Neurons and Astrocytes during Network Activity in Hippocampal Slices. J. Cereb. Blood Flow Metab. *34*, 397–407. https://doi.org/10.1038/jcbfm.2013.222.
80. Bak, L.K., Schousboe, A., Sonnewald, U., and Waagepetersen, H.S. (2006). Glucose is Necessary to Maintain Neurotransmitter Homeostasis during Synaptic Activity in Cultured Glutamatergic Neurons. J. Cereb. Blood Flow Metab. *26*, 1285–1297. https://doi.org/10.1038/sj.jcbfm.9600281.
81. Segarra-Mondejar, M., Casellas-Díaz, S., Ramiro-Pareta, M., Müller-Sánchez, C., Martorell-Riera, A., Hermelo, I., Reina, M., Aragonés, J., Martínez-Estrada, O.M., and Soriano, F.X. (2018). Synaptic activity-induced glycolysis facilitates membrane lipid provision and neurite outgrowth. EMBO J. *37*, 1–16. https://doi.org/10.15252/embj.201797368.
82. Schönig, K., and Bujard, H. (2013). Generating Conditional Mouse Mutants via Tetracycline-Controlled Gene Expression. In Transgenic Mouse Methods and Protocols (Humana Press), pp. 69–104. https://doi.org/10.1385/1-59259-340-2:69.
83. Gossen, M., and Bujard, H. (1992). Tight control of gene expression in mammalian cells by tetracycline-responsive promoters. Proc. Natl. Acad. Sci. USA *89*, 5547–5551. https://doi.org/10.1073/pnas.89.12.5547.
84. Wang, X., Zhang, C., Szábo, G., and Sun, Q.-Q. (2013). Distribution of CaMKIIα expression in the brain *in vivo*, studied by CaMKIIα-GFP mice. Brain Res. *1518*, 9–25. https://doi.org/10.1016/j.brainres.2013.04.042.
85. Blake, J.A., Baldarelli, R., Kadin, J.A., Richardson, J.E., Smith, C.L., and Bult, C.J.; Mouse Genome Database Group (2021). Mouse Genome Database (MGD): Knowledgebase for mouse-human comparative biology. Nucleic Acids Res. *49*, D981–D987. https://doi.org/10.1093/nar/gkaa1083.
86. Feil, R., Wagner, J., Metzger, D., and Chambon, P. (1997). Regulation of Cre Recombinase Activity by Mutated Estrogen Receptor Ligand-Binding Domains. Biochem. Biophys. Res. Commun. *237*, 752–757. https://doi.org/10.1006/bbrc.1997.7124.
87. Feil, R., Brocard, J., Mascrez, B., LeMeur, M., Metzger, D., and Chambon, P. (1996). Ligand-activated site-specific recombination in mice. Proc. Natl. Acad. Sci. USA *93*, 10887–10890. https://doi.org/10.1073/pnas.93.20.10887.
88. Kazlauckas, V., Schuh, J., Dall'Igna, O.P., Pereira, G.S., Bonan, C.D., and Lara, D.R. (2005). Behavioral and cognitive profile of mice with high and low exploratory phenotypes. Behav. Brain Res. *162*, 272–278. https://doi.org/10.1016/j.bbr.2005.03.021.
89. Trevarthen, A.C., Kappel, S., Roberts, C., Finnegan, E.M., Paul, E.S., Planas-Sitjà, I., Mendl, M.T., and Fureix, C. (2019). Measuring affect-related cognitive bias: Do mice in opposite affective states react differently to negative and positive stimuli? PLoS One *14*, e0226438. https://doi.org/10.1371/journal.pone.0226438.

90. Simon, P., Dupuis, R., and Costentin, J. (1994). Thigmotaxis as an index of anxiety in mice. Influence of dopaminergic transmissions. Behav. Brain Res. *61*, 59–64. https://doi.org/10.1016/0166-4328(94)90008-6.
91. Valle, F.P. (1971). Rats' performance on repeated tests in the open field as a function of age. Psychon. Sci. *23*, 333–334. https://doi.org/10.3758/BF03336137.
92. Belzung, C., and Berton, F. (1997). Further pharmacological validation of the BALB/c neophobia in the free exploratory paradigm as an animal model of trait anxiety. Behav. Pharmacol. *8*, 541–548. https://doi.org/10.1097/00008877-199711000-00012.
93. Clément, Y., Joubert, C., Kopp, C., Lepicard, E.M., Venault, P., Misslin, R., Cadot, M., and Chapouthier, G. (2007). Anxiety in Mice: A Principal Component Analysis Study. Neural Plast. *2007*, 1–8. https://doi.org/10.1155/2007/35457.
94. Winters, B.D., Saksida, L.M., and Bussey, T.J. (2008). Object recognition memory: Neurobiological mechanisms of encoding, consolidation and retrieval. Neurosci. Biobehav. Rev. *32*, 1055–1070. https://doi.org/10.1016/j.neubiorev.2008.04.004.
95. Murray, E.A., and Bussey, T.J. (1999). Perceptual-mnemonic functions of the perirhinal cortex. Trends Cogn. Sci. *3*, 142–151. https://doi.org/10.1016/S1364-6613(99)01303-0.
96. Winters, B.D., Forwood, S.E., Cowell, R.A., Saksida, L.M., and Bussey, T.J. (2004). Double dissociation between the effects of peri-postrhinal cortex and hippocampal lesions on tests of object recognition and spatial memory: heterogeneity of function within the temporal lobe. J. Neurosci. *24*, 5901–5908. https://doi.org/10.1523/JNEUROSCI.1346-04.2004.
97. Reichelt, A.C., Kramar, C.P., Ghosh-Swaby, O.R., Sheppard, P.A.S., Kent, B.A., Bekinschtein, P., Saksida, L.M., and Bussey, T.J. (2021). The spontaneous location recognition task for assessing spatial pattern separation and memory across a delay in rats and mice. Nat. Protoc. *16*, 5616–5633. https://doi.org/10.1038/s41596-021-00627-w.
98. Ben Abdallah, N.M.B., Fuss, J., Trusel, M., Galsworthy, M.J., Bobsin, K., Colacicco, G., Deacon, R.M.J., Riva, M.A., Kellendonk, C., Sprengel, R., et al. (2011). The puzzle box as a simple and efficient behavioral test for exploring impairments of general cognition and executive functions in mouse models of schizophrenia. Exp. Neurol. *227*, 42–52. https://doi.org/10.1016/j.expneurol.2010.09.008.
99. Venkov, L., Rosental, L., and Manolova, M. (1976). Subcellular distribution of LDH isoenzymes in neuronal- and glial-enriched fractions. Brain Res. *109*, 323–333. https://doi.org/10.1016/0006-8993(76)90533-3.
100. Brooks, G.A., Dubouchaud, H., Brown, M., Sicurello, J.P., and Butz, C.E. (1999). Role of mitochondrial lactate dehydrogenase and lactate oxidation in the intracellular lactate shuttle. Proc. Natl. Acad. Sci. USA *96*, 1129–1134. https://doi.org/10.1073/pnas.96.3.1129.
101. Brooks, G.A. (2018). The Science and Translation of Lactate Shuttle Theory. Cell Metab. *27*, 757–785. https://doi.org/10.1016/j.cmet.2018.03.008.
102. McIlwain, H. (1953). Substances Which Support Respiration and Metabolic Response to Electrical Impulses in Human Cerebral Tissues. J. Neurol. Neurosurg. Psychiatry *16*, 257–266. https://doi.org/10.1136/jnnp.16.4.257.
103. Schurr, A., West, C.A., and Rigor, B.M. (1988). Lactate-Supported Synaptic Function in the Rat Hippocampal Slice Preparation. Science *240*, 1326–1328. https://doi.org/10.1126/science.3375817.
104. Vaccari-Cardoso, B., Antipina, M., Teschemacher, A.G., and Kasparov, S. (2022). Lactate-Mediated Signaling in the Brain—An Update. Brain Sci. *13*, 49. https://doi.org/10.3390/brainsci13010049.
105. Doyle, D.Z., and Kwan, K.Y. (2022). Neurogenic–angiogenic synchrony via lactate. Nat. Neurosci. *25*, 839–840. https://doi.org/10.1038/s41593-022-01111-8.
106. Nicola, R., and Okun, E. (2021). Adult Hippocampal Neurogenesis: One Lactate to Rule Them All. NeuroMolecular Med. *23*, 445–448. https://doi.org/10.1007/s12017-021-08658-y.
107. Wang, J., Cui, Y., Yu, Z., Wang, W., Cheng, X., Ji, W., Guo, S., Zhou, Q., Wu, N., Chen, Y., et al. (2019). Brain Endothelial Cells Maintain Lactate Homeostasis and Control Adult Hippocampal Neurogenesis. Cell Stem Cell *25*, 754–767.e9. https://doi.org/10.1016/j.stem.2019.09.009.
108. Lee, H.W., Xu, Y., Zhu, X., Jang, C., Choi, W., Bae, H., Wang, W., He, L., Jin, S.W., Arany, Z., and Simons, M. (2022). Endothelium-derived lactate is required for pericyte function and blood–brain barrier maintenance. EMBO J. *41*, e109890. https://doi.org/10.15252/embj.2021109890.
109. Yang, J., Ruchti, E., Petit, J.-M., Jourdain, P., Grenningloh, G., Allaman, I., and Magistretti, P.J. (2014). Lactate promotes plasticity gene expression by potentiating NMDA signaling in neurons. Proc. Natl. Acad. Sci. USA *111*, 12228–12233. https://doi.org/10.1073/pnas.1322912111.
110. Pötzsch, A., Zocher, S., Bernas, S.N., Leiter, O., Rünker, A.E., and Kempermann, G. (2021). L-lactate exerts a pro-proliferative effect on adult hippocampal precursor cells *in vitro*. iScience *24*, 102126. https://doi.org/10.1016/j.isci.2021.102126.
111. Bekinschtein, P., Kent, B.A., Oomen, C.A., Clemenson, G.D., Gage, F.H., Saksida, L.M., and Bussey, T.J. (2014). Brain-derived neurotrophic factor interacts with adult-born immature cells in the dentate gyrus during consolidation of overlapping memories. Hippocampus *24*, 905–911. https://doi.org/10.1002/hipo.22304.
112. Bekinschtein, P., Kent, B.A., Oomen, C.A., Clemenson, G.D., Gage, F.H., Saksida, L.M., and Bussey, T.J. (2013). BDNF in the dentate gyrus is required for consolidation of "pattern-separated" memories. Cell Rep. *5*, 759–768. https://doi.org/10.1016/j.celrep.2013.09.027.
113. Sahay, A., Scobie, K.N., Hill, A.S., O'Carroll, C.M., Kheirbek, M.A., Burghardt, N.S., Fenton, A.A., Dranovsky, A., and Hen, R. (2011). Increasing adult hippocampal neurogenesis is sufficient to improve pattern separation. Nature *472*, 466–470. https://doi.org/10.1038/nature09817.
114. Clelland, C.D., Choi, M., Romberg, C., Clemenson, G.D., Jr., Fragniere, A., Tyers, P., Jessberger, S., Saksida, L.M., Barker, R.A., Gage, F.H., and Bussey, T.J. (2009). A Functional Role for Adult Hippocampal Neurogenesis in Spatial Pattern Separation. Science *325*, 210–213. https://doi.org/10.1126/science.1173215.
115. Cès, A., Burg, T., Herbeaux, K., Héraud, C., Bott, J.-B., Mensah-Nyagan, A.G., and Mathis, C. (2018). Age-related vulnerability of pattern separation in C57BL/6J mice. Neurobiol. Aging *62*, 120–129. https://doi.org/10.1016/j.neurobiolaging.2017.10.013.
116. Bonafina, A., Trinchero, M.F., Ríos, A.S., Bekinschtein, P., Schinder, A.F., Paratcha, G., and Ledda, F. (2019). GDNF and GFRα1 Are Required for Proper Integration of Adult-Born Hippocampal Neurons. Cell Rep. *29*, 4308–4319.e4. https://doi.org/10.1016/j.celrep.2019.11.100.
117. Shors, T.J., Miesegaes, G., Beylin, A., Zhao, M., Rydel, T., and Gould, E. (2001). Neurogenesis in the adult is involved in the formation of trace memories. Nature *410*, 372–376. https://doi.org/10.1038/35066584.
118. Shors, T.J., Townsend, D.A., Zhao, M., Kozorovitskiy, Y., and Gould, E. (2002). Neurogenesis may relate to some but not all types of hippocampal-dependent learning. Hippocampus *12*, 578–584. https://doi.org/10.1002/hipo.10103.
119. Snyder, J.S., Hong, N.S., McDonald, R.J., and Wojtowicz, J.M. (2005). A role for adult neurogenesis in spatial long-term memory. Neuroscience *130*, 843–852. https://doi.org/10.1016/j.neuroscience.2004.10.009.
120. Zhang, C.-L., Zou, Y., He, W., Gage, F.H., and Evans, R.M. (2008). A role for adult TLX-positive neural stem cells in learning and behaviour. Nature *451*, 1004–1007. https://doi.org/10.1038/nature06562.
121. Hernández-Rabaza, V., Llorens-Martín, M., Velázquez-Sánchez, C., Ferragud, A., Arcusa, A., Gumus, H.G., Gómez-Pinedo, U., Pérez-Villalba, A., Roselló, J., Trejo, J.L., et al. (2009). Inhibition of adult hippocampal neurogenesis disrupts contextual learning but spares spatial working memory, long-term conditional rule retention and spatial reversal. Neuroscience *159*, 59–68. https://doi.org/10.1016/j.neuroscience.2008.11.054.
122. Garthe, A., Behr, J., and Kempermann, G. (2009). Adult-Generated Hippocampal Neurons Allow the Flexible Use of Spatially Precise Learning Strategies. PLoS One *4*, e5464. https://doi.org/10.1371/journal.pone.0005464.
123. Tronel, S., Belnoue, L., Grosjean, N., Revest, J.M., Piazza, P.V., Koehl, M., and Abrous, D.N. (2012). Adult-born neurons are necessary for extended contextual discrimination. Hippocampus *22*, 292–298. https://doi.org/10.1002/hipo.20895.
124. Burghardt, N.S., Park, E.H., Hen, R., and Fenton, A.A. (2012). Adult-born hippocampal neurons promote cognitive flexibility in mice. Hippocampus *22*, 1795–1808. https://doi.org/10.1002/hipo.22013.
125. Creer, D.J., Romberg, C., Saksida, L.M., Van Praag, H., and Bussey, T.J. (2010). Running enhances spatial pattern separation in mice. Proc. Natl. Acad. Sci. USA *107*, 2367–2372. https://doi.org/10.1073/pnas.0911725107.
126. Drew, M.R., Denny, C.A., and Hen, R. (2010). Arrest of adult hippocampal neurogenesis in mice impairs single- but not multiple-trial contextual fear conditioning. Behav. Neurosci. *124*, 446–454. https://doi.org/10.1037/a0020081.
127. Gao, A., Xia, F., Guskjolen, A.J., Ramsaran, A.I., Santoro, A., Josselyn, S.A., and Frankland, P.W. (2018). Elevation of Hippocampal Neurogenesis Induces a

Temporally Graded Pattern of Forgetting of Contextual Fear Memories. J. Neurosci. *38*, 3190–3198. https://doi.org/10.1523/JNEUROSCI.3126-17.2018.

128. Deng, W., Aimone, J.B., and Gage, F.H. (2010). New neurons and new memories: How does adult hippocampal neurogenesis affect learning and memory? Nat. Rev. Neurosci. *11*, 339–350. https://doi.org/10.1038/nrn2822.
129. Oomen, C.A., Bekinschtein, P., Kent, B.A., Saksida, L.M., and Bussey, T.J. (2014). Adult hippocampal neurogenesis and its role in cognition. Wiley Interdiscip. Rev. Cogn. Sci. *5*, 573–587. https://doi.org/10.1002/wcs.1304.
130. Aimone, J.B., Wiles, J., and Gage, F.H. (2006). Potential role for adult neurogenesis in the encoding of time in new memories. Nat. Neurosci. *9*, 723–727. https://doi.org/10.1038/nn1707.
131. Deng, W., Saxe, M.D., Gallina, I.S., and Gage, F.H. (2009). Adult-Born Hippocampal Dentate Granule Cells Undergoing Maturation Modulate Learning and Memory in the Brain. J. Neurosci. *29*, 13532–13542. https://doi.org/10.1523/JNEUROSCI.3362-09.2009.
132. Nakashiba, T., Cushman, J.D., Pelkey, K.A., Renaudineau, S., Buhl, D.L., McHugh, T.J., Rodriguez Barrera, V., Chittajallu, R., Iwamoto, K.S., McBain, C.J., et al. (2012). Young Dentate Granule Cells Mediate Pattern Separation, whereas Old Granule Cells Facilitate Pattern Completion. Cell *149*, 188–201. https://doi.org/10.1016/j.cell.2012.01.046.
133. Yamada, K., and Nabeshima, T. (2003). Brain-Derived Neurotrophic Factor/TrkB Signaling in Memory Processes. J. Pharmacol. Sci. *91*, 267–270. https://doi.org/10.1254/jphs.91.267.
134. Schildt, S., Endres, T., Lessmann, V., and Edelmann, E. (2013). Acute and chronic interference with BDNF/TrkB-signaling impair LTP selectively at mossy fiber synapses in the CA3 region of mouse hippocampus. Neuropharmacology *71*, 247–254. https://doi.org/10.1016/j.neuropharm.2013.03.041.
135. Panja, D., and Bramham, C.R. (2014). BDNF mechanisms in late LTP formation: A synthesis and breakdown. Neuropharmacology *76*, 664–676. https://doi.org/10.1016/j.neuropharm.2013.06.024.
136. McHugh, S.B., Lopes-dos-Santos, V., Gava, G.P., Hartwich, K., Tam, S.K.E., Bannerman, D.M., and Dupret, D. (2022). Adult-born dentate granule cells promote hippocampal population sparsity. Nat. Neurosci. *25*, 1481–1491. https://doi.org/10.1038/s41593-022-01176-5.
137. Schmidt-Hieber, C., Jonas, P., and Bischofberger, J. (2004). Enhanced synaptic plasticity in newly generated granule cells of the adult hippocampus. Nature *429*, 184–187. https://doi.org/10.1038/nature02553.
138. Ge, S., Yang, C.H., Hsu, K.S., Ming, G.L., and Song, H. (2007). A Critical Period for Enhanced Synaptic Plasticity in Newly Generated Neurons of the Adult Brain. Neuron *54*, 559–566. https://doi.org/10.1016/j.neuron.2007.05.002.
139. Sivakumaran, S., Mohajerani, M.H., and Cherubini, E. (2009). At Immature Mossy-Fiber–CA3 Synapses, Correlated Presynaptic and Postsynaptic Activity Persistently Enhances GABA Release and Network Excitability via BDNF and cAMP-Dependent PKA. J. Neurosci. *29*, 2637–2647. https://doi.org/10.1523/JNEUROSCI.5019-08.2009.
140. Mongiat, L.A., Espósito, M.S., Lombardi, G., and Schinder, A.F. (2009). Reliable Activation of Immature Neurons in the Adult Hippocampus. PLoS One *4*, e5320. https://doi.org/10.1371/journal.pone.0005320.
141. Rossi, C., Angelucci, A., Costantin, L., Braschi, C., Mazzantini, M., Babbini, F., Fabbri, M.E., Tessarollo, L., Maffei, L., Berardi, N., and Caleo, M. (2006). Brain-derived neurotrophic factor (BDNF) is required for the enhancement of hippocampal neurogenesis following environmental enrichment. Eur. J. Neurosci. *24*, 1850–1856. https://doi.org/10.1111/j.1460-9568.2006.05059.x.
142. Scharfman, H., Goodman, J., Macleod, A., Phani, S., Antonelli, C., and Croll, S. (2005). Increased neurogenesis and the ectopic granule cells after intrahippocampal BDNF infusion in adult rats. Exp. Neurol. *192*, 348–356. https://doi.org/10.1016/j.expneurol.2004.11.016.
143. Vilar, M., and Mira, H. (2016). Regulation of Neurogenesis by Neurotrophins during Adulthood: Expected and Unexpected Roles. Front. Neurosci. *10*, 26. https://doi.org/10.3389/fnins.2016.00026.
144. Hwang, D., Kim, J., Kyun, S., Jang, I., Kim, T., Park, H.Y., and Lim, K. (2023). Exogenous lactate augments exercise-induced improvement in memory but not in hippocampal neurogenesis. Sci. Rep. *13*, 5838. https://doi.org/10.1038/s41598-023-33017-1.
145. Jourdain, P., Rothenfusser, K., Ben-Adiba, C., Allaman, I., Marquet, P., and Magistretti, P.J. (2018). Dual action of L-Lactate on the activity of NR2B-containing NMDA receptors: from potentiation to neuroprotection. Sci. Rep. *8*, 13472. https://doi.org/10.1038/s41598-018-31534-y.
146. Skwarzynska, D., Sun, H., Williamson, J., Kasprzak, I., and Kapur, J. (2023). Glycolysis regulates neuronal excitability via lactate receptor, HCA1R. Brain *146*, 1888–1902. https://doi.org/10.1093/brain/awac419.
147. Briquet, M., Rocher, A.-B., Alessandri, M., Rosenberg, N., de Castro Abrantes, H., Wellbourne-Wood, J., Schmuziger, C., Ginet, V., Puyal, J., Pralong, E., et al. (2022). Activation of lactate receptor HCAR1 down-modulates neuronal activity in rodent and human brain tissue. J. Cereb. Blood Flow Metab. *42*, 1650–1665. https://doi.org/10.1177/0271678X221080324.
148. de Castro Abrantes, H., Briquet, M., Schmuziger, C., Restivo, L., Puyal, J., Rosenberg, N., Rocher, A.-B., Offermanns, S., and Chatton, J.-Y. (2019). The Lactate Receptor HCAR1 Modulates Neuronal Network Activity through the Activation of G α and G $\beta\gamma$ Subunits. J. Neurosci. *39*, 4422–4433. https://doi.org/10.1523/JNEUROSCI.2092-18.2019.
149. Bozzo, L., Puyal, J., and Chatton, J.-Y. (2013). Lactate Modulates the Activity of Primary Cortical Neurons through a Receptor-Mediated Pathway. PLoS One *8*, e71721. https://doi.org/10.1371/journal.pone.0071721.
150. Morland, C., Andersson, K.A., Haugen, Ø.P., Hadzic, A., Kleppa, L., Gille, A., Rinholm, J.E., Palibrk, V., Diget, E.H., Kennedy, L.H., et al. (2017). Exercise induces cerebral VEGF and angiogenesis via the lactate receptor HCAR1. Nat. Commun. *8*, 15557. https://doi.org/10.1038/ncomms15557.
151. Li, G., Wang, H.Q., Wang, L.H., Chen, R.P., and Liu, J.P. (2014). Distinct Pathways of ERK1/2 Activation by Hydroxy-Carboxylic Acid Receptor-1. PLoS One *9*, e93041. https://doi.org/10.1371/journal.pone.0093041.
152. Lundquist, A.J., Gallagher, T.J., Petzinger, G.M., and Jakowec, M.W. (2021). Exogenous l-lactate promotes astrocyte plasticity but is not sufficient for enhancing striatal synaptogenesis or motor behavior in mice. J. Neurosci. Res. *99*, 1433–1447. https://doi.org/10.1002/jnr.24804.
153. Coco, M., Caggia, S., Musumeci, G., Perciavalle, V., Graziano, A.C.E., Pannuzzo, G., and Cardile, V. (2013). Sodium L-lactate differently affects brain-derived neurothrophic factor, inducible nitric oxide synthase, and heat shock protein 70 kDa production in human astrocytes and SH-SY5Y cultures. J. Neurosci. Res. *91*, 313–320. https://doi.org/10.1002/jnr.23154.
154. Liu, W., Wang, Y., Bozi, L.H.M., Fischer, P.D., Jedrychowski, M.P., Xiao, H., Wu, T., Darabedian, N., He, X., Mills, E.L., et al. (2023). Lactate regulates cell cycle by remodeling the anaphase promoting complex. Nature *616*, 790–797. https://doi.org/10.1038/s41586-023-05939-3.
155. Singh, M., Meyer, E.M., and Simpkins, J.W. (1995). The effect of ovariectomy and estradiol replacement on brain-derived neurotrophic factor messenger ribonucleic acid expression in cortical and hippocampal brain regions of female Sprague-Dawley rats. Endocrinology *136*, 2320–2324. https://doi.org/10.1210/endo.136.5.7720680.
156. Sohrabji, F., Miranda, R.C., and Toran-Allerand, C.D. (1995). Identification of a putative estrogen response element in the gene encoding brain-derived neurotrophic factor. Proc. Natl. Acad. Sci. USA *92*, 11110–11114. https://doi.org/10.1073/pnas.92.24.11110.
157. Sohrabji, F., and Lewis, D.K. (2006). Estrogen–BDNF interactions: Implications for neurodegenerative diseases. Front. Neuroendocrinol. *27*, 404–414. https://doi.org/10.1016/j.yfrne.2006.09.003.
158. Wolf, D.C., Sanon, N.T., Cunha, A.O.S., Chen, J.-S., Shaker, T., Elhassan, A.-R., do Nascimento, A.S.F., Di Cristo, G., and Weil, A.G. (2022). Sex-specific differences in KCC2 localisation and inhibitory synaptic transmission in the rat hippocampus. Sci. Rep. *12*, 3186. https://doi.org/10.1038/s41598-022-06769-5.
159. Brandt, N., Löffler, T., Fester, L., and Rune, G.M. (2020). Sex-specific features of spine densities in the hippocampus. Sci. Rep. *10*, 11405. https://doi.org/10.1038/s41598-020-68371-x.
160. Silhol, M., Bonnichon, V., Rage, F., and Tapia-Arancibia, L. (2005). Age-related changes in brain-derived neurotrophic factor and tyrosine kinase receptor isoforms in the hippocampus and hypothalamus in male rats. Neuroscience *132*, 613–624. https://doi.org/10.1016/j.neuroscience.2005.01.008.
161. Costa, M.S., Ardais, A.P., Fioreze, G.T., Mioranzza, S., Botton, P.H.S., Souza, D.O., Rocha, J.B.T., and Porciúncula, L.O. (2012). The impact of the frequency of moderate exercise on memory and brain-derived neurotrophic factor signaling in young adult and middle-aged rats. Neuroscience *222*,

100–109. https://doi.org/10.1016/j.neuroscience.2012.06.068.
162. Hattiangady, B., Rao, M.S., Shetty, G.A., and Shetty, A.K. (2005). Brain-derived neurotrophic factor, phosphorylated cyclic AMP response element binding protein and neuropeptide Y decline as early as middle age in the dentate gyrus and CA1 and CA3 subfields of the hippocampus. Exp. Neurol. *195*, 353–371. https://doi.org/10.1016/j.expneurol.2005.05.014.
163. Gil-Mohapel, J., Brocardo, P.S., Choquette, W., Gothard, R., Simpson, J.M., and Christie, B.R. (2013). Hippocampal Neurogenesis Levels Predict WATERMAZE Search Strategies in the Aging Brain. PLoS One *8*, e75125. https://doi.org/10.1371/journal.pone.0075125.
164. Berdugo-Vega, G., Arias-Gil, G., López-Fernández, A., Artegiani, B., Wasielewska, J.M., Lee, C.-C., Lippert, M.T., Kempermann, G., Takagaki, K., and Calegari, F. (2020). Increasing neurogenesis refines hippocampal activity rejuvenating navigational learning strategies and contextual memory throughout life. Nat. Commun. *11*, 135. https://doi.org/10.1038/s41467-019-14026-z.
165. Amrein, I., Isler, K., and Lipp, H.-P. (2011). Comparing adult hippocampal neurogenesis in mammalian species and orders: influence of chronological age and life history stage. Eur. J. Neurosci. *34*, 978–987. https://doi.org/10.1111/j.1460-9568.2011.07804.x.
166. Bondolfi, L., Ermini, F., Long, J.M., Ingram, D.K., and Jucker, M. (2004). Impact of age and caloric restriction on neurogenesis in the dentate gyrus of C57BL/6 mice. Neurobiol. Aging *25*, 333–340. https://doi.org/10.1016/S0197-4580(03)00083-6.
167. Lugert, S., Basak, O., Knuckles, P., Haussler, U., Fabel, K., Götz, M., Haas, C.A., Kempermann, G., Taylor, V., and Giachino, C. (2010). Quiescent and Active Hippocampal Neural Stem Cells with Distinct Morphologies Respond Selectively to Physiological and Pathological Stimuli and Aging. Cell Stem Cell *6*, 445–456. https://doi.org/10.1016/j.stem.2010.03.017.
168. Kennard, J.A., and Woodruff-Pak, D.S. (2011). Age sensitivity of behavioral tests and brain substrates of normal aging in mice. Front. Aging Neurosci. *3*, 9. https://doi.org/10.3389/fnagi.2011.00009.
169. López-Otín, C., Blasco, M.A., Partridge, L., Serrano, M., and Kroemer, G. (2013). The Hallmarks of Aging. Cell *153*, 1194–1217. https://doi.org/10.1016/j.cell.2013.05.039.
170. López-Otín, C., Blasco, M.A., Partridge, L., Serrano, M., and Kroemer, G. (2023). Hallmarks of aging: An expanding universe. Cell *186*, 243–278. https://doi.org/10.1016/j.cell.2022.11.001.
171. Flores, A., Schell, J., Krall, A.S., Jelinek, D., Miranda, M., Grigorian, M., Braas, D., White, A.C., Zhou, J.L., Graham, N.A., et al. (2017). Lactate dehydrogenase activity drives hair follicle stem cell activation. Nat. Cell Biol. *19*, 1017–1026. https://doi.org/10.1038/ncb3575.
172. Theret, M., Gsaier, L., Schaffer, B., Juban, G., Ben Larbi, S., Weiss-Gayet, M., Bultot, L., Collodet, C., Foretz, M., Desplanches, D., et al. (2017). AMPKα1-LDH pathway regulates muscle stem cell self-renewal by controlling metabolic homeostasis. EMBO J. *36*, 1946–1962. https://doi.org/10.15252/embj.201695273.
173. Wang, Y.-H., Israelsen, W.J., Lee, D., Yu, V.W.C., Jeanson, N.T., Clish, C.B., Cantley, L.C., Vander Heiden, M.G., and Scadden, D.T. (2014). Cell-State-Specific Metabolic Dependency in Hematopoiesis and Leukemogenesis. Cell *158*, 1309–1323. https://doi.org/10.1016/j.cell.2014.07.048.
174. Zheng, X., Boyer, L., Jin, M., Mertens, J., Kim, Y., Ma, L., Ma, L., Hamm, M., Gage, F.H., and Hunter, T. (2016). Metabolic reprogramming during neuronal differentiation from aerobic glycolysis to neuronal oxidative phosphorylation. Elife *5*, 1–25. https://doi.org/10.7554/eLife.13374.
175. Drulis-Fajdasz, D., Wójtowicz, T., Wawrzyniak, M., Wlodarczyk, J., Mozrzymas, J.W., and Rakus, D. (2015). Involvement of cellular metabolism in age-related LTP modifications in rat hippocampal slices. Oncotarget *6*, 14065–14081. https://doi.org/10.18632/oncotarget.4188.
176. Hagihara, H., Shoji, H., Hattori, S., Sala, G., Takamiya, Y., Tanaka, M., Ihara, M., Shibutani, M., Hatada, I., Hori, K., et al. (2024). Large-scale animal model study uncovers altered brain pH and lactate levels as a transdiagnostic endophenotype of neuropsychiatric disorders involving cognitive impairment. Elife *12*, 1–27. https://doi.org/10.7554/eLife.89376.3.
177. Bajaffer, A., Mineta, K., Magistretti, P., and Gojobori, T. (2022). Lactate-mediated neural plasticity genes emerged during the evolution of memory systems. Sci. Rep. *12*, 19238. https://doi.org/10.1038/s41598-022-23784-8.
178. Jang, S., Nelson, J.C., Bend, E.G., Rodríguez-Laureano, L., Tueros, F.G., Cartagenova, L., Underwood, K., Jorgensen, E.M., and Colón-Ramos, D.A. (2016). Glycolytic Enzymes Localize to Synapses under Energy Stress to Support Synaptic Function. Neuron *90*, 278–291. https://doi.org/10.1016/j.neuron.2016.03.011.
179. Drulis-Fajdasz, D., Gizak, A., Wójtowicz, T., Wiśniewski, J.R., and Rakus, D. (2018). Aging-associated changes in hippocampal glycogen metabolism in mice. Evidence for and against astrocyte-to-neuron lactate shuttle. Glia *66*, 1481–1495. https://doi.org/10.1002/glia.23319.
180. Mc Cluskey, M., Dubouchaud, H., Nicot, A.S., and Saudou, F. (2024). A vesicular Warburg effect: Aerobic glycolysis occurs on axonal vesicles for local NAD+ recycling and transport. Traffic *25*, e12926. https://doi.org/10.1111/tra.12926.
181. Duran, J., Gruart, A., Varea, O., López-Soldado, I., Delgado-García, J.M., and Guinovart, J.J. (2019). Lack of Neuronal Glycogen Impairs Memory Formation and Learning-Dependent Synaptic Plasticity in Mice. Front. Cell. Neurosci. *13*, 374. https://doi.org/10.3389/fncel.2019.00374.
182. Duran, J., Saez, I., Gruart, A., Guinovart, J.J., and Delgado-García, J.M. (2013). Impairment in Long-Term Memory Formation and Learning-Dependent Synaptic Plasticity in Mice Lacking Glycogen Synthase in the Brain. J. Cereb. Blood Flow Metab. *33*, 550–556. https://doi.org/10.1038/jcbfm.2012.200.
183. Lujan, B., Kushmerick, C., Banerjee, T.D., Dagda, R.K., and Renden, R. (2016). Glycolysis selectively shapes the presynaptic action potential waveform. J. Neurophysiol. *116*, 2523–2540. https://doi.org/10.1152/jn.00629.2016.
184. Rangaraju, V., Calloway, N., and Ryan, T.A. (2014). Activity-driven local ATP synthesis is required for synaptic function. Cell *156*, 825–835. https://doi.org/10.1016/j.cell.2013.12.042.
185. ter Horst, J.P., de Kloet, E.R., Schächinger, H., and Oitzl, M.S. (2012). Relevance of Stress and Female Sex Hormones for Emotion and Cognition. Cell. Mol. Neurobiol. *32*, 725–735. https://doi.org/10.1007/s10571-011-9774-2.
186. Bertholomey, M.L., Nagarajan, V., Smith, D.M., and Torregrossa, M.M. (2022). Sex- and age-dependent effects of chronic corticosterone exposure on depressive-like, anxiety-like, and fear-related behavior: Role of amygdala glutamate receptors in the rat. Front. Behav. Neurosci. *16*, 950000. https://doi.org/10.3389/fnbeh.2022.950000.
187. Shors, T.J., Chua, C., and Falduto, J. (2001). Sex Differences and Opposite Effects of Stress on Dendritic Spine Density in the Male Versus Female Hippocampus. J. Neurosci. *21*, 6292–6297. https://doi.org/10.1523/JNEUROSCI.21-16-06292.2001.
188. Bowman, R., Frankfurt, M., and Luine, V. (2022). Sex differences in cognition following variations in endocrine status. Learn. Mem. *29*, 234–245. https://doi.org/10.1101/lm.053509.121.
189. Dupret, D., Revest, J.M., Koehl, M., Ichas, F., De Giorgi, F., Costet, P., Abrous, D.N., and Piazza, P.V. (2008). Spatial relational memory requires hippocampal adult neurogenesis. PLoS One *3*, e1959. https://doi.org/10.1371/journal.pone.0001959.
190. Fölsz, O., Trouche, S., and Croset, V. (2023). Adult-born neurons add flexibility to hippocampal memories. Front. Neurosci. *17*, 1–9. https://doi.org/10.3389/fnins.2023.1128623.
191. Dias, C., Fernandes, E., Barbosa, R.M., Laranjinha, J., and Ledo, A. (2023). Astrocytic aerobic glycolysis provides lactate to support neuronal oxidative metabolism in the hippocampus. Biofactors *49*, 875–886. https://doi.org/10.1002/biof.1951.
192. Herbst, E.A.F., George, M.A.J., Brebner, K., Holloway, G.P., and Kane, D.A. (2018). Lactate is oxidized outside of the mitochondrial matrix in rodent brain. Appl. Physiol. Nutr. Metab. *43*, 467–474. https://doi.org/10.1139/apnm-2017-0450.
193. Chen, Y.-J., Mahieu, N.G., Huang, X., Singh, M., Crawford, P.A., Johnson, S.L., Gross, R.W., Schaefer, J., and Patti, G.J. (2016). Lactate metabolism is associated with mammalian mitochondria. Nat. Chem. Biol. *12*, 937–943. https://doi.org/10.1038/nchembio.2172.
194. Akter, M., Ma, H., Hasan, M., Karim, A., Zhu, X., Zhang, L., and Li, Y. (2023). Exogenous L-lactate administration in rat hippocampus increases expression of key regulators of mitochondrial biogenesis and antioxidant defense. Front. Mol. Neurosci. *16*, 1117146. https://doi.org/10.3389/fnmol.2023.1117146.
195. Yang, S.-H., Sarkar, S.N., Liu, R., Perez, E.J., Wang, X., Wen, Y., Yan, L.-J., and Simpkins, J.W. (2009). Estrogen Receptor β as a Mitochondrial Vulnerability Factor. J. Biol. Chem. *284*, 9540–9548. https://doi.org/10.1074/jbc.M808246200.
196. Chen, J.Q., Delannoy, M., Cooke, C., and Yager, J.D. (2004). Mitochondrial localization of ERalpha and ERbeta in human MCF7 cells. Am. J. Physiol. Metab

286, E1011–E1022. https://doi.org/10.1152/ajpendo.00508.2003.

197. Yang, S.-H., Liu, R., Perez, E.J., Wen, Y., Stevens, S.M., Valencia, T., Brun-Zinkernagel, A.-M., Prokai, L., Will, Y., Dykens, J., et al. (2004). Mitochondrial localization of estrogen receptor beta. Proc. Natl. Acad. Sci. USA *101*, 4130–4135. https://doi.org/10.1073/pnas.0306948101.
198. Nilsen, J., Irwin, R.W., Gallaher, T.K., and Brinton, R.D. (2007). Estradiol In Vivo Regulation of Brain Mitochondrial Proteome. J. Neurosci. *27*, 14069–14077. https://doi.org/10.1523/JNEUROSCI.4391-07.2007.
199. Chen, J.Q., Eshete, M., Alworth, W.L., and Yager, J.D. (2004). Binding of MCF-7 cell mitochondrial proteins and recombinant human estrogen receptors α and β to human mitochondrial DNA estrogen response elements. J. Cell. Biochem. *93*, 358–373. https://doi.org/10.1002/jcb.20178.
200. Demonacos, C.V., Karayanni, N., Hatzoglou, E., Tsiriyiotis, C., Spandidos, D.A., and Sekeris, C.E. (1996). Mitochondrial genes as sites of primary action of steroid hormones. Steroids *61*, 226–232. https://doi.org/10.1016/0039-128X(96)00019-0.
201. Van Itallie, C.M., and Dannies, P.S. (1988). Estrogen Induces Accumulation of the Mitochondrial Ribonucleic Acid for Subunit II of Cytochrome Oxidase in Pituitary Tumor Cells. Mol. Endocrinol. *2*, 332–337. https://doi.org/10.1210/mend-2-4-332.
202. Bettini, E., and Maggi, A. (1992). Estrogen Induction of Cytochrome c Oxidase Subunit III in Rat Hippocampus. J. Neurochem. *58*, 1923–1929. https://doi.org/10.1111/j.1471-4159.1992.tb10070.x.
203. Kim, H.I., Lee, S., Lim, J., Chung, S., Koo, T.-S., Ji, Y.-G., Suh, Y.-G., Son, W.S., Kim, S.-H., and Choi, H.J. (2021). ERRγ ligand HPB2 upregulates BDNF-TrkB and enhances dopaminergic neuronal phenotype. Pharmacol. Res. *165*, 105423. https://doi.org/10.1016/j.phrs.2021.105423.
204. Fox, S.N., McMeekin, L.J., Savage, C.H., Joyce, K.L., Boas, S.M., Simmons, M.S., Farmer, C.B., Ryan, J., Pereboeva, L., Becker, K., et al. (2022). Estrogen-related receptor gamma regulates mitochondrial and synaptic genes and modulates vulnerability to synucleinopathy. NPJ Parkinsons Dis. *8*, 106. https://doi.org/10.1038/s41531-022-00369-w.
205. Giguère, V. (2008). Transcriptional control of energy homeostasis by the estrogen-related receptors. Endocr. Rev. *29*, 677–696. https://doi.org/10.1210/er.2008-0017.
206. McMeekin, L.J., Joyce, K.L., Jenkins, L.M., Bohannon, B.M., Patel, K.D., Bohannon, A.S., Patel, A., Fox, S.N., Simmons, M.S., Day, J.J., et al. (2021). Estrogen-related Receptor Alpha (ERRα) is Required for PGC-1α-dependent Gene Expression in the Mouse Brain. Neuroscience *479*, 70–90. https://doi.org/10.1016/j.neuroscience.2021.10.007.
207. Tanida, T., Matsuda, K.I., Yamada, S., Kawata, M., and Tanaka, M. (2017). Immunohistochemical profiling of estrogen-related receptor gamma in rat brain and colocalization with estrogen receptor alpha in the preoptic area. Brain Res. *1659*, 71–80. https://doi.org/10.1016/j.brainres.2017.01.024.
208. Pei, L., Mu, Y., Leblanc, M., Alaynick, W., Barish, G.D., Pankratz, M., Tseng, T.W., Kaufman, S., Liddle, C., Yu, R.T., et al. (2015). Dependence of Hippocampal Function on ERRγ-Regulated Mitochondrial Metabolism. Cell Metab. *21*, 628–636. https://doi.org/10.1016/j.cmet.2015.03.004.
209. Castro, M.A., Beltrán, F.A., Brauchi, S., and Concha, I.I. (2009). A metabolic switch in brain: glucose and lactate metabolism modulation by ascorbic acid. J. Neurochem. *110*, 423–440. https://doi.org/10.1111/j.1471-4159.2009.06151.x.
210. Holeček, M. (2023). Aspartic Acid in Health and Disease. Nutrients *15*, 4023. https://doi.org/10.3390/nu15184023.
211. Kane, D.A. (2014). Lactate oxidation at the mitochondria: a lactate-malate-aspartate shuttle at work. Front. Neurosci. *8*, 366. https://doi.org/10.3389/fnins.2014.00366.
212. Wan, H., Aggleton, J.P., and Brown, M.W. (1999). Different contributions of the hippocampus and perirhinal cortex to recognition memory. J. Neurosci. *19*, 1142–1148. https://doi.org/10.1523/jneurosci.19-03-01142.1999.
213. Balderas, I., Rodriguez-Ortiz, C.J., Salgado-Tonda, P., Chavez-Hurtado, J., McGaugh, J.L., and Bermudez-Rattoni, F. (2008). The consolidation of object and context recognition memory involve different regions of the temporal lobe. Learn. Mem. *15*, 618–624. https://doi.org/10.1101/lm.1028008.
214. Bussey, T.J., and Saksida, L.M. (2005). Object memory and perception in the medial temporal lobe: an alternative approach. Curr. Opin. Neurobiol. *15*, 730–737. https://doi.org/10.1016/j.conb.2005.10.014.
215. Winters, B.D., and Bussey, T.J. (2005). Transient Inactivation of Perirhinal Cortex Disrupts Encoding, Retrieval, and Consolidation of Object Recognition Memory. J. Neurosci. *25*, 52–61. https://doi.org/10.1523/JNEUROSCI.3827-04.2005.
216. Fan, J., Hitosugi, T., Chung, T.-W., Xie, J., Ge, Q., Gu, T.-L., Polakiewicz, R.D., Chen, G.Z., Boggon, T.J., Lonial, S., et al. (2011). Tyrosine Phosphorylation of Lactate Dehydrogenase A Is Important for NADH/NAD+ Redox Homeostasis in Cancer Cells. Mol. Cell Biol. *31*, 4938–4950. https://doi.org/10.1128/mcb.06120-11.
217. Yasykova, M.Y., Petukhov, S.P., and Muronetz, V.I. (2000). Phosphorylation of lactate dehydrogenase by protein kinases. Biochemistry *65*, 1192–1196.
218. Cooper, J.A., Esch, F.S., Taylor, S.S., and Hunter, T. (1984). Phosphorylation sites in enolase and lactate dehydrogenase utilized by tyrosine protein kinases *in vivo* and *in vitro*. J. Biol. Chem. *259*, 7835–7841. https://doi.org/10.1016/S0021-9258(17)42869-9.
219. Hornbeck, P.V., Zhang, B., Murray, B., Kornhauser, J.M., Latham, V., and Skrzypek, E. (2015). PhosphoSitePlus, 2014: mutations, PTMs and recalibrations. Nucleic Acids Res. *43*, D512–D520. https://doi.org/10.1093/nar/gku1267.
220. Aleshin, V.A., Artiukhov, A.V., Kaehne, T., Graf, A.V., and Bunik, V.I. (2021). Daytime Dependence of the Activity of the Rat Brain Pyruvate Dehydrogenase Corresponds to the Mitochondrial Sirtuin 3 Level and Acetylation of Brain Proteins, All Regulated by Thiamine Administration Decreasing Phosphorylation of PDHA Ser293. Int. J. Mol. Sci. *22*, 8006. https://doi.org/10.3390/ijms22158006.
221. Zhao, D., Zou, S.-W., Liu, Y., Zhou, X., Mo, Y., Wang, P., Xu, Y.-H., Dong, B., Xiong, Y., Lei, Q.-Y., and Guan, K.L. (2013). Lysine-5 Acetylation Negatively Regulates Lactate Dehydrogenase A and Is Decreased in Pancreatic Cancer. Cancer Cell *23*, 464–476. https://doi.org/10.1016/j.ccr.2013.02.005.
222. Cui, Y., Qin, L., Wu, J., Qu, X., Hou, C., Sun, W., Li, S., Vaughan, A.T.M., Li, J.J., and Liu, J. (2015). SIRT3 Enhances Glycolysis and Proliferation in SIRT3-Expressing Gastric Cancer Cells. PLoS One *10*, e0129834. https://doi.org/10.1371/journal.pone.0129834.
223. Li, X., Zhang, C., Zhao, T., Su, Z., Li, M., Hu, J., Wen, J., Shen, J., Wang, C., Pan, J., et al. (2020). Lysine-222 succinylation reduces lysosomal degradation of lactate dehydrogenase a and is increased in gastric cancer. J. Exp. Clin. Cancer Res. *39*, 172. https://doi.org/10.1186/s13046-020-01681-0.
224. Dawson, N.J., Bell, R.A.V., and Storey, K.B. (2013). Purification and Properties of White Muscle Lactate Dehydrogenase from the Anoxia-Tolerant Turtle, the Red-Eared Slider, Trachemys scripta elegans. Enzyme Res. *2013*, 784973. https://doi.org/10.1155/2013/784973.
225. Storey, K.B. (2016). Comparative enzymology—new insights from studies of an "old" enzyme, lactate dehydrogenase. Comp. Biochem. Physiol. B Biochem. Mol. Biol. *199*, 13–20. https://doi.org/10.1016/j.cbpb.2015.12.004.
226. Yin, D., Jiang, N., Cheng, C., Sang, X., Feng, Y., Chen, R., and Chen, Q. (2023). Protein Lactylation and Metabolic Regulation of the Zoonotic Parasite Toxoplasma gondii. Dev. Reprod. Biol. *21*, 1163–1181. https://doi.org/10.1016/j.gpb.2022.09.010.
227. Yang, D., Yin, J., Shan, L., Yi, X., Zhang, W., and Ding, Y. (2022). Identification of lysine-lactylated substrates in gastric cancer cells. iScience *25*, 104630. https://doi.org/10.1016/j.isci.2022.104630.
228. de Toeuf, B., Soin, R., Nazih, A., Dragojevic, M., Jurėnas, D., Delacourt, N., Vo Ngoc, L., Garcia-Pino, A., Kruys, V., and Gueydan, C. (2018). ARE-mediated decay controls gene expression and cellular metabolism upon oxygen variations. Sci. Rep. *8*, 5211. https://doi.org/10.1038/s41598-018-23551-8.
229. Huang, D., Hubbard, C.J., and Jungmann, R.A. (1995). Lactate dehydrogenase A subunit messenger RNA stability is synergistically regulated via the protein kinase A and C signal transduction pathways. Mol. Endocrinol. *9*, 994–1004. https://doi.org/10.1210/mend.9.8.7476996.
230. Jungmann, R.A., and Kiryukhina, O. (2005). Cyclic AMP and AKAP-mediated Targeting of Protein Kinase A Regulates Lactate Dehydrogenase Subunit A mRNA Stability. J. Biol. Chem. *280*, 25170–25177. https://doi.org/10.1074/jbc.M502514200.
231. Wang, C., Li, Y., Yan, S., Wang, H., Shao, X., Xiao, M., Yang, B., Qin, G., Kong, R., Chen, R., and Zhang, N. (2020). Interactome analysis reveals that lncRNA HULC promotes aerobic glycolysis through LDHA and PKM2. Nat. Commun. *11*, 3162. https://doi.org/10.1038/s41467-020-16966-3.
232. Zhu, Y., Jin, L., Shi, R., Li, J., Wang, Y., Zhang, L., Liang, C.-Z., Narayana, V.K., De Souza, D.P., Thorne, R.F., et al. (2022). The long noncoding RNA glycoLINC assembles a lower glycolytic metabolon to promote

glycolysis. Mol. Cell *82*, 542–554.e6. https://doi.org/10.1016/j.molcel.2021.11.017.
233. Hicks, K.G., Cluntun, A.A., Schubert, H.L., Hackett, S.R., Berg, J.A., Leonard, P.G., Ajalla Aleixo, M.A., Zhou, Y., Bott, A.J., Salvatore, S.R., et al. (2023). Protein-metabolite interactomics of carbohydrate metabolism reveal regulation of lactate dehydrogenase. Science *379*, 996–1003. https://doi.org/10.1126/science.abm3452.
234. Mayford, M., Bach, M.E., Huang, Y.-Y., Wang, L., Hawkins, R.D., and Kandel, E.R. (1996). Control of Memory Formation Through Regulated Expression of a CaMKII Transgene. Science *274*, 1678–1683. https://doi.org/10.1126/science.274.5293.1678.
235. Kistner, A., Gossen, M., Zimmermann, F., Jerecic, J., Ullmer, C., Lübbert, H., and Bujard, H. (1996). Doxycycline-mediated quantitative and tissue-specific control of gene expression in transgenic mice. Proc. Natl. Acad. Sci. USA *93*, 10933–10938. https://doi.org/10.1073/pnas.93.20.10933.
236. Madisen, L., Zwingman, T.A., Sunkin, S.M., Oh, S.W., Zariwala, H.A., Gu, H., Ng, L.L., Palmiter, R.D., Hawrylycz, M.J., Jones, A.R., et al. (2010). A robust and high-throughput Cre reporting and characterization system for the whole mouse brain. Nat. Neurosci. *13*, 133–140. https://doi.org/10.1038/nn.2467.
237. Yoshinobu, K., Araki, M., Morita, A., Araki, M., Kokuba, S., Nakagata, N., and Araki, K. (2021). Tamoxifen feeding method is suitable for efficient conditional knockout. Exp. Anim. *70*, 91–100. https://doi.org/10.1538/expanim.19-0138.
238. Bartha, R., Drost, D.J., and Williamson, P.C. (1999). Factors affecting the quantification of short echoin-vivo1H MR spectra: prior knowledge, peak elimination, and filtering. NMR Biomed. *12*, 205–216. https://doi.org/10.1002/(SICI)1099-1492(199906)12:4<205::AID-NBM558>3.0.CO;2-1.
239. Kassem, M.N.E., and Bartha, R. (2003). Quantitative proton short-echo-time LASER spectroscopy of normal human white matter and hippocampus at 4 Tesla incorporating macromolecule subtraction. Magn. Reson. Med. *49*, 918–927. https://doi.org/10.1002/mrm.10443.
240. Wong, D., Schranz, A.L., and Bartha, R. (2018). Optimized *in vivo* brain glutamate measurement using long-echo-time semi-LASER at 7 T. NMR Biomed. *31*, e4002. https://doi.org/10.1002/nbm.4002.
241. Ding, J., Ji, J., Rabow, Z., Shen, T., Folz, J., Brydges, C.R., Fan, S., Lu, X., Mehta, S., Showalter, M.R., et al. (2021). A metabolome atlas of the aging mouse brain. Nat. Commun. *12*, 6021. https://doi.org/10.1038/s41467-021-26310-y.
242. Fiehn, O. (2016). Metabolomics by Gas Chromatography–Mass Spectrometry: Combined Targeted and Untargeted Profiling. Curr. Protoc. Mol. Biol. *114*, 1–32. https://doi.org/10.1002/0471142727.mb3004s114.
243. Jones, B.J., and Roberts, D.J. (1968). A rotarod suitable for quantitative measurements of motor incoordination in naive mice. Naunyn-Schmiedebergs Arch. Exp. Pathol. Pharmakol. *259*, 211. https://doi.org/10.1007/BF00537801.
244. Tung, V.W.K., Burton, T.J., Dababneh, E., Quail, S.L., and Camp, A.J. (2014). Behavioral Assessment of the Aging Mouse Vestibular System. J. Vis. Exp. *89*, 51605. https://doi.org/10.3791/51605.
245. Karl, T., Pabst, R., and von Hörsten, S. (2003). Behavioral phenotyping of mice in pharmacological and toxicological research. Exp. Toxicol. Pathol. *55*, 69–83. https://doi.org/10.1078/0940-2993-00301.
246. Crawley, J., and Goodwin, F.K. (1980). Preliminary report of a simple animal behavior model for the anxiolytic effects of benzodiazepines. Pharmacol. Biochem. Behav. *13*, 167–170. https://doi.org/10.1016/0091-3057(80)90067-2.
247. Costall, B., Jones, B.J., Kelly, M.E., Naylor, R.J., and Tomkins, D.M. (1989). Exploration of mice in a black and white test box: Validation as a model of anxiety. Pharmacol. Biochem. Behav. *32*, 777–785. https://doi.org/10.1016/0091-3057(89)90033-6.
248. Bourin, M., and Hascoët, M. (2003). The mouse light/dark box test. Eur. J. Pharmacol. *463*, 55–65. https://doi.org/10.1016/S0014-2999(03)01274-3.
249. Serchov, T., van Calker, D., and Biber, K. (2016). Light/Dark Transition Test to Assess Anxiety-like Behavior in Mice. Bio-Protocol *6*, 4. https://doi.org/10.21769/BioProtoc.1957.
250. Tucker, L.B., and McCabe, J.T. (2021). Measuring Anxiety-Like Behaviors in Rodent Models of Traumatic Brain Injury. Front. Behav. Neurosci. *15*, 682935. https://doi.org/10.3389/fnbeh.2021.682935.
251. Dawson, G.R., and Tricklebank, M.D. (1995). Use of the elevated plus maze in the search for novel anxiolytic agents. Trends Pharmacol. Sci. *16*, 33–36. https://doi.org/10.1016/S0165-6147(00)88973-7.
252. Weiss, S.M., Wadsworth, G., Fletcher, A., and Dourish, C.T. (1998). Utility of ethological analysis to overcome locomotor confounds in elevated maze models of anxiety. Neurosci. Biobehav. Rev. *23*, 265–271. https://doi.org/10.1016/S0149-7634(98)00027-X.
253. Cryan, J.F., and Holmes, A. (2005). The ascent of mouse: advances in modelling human depression and anxiety. Nat. Rev. Drug Discov. *4*, 775–790. https://doi.org/10.1038/nrd1825.
254. HascoëT, M., and Bourin, M. (1998). A New Approach to the Light/Dark Test Procedure in Mice. Pharmacol. Biochem. Behav. *60*, 645–653. https://doi.org/10.1016/S0091-3057(98)00031-8.
255. Vogel-Ciernia, A., and Wood, M.A. (2014). Examining Object Location and Object Recognition Memory in Mice. Curr. Protoc. Neurosci. *69*, 1–17. https://doi.org/10.1002/0471142301.ns0831s69.
256. Seibenhener, M.L., and Wooten, M.C. (2015). Use of the Open Field Maze to Measure Locomotor and Anxiety-like Behavior in Mice. J. Vis. Exp. *96*, e52434. https://doi.org/10.3791/52434.
257. Morris, R.G. (1981). Spatial localization does not require the presence of local cues. Learn. Motiv. *12*, 239–260. https://doi.org/10.1016/0023-9690(81)90020-5.
258. Frame, A.K., Lone, A., Harris, R.A., and Cumming, R.C. (2019). Simple Protocol for Distinguishing Drug-induced Effects on Spatial Memory Acquisition, Consolidation and Retrieval in Mice Using the Morris Water Maze. Bio. Protoc. *9*, e3376. https://doi.org/10.21769/BioProtoc.3376.
259. O'Connor, A.M., Burton, T.J., Leamey, C.A., and Sawatari, A. (2014). The Use of the Puzzle Box as a Means of Assessing the Efficacy of Environmental Enrichment. J. Vis. Exp. *94*, 52225. https://doi.org/10.3791/52225.
260. Xia, J., Psychogios, N., Young, N., and Wishart, D.S. (2009). MetaboAnalyst: a web server for metabolomic data analysis and interpretation. Nucleic Acids Res. *37*, W652–W660. https://doi.org/10.1093/nar/gkp356.
261. Pang, Z., Chong, J., Zhou, G., de Lima Morais, D.A., Chang, L., Barrette, M., Gauthier, C., Jacques, P.É., Li, S., and Xia, J. (2021). MetaboAnalyst 5.0: narrowing the gap between raw spectra and functional insights. Nucleic Acids Res. *49*, W388–W396. https://doi.org/10.1093/nar/gkab382.

STAR★METHODS

KEY RESOURCES TABLE

REAGENT or RESOURCE	SOURCE	IDENTIFIER
Experimental models: organisms/strains		
Mouse: TRE-LDHA	This paper	RRID:MGI:7645158
Mouse: CaMKII-tTA	The Jackson Laboratory	RRID:IMSR_JAX:007004
Mouse: C57BL/6NCrl	Charles River	RRID:IMSR_CRL:027
Mouse: Ldha^{flox}	The Jackson Laboratory	RRID:IMSR_JAX:030112
Mouse: CaMK2α-CreERT2	The Jackson Laboratory	RRID:IMSR_JAX:012362
Antibodies		
Mouse anti-HA.11 epitope tag	BioLegend	BioLegend Cat# 901513, RRID:AB_2565335
Rabbit anti-LDHA	Cell Signaling Technology	Cat# 2012, RRID:AB_2137173
Rabbit anti-LDHB	Proteintech	Cat# 19988-1-AP, RRID:AB_10638780
Goat anti-mouse, HRP conjugated	Millipore Sigma	Cat# AP130P, RRID:AB_91266
Goat anti-rabbit, HRP conjugated	Millipore Sigma	Cat# AP132P, RRID:AB_90264
Goat anti-mouse, affinity-purified fab fragment	Jackson ImmunoResearch	Cat# 115-007-003, RRID:AB_2338476
Rabbit anti-MAP2	Abcam	Cat# ab32454, RRID:AB_776174
Rabbit anti-LDHA	Proteintech	Cat# 19987-1-AP, RRID:AB_10646429
Mouse anti-CaMKIIα	Cell Signaling Technology	Cat# 50049, RRID:AB_2721906
Goat anti-rabbit, Alexa Fluor 647	ThermoFisher Scientific	Cat# A-21244, RRID:AB_2535812
Goat anti-mouse, Alexa Fluor 568	ThermoFisher Scientific	Cat# A-11031, RRID:AB_144696
Goat anti-rabbit, Alexa Fluor Plus 800	ThermoFisher Scientific	Cat# A32735, RRID:AB_2633284
Software and algorithms		
GraphPad Prism	GraphPad Software	https://www.graphpad.com, RRID:SCR_002798
NIS-Elements AR	Nikon Instruments	https://www.nikoninstruments.com/Products/Software, RRID:SCR_014329
Image Lab	Bio-Rad	http://www.bio-rad.com/en-us/sku/1709690-image-lab-software, RRID:SCR_014210
ANY-maze	Stoelting	https://www.any-maze.com, RRID:SCR_014289
LECO ChromaTOF-Sync software	LECO	https://www.leco.com/product/chromatof-sync, RRID:SCR_023077
Metaboanalyst	Jeff Xia Lab, McGill University	https://www.metaboanalyst.ca/, RRID:SCR_015539
Deposited data		
Raw and analyzed data	This paper	https://doi.org/10.5683/SP3/PWONIY

RESOURCE AVAILABILITY

Lead contact

Further information and requests for resources and reagents should be directed to and will be fulfilled by the Lead Contact, Robert C. Cumming (rcummin5@uwo.ca).

Materials availability

This study did not generate new unique reagents. The TRE-LDHA mouse line is available upon request from the lead contact.

Data and code availability

- All raw data and output from statistical analyses, including metabolomic data, have been deposited at the Borealis data repository and are available as of the date of this publication. Accession numbers are listed in the key resources table.
- This paper does not report original code.
- Any additional information required to reanalyze the data reported in this paper is available from the lead contact upon request.

EXPERIMENTAL MODEL AND STUDY PARTICIPANT DETAILS

Mice

This study was performed in accordance with Canadian Council of Animal Care guidelines. All animals were handled according to protocols approved by the animal care committee (ACC) of Western University (Protocol 2011-079 and 2020-112). Male and female mice were housed individually or grouped by sex in shoebox cages in a temperature-controlled room (22-25°C) with a 12 hour light-dark cycle in a plastic house (ACRE011, Techniplast) and with *ad libitum* access to food (Teklad 2018, Envigo) and water. Neuronal *Ldha* induction transgenic mice were generated using the Tet-Off system[82,83] as described in Figure 1A. Neuronal *Ldha* induction transgenic and littermate control mice were bred by crossing mice containing a transgene with a neuronal calcium-calmodulin-dependent kinase II (CaMKIIα) promoter driving tTA expression (CaMKII-tTA; 007004, The Jackson Laboratory)[234] and mice containing a transgene with a TRE promoter driving HA-tagged *Ldha* expression (TRE-LDHA). The mouse *Ldha* cDNA sequence fused to an HA tag sequence on the 3′ terminal was ligated into the multiple cloning site of the pTRE-Tight Vector (631059, Clontech) and linearized using the restriction enzyme Xho1. Pronuclear injection of the linearized insert was conducted by London Regional Transgenic and Gene Targeting Facility, Victoria Research Laboratories, London, ON to generate the TRE-LDHA line. CaMKII-tTA and TRE-LDHA mice were maintained hemizygous on a C57BL/6NCrl background (027, Charles River). Offspring from crossing CaMKII-tTA and TRE-LDHA mice were genotyped using endpoint polymerase chain reaction (PCR). Offspring carrying both transgenes were designated neuronal *Ldha* induction transgenic mice whereas those carrying only one transgene or neither were designated control mice. Neuronal *Ldha* induction and littermate control mice were provided 200 mg/kg doxycycline in their diet (S3888, Bio-Serv) during embryonic and early age development to prevent tTA-induced HA-tagged *Ldha* expression in transgenic until 1.5 months of age.[235] Neuronal *Ldha* knockout (KO) mice were generated using the ligand-activated site-specific Cre-lox system[86,87] as described in Figure 2A. Neuronal *Ldha* KO mice and littermate control mice were bred by crossing mice homozygous for exon 3 *loxp*-flanked *Ldha* ($Ldha^{flox}$; 030112, The Jackson Laboratory)[173] and hemizygous for a transgene with a neuronal CaMKIIα promoter driving CreERT2 expression (CaMK2α-CreERT2; 012362, The Jackson Laboratory)[236] to mice homozygous for $Ldha^{flox}$ without the CaMK2α-CreERT2 transgene. The CaMK2a-CreERT2;$Ldha^{flox}$ and $Ldha^{flox}$ mice were maintained on the mixed C57BL/6N;C57BL/6J genetic background which the $Ldha^{flox}$ were provided on from The Jackson Laboratory. Offspring from crossing CaMK2α-CreERT2;$Ldha^{flox}$ to $Ldha^{flox}$ mice were genotyped using endpoint PCR. Offspring carrying the CaMK2α-CreERT2 transgene were designated neuronal *Ldha* KO mice whereas those without it were designated control mice. Neuronal *Ldha* KO and littermate control mice were provided 500 mg/kg tamoxifen in their diet (TD130857, Envigo) at 4-5 months of age for a month to activate CreERT2 recombination-induced *Ldha* knockout[237] and a similar tasting diet without tamoxifen (TD0757, Envigo) for five days prior. Transgenic and age-matched controls underwent behavioural testing simultaneously at young and old ages at least one month after having the transgenic system induced (Figure 9). Cognitive behaviour in spontaneously elicited object-based tasks, and the puzzle box were repeatedly tested at young and old age. Cognitive behaviour in the Morris Water Maze was tested in separate cohorts for young (6-7 months) and old age (13 months). Locomotor ability on the rotarod and anxiety-like behaviour in the light-dark box were tested only at old and young age, respectively. *In vivo* ^{1}H-MRS analysis was performed on mice only after completing behavioural testing. Mice were euthanized with carbon dioxide, cardiac perfused with phosphate buffered saline (PBS) containing phenylmethylsulfonyl fluoride (PMSF) protease inhibitor (P7626, Millipore Sigma) and sodium orthovanadate phosphatase inhibitor (S6508, Millipore Sigma), and then had brains harvested for further analysis.

METHOD DETAILS

Western blotting

Brain tissues dissected from particular brain regions in the right hemisphere of each mouse were extracted using lysis buffer containing 250mM sucrose (S0389, Millipore Sigma), 50mM tris (BP152, ThermoFisher Scientific), 25mM potassium chloride (P4504, Millipore Sigma), 1% triton X (T9284, Millipore Sigma), 0.5mM PMSF (P7626, Millipore Sigma), 1X Halt™ protease inhibitor cocktail (87786, ThermoFisher Scientific), and 0.1mM sodium orthovanadate (S6508, Millipore Sigma). Brain tissue was dounce homogenized, centrifuged, and protein concentration in the supernatant was determined using a detergent compatible assay (5000111, Bio-Rad). Protein extracts were combined with a bromophenol blue based loading buffer and boiled for five minutes. For each experiment, an equal fraction of samples from each replicate were combined to create a pooled sample. Protein extracts and the pooled sample were resolved by sodium dodecyl sulfate–polyacrylamide gel electrophoresis (SDS-PAGE) and transferred to a polyvinylidene fluoride (PVDF) membrane blot. For each gel, protein standards (1610373, Bio-Rad) were run alongside the protein samples. Total protein level for each blot was quantified from images generated using staining with

0.1% Ponceau S (P3504, Millipore Sigma) in 5% glacial acetic acid. Blots were blocked with 1% w/v bovine serum albumin (BSA) in tris buffered saline containing 0.1% tween 20 (TBST) and 3% w/v milk at room temperature, probed with primary antibodies in at 4°C overnight, and secondary antibodies at room temperature for 2 hours. Primary antibodies were made in TBST with 0.01% sodium azide, and blots were washed in TBST before and after each probe. Primary antibodies included mouse anti-HA.11 epitope tag (901513, BioLegend; 1:1000), rabbit anti-LDHA (2012S, Cell Signaling; 1:1000), and rabbit anti-LDHB (19988-1-AP, Proteintech; 1:3000). Secondary antibodies conjugated with horseradish peroxidase (HRP) included goat anti-mouse (AP130P, Millipore Sigma; 1:10000), and goat anti-rabbit (AP132P, Millipore Sigma; 1:6666). Immobilon Classico or Forte Western HRP substrate (WBLUC, WBLUF, Millipore Sigma) were used to produce chemiluminescent signals on probed blots. A ChemiDoc XRS imaging system (170-8070, Bio-Rad) was used to image chemiluminescence and Ponceaus S signal density and quantified using Image Lab software (RRID:SCR_014210, Bio-Rad). For quantification purposes, western blot band intensity was standardized to total Ponceaus S signal density for each lane then normalized to the pooled sample on each blot. Males and females were analyzed and graphed separately if there were sex-specific statistical effects.

Immunofluorescence microscopy

The left hemisphere of brains harvested from each mouse were post-fixed in 4% paraformaldehyde (15713, Electron Microscopy Sciences) in phosphate buffer for three days then stored in 70% ethanol. Fixed brains were embedded in paraffin wax and sectioned with a rotary microtome (RM2055, Leica Biosystems) at a thickness of 5μm along the sagittal plane until the polymorph layer of the hippocampal dentate gyrus was visible. Sections were baked onto glass slides (12-550-15, ThermoFisher Scientific), deparaffinized using xylene, rehydrated with successive solutions of increasingly diluted ethanol, and then subjected to heat-induced epitope retrieval with 10mM sodium citrate buffer pH 6.0 (C7129, Millipore Sigma) at 90°C for 15min. Sections were exposed to ultraviolet (UV) light to quench general autofluorescence, 1mg/ml sodium borohydride (452882, Millipore Sigma) in PBS to quench fixative-derived autofluorescence, and TrueBlack or TrueBlack Plus (23007, 23014, Biotium; 1:20, 1:50) to quench lipofuscin-derived autofluorescence. Sections were treated with goat anti-mouse affinity-purified fab fragment antibodies (115-007-003, Jackson ImmunoResearch Inc.; 1:40) and Background Sniper (BS966, Biocare Medical) for 7 minutes or Ultra Cruz (sc-516214, Santa Cruz) for 1 hour to block non-specific signal. Sections in a humidity chamber were hybridized with primary antibody at 4°C overnight, secondary antibody for 45-60 minutes at room temperature, and counter stained with 1:300 4′,6-diamidino-2-phenylindole (DAPI; D1306, ThermoFisher Scientific) in PBS for 2 minutes at room temperature. Sections were mounted under coverslips using Prolong Gold Antifade reagent (P36930, ThermoFisher Scientific). Antibodies were prepared in Dako antibody diluent (S0809, Agilent Technologies). Primary antibodies included mouse anti-HA.11 epitope tag (901513, BioLegend; 1:500), rabbit anti-MAP2 (ab32454, Abcam; 1:700), rabbit anti-LDHA (19987-1-AP, Proteintech; 1:250), mouse anti-CaMKIIα (50049, Cell Signaling; 1:250). Secondary antibodies conjugated to fluorophores included goat anti-rabbit Alexa Fluor 647 (A21244, ThermoFisher Scientific; 1:500), goat anti-mouse Alexa Fluor 568 (A11031, ThermoFisher Scientific; 1:500 / 1:400), goat anti-rabbit Alexa Fluor Plus 800 (A32735, ThermoFisher scientific; 1:350). Sections were washed with PBS between each step of the staining process from quenching onwards. Fluorescence microscopy images were taken of each section using a Nikon ECLIPSE Ti2-E microscope system with plan apochromatic lambda dry 20x objective (MRD00205, Nikon Instruments) and a monochrome backside illuminated scientific complementary metal–oxide–semiconductor image sensor (pco.edge 4.2 bi, Excelitas Technologies). The excitation and emission wavelengths (nm) used for detection of fluorescence from Alexa Fluor 568 were 554 and 595, from Alexa Fluor 647 and Alexa Fluor Plus 647 were 635 and 681, for Alexa Fluor Plus 800 were 735 and 809, for DAPI were 378 and 432, respectively. 3x3 tiled and stitched images were created for each brain region: hippocampus, cerebellum, and frontal cortex. Within NIS-Elements AR (RRID:SCR_014329, Nikon Instruments) the Clarify.ai module was used to automatically remove blur from images. Signal quantification was performed using a custom-made GA3 analysis pipeline. Thresholds based on fluorescent signal intensity were determined for each channel before being systematically applied to quantify total signal area across all images. Percent MAP2+ neurons with HA equals the area of HA and MAP2 signal overlap divided by total MAP2 signal area. Percent CaMKIIα+ neurons with LDHA equals the area of LDHA and CaMKIIα signal overlap divided by total CaMKIIα signal area. Males and females were analyzed and graphed separately if there were statistical effects including sex.

^{1}H magnetic resonance spectroscopy

Magnetic resonance imaging (MRI) experiments were performed on a 9.4-T/31-cm small animal MRI scanner (Agilent, Palo Alto, CA, USA) interfaced to a Bruker Avance III HD console (Bruker BioSpin Corp, Billerica, MA) and equipped with a 6-cm gradient coil of 1000mT/m strength, with software package of Paravision-6 at the Centre for Functional and Metabolic Mapping located within the Robarts Research Institute at the University of Western Ontario. A Varian 30-mm millipede volume RF coil was used for data collection. Mice were anesthetized using isoflurane maintained between 1.5% and 2.5% with an oxygen flow rate of 1−1.5 L/min through a custom-built nose cone. Animal temperature was monitored with a rectal temperature probe and respiration was monitored with a pneumatic pillow connected to a pressure transducer that was placed on the thoracic region. Body temperature was maintained at 36.9−37.1°C throughout imaging by blowing warm air over the animal using a model 1025 small-animal monitoring and gating system (SA Instruments Inc., Stony Brook, NY, USA). At the beginning of each scan, the T2-weighted anatomical images were acquired to plan the MRS voxel. This T2-weighted anatomical image was acquired using a TurboRARE2D pulse sequence (16 averages, 31 slices with slice thickness of 0.5 mm, FOV = 19.2 × 19.2 mm^2, matrix size = 128 × 128, in-plane resolution = 0.15 × 0.15 mm^2, TE = 40 ms, TR = 5.0 s, echo spacing = 10 ms, and Rare factor = 8). Subsequently, a 2 x 6 x 3 mm^3 voxel was positioned to both hippocampi for MRS data acquisition using a semi-LASER (Semi-Localization by Adiabatic Selective Refocusing, provides localized spectra from rectangular voxels selected with a sequence of an 90° excitation pulse and two pairs of

180° adiabatic refocusing pulses. Four spin echoes are produced from which the last one is acquired) pulse sequence with parameters: TR/TE = 5000/136ms. Lactate was identified as an inverted doublet peak at 1.33ppm. A water spectrum with 8-average was acquired first, then a 128-averaged metabolite spectrum with water suppression was acquired. Metabolite spectra were fitted using fitMAN software[238] incorporated into a graphical user interface written in the IDL (Interactive Data Language) programming language[239] to determine the amplitude of lactate and creatine resonances. The lactate over creatine ratio was calculated by dividing the sum of each amplitude resonance after T2 correction.[240] Males and females were analyzed and graphed separately if there were statistical effects including sex.

Gas chromatography-mass spectrometry

Primary metabolites were extracted with methanol-methyltertbutyl ether- water, as modified from Ding et al., (2021).[241] In brief, frozen hippocampus tissue was ground with a pestle, of which 5 mg was suspended in 225 μL of cold (-20°C) methanol (MeOH) . Cold (-20°C) methyl *tert*-butyl ether (MTBE; 750 μL) was added and the samples were vortexed, placed on a rotating mixer at 4°C for 30 mins, and transferred to a sonicating bath at 4°C for 15 mins. To induce phase separation, 188 μL room temperature ultra-pure water containing 0.044 mg/mL adonitol (02240, BioChemika) as an internal standard was added, and the samples were vortexed and centrifuged for 10 mins at 13,000 rpm to pellet insoluble material. For recovery of polar metabolites, two 125 μL aliquots of the MeOH-water (lower) phase were transferred to separate, clean microcentrifuge tubes.[241] After the addition of 10 μL of 0.1mg/mL mixture of *n*-alkane retention index standards (C12, C15, C19, C22, C26, and C30), the samples were dried under a stream of N_2. Samples were stored at -20°C until further analysis. Dried polar extracts are derivatized using a two-step process involving methoximation followed by trimethylsilylation, using a protocol adapted from Fiehn (2016).[242] Briefly, 20 μL of 20 mg/mL methoxyamine-HCL (226904, Millipore Sigma) in pyridine was added to the dried extract residues and the samples incubated at 30°C for 90 min. Next, 80 μL of N-methyl-N-(trimethylsilyl)triflouroacetamide (MSTFA) (69479, Millipore Sigma) was added to each sample and incubated for 30 min at 37°C. Derivatized samples were cooled to room temperature, centrifuged, and 10 μL was transferred to chromatography vials fitted with glass micro-volume inserts and diluted with chloroform to a final volume of 100 μL. Samples were immediately analyzed via GCMS. A composite sample, created by pooling equal amounts from all samples, was prepared in the same way as detailed above; the composite sample was run every 10 injections. Samples were run in two cohorts to reflect the experimental design. Each cohort included an injection of chloroform, 6-point quality control mix (Fiehn 2016),[242] retention index mix, and reagent blank at the start of each cohort. For calibration, a dilution series was prepared with sodium lactate (200 μg/mL – 0.0002 μg/mL) and derivatized as above. Samples (1 μL) were injected into an Agilent 7890A GC system configured with a RESTEK Rxi-5ms Low bleed GC column (30 m, 250 μm internal diameter and 0.25 μm film thickness) (709-809-508, Restek) and eluted with the following oven temperature program: initial temperature at 50°C held for 0.5 mins followed by a temperature ramp at 20°C min^{-1} to a final temperature of 325°C and held at 325°C for 5.75 mins. Data acquisition was turned on after a 3-minute delay to allow the solvent to clear the system. Injector and transfer line temperatures were set to 250°C. High purity helium was used as carrier gas at a flow rate of 1 mL min^{-1}. Mass data were collected over an 85-500 m/z range using a LECO Pegasus BT MS. Data produced (i.e. sample files, five reagent blanks, and five 6-point quality control mixes) were baseline corrected, deconvoluted, aligned, and peak areas were integrated using LECO ChromaTOF-Sync software (RRID:SCR_023077). To control for efficiency of derivatization, a comparative check on the 6pt – quality control mix was performed with each batch as detailed in Fiehn (2016).[242] Integrated peak areas were normalized between chromatograms based on peak area of adonitol. Only components with peak areas greater than the average peak area of five reagent blanks were retained. Analyte annotation of mass spectra features was based on the National Institute of Standards and Technology (NIST) library. Metabolites that could not be identified in the NIST database were numbered based on their mean retention time.

Rotarod

A rotarod (EZ-Rod, AccuScan Instruments) was used to test locomotor ability[243] according to a modified protocol[244,245] depicted in Figure 4A. Mice were habituated to the testing room for at least one hour prior to beginning the protocol. On day 1, mice were placed on the rotarod for two minutes with the 3 cm diameter rod spinning at a constant 10.5 revolutions per minute and the mouse returned to the rod each time after a fall. On day 2, mice were subjected to six trials separated by 10 minute intertrial intervals with each trial involving mice being placed on the rod spinning at 4.3 revolutions per minute with the speed increased by 4 revolutions per minute every 30 seconds for a maximum of five minutes or until the mice fell off. The apparatus was cleaned with 70% ethanol between mice and between trials. A lower number of falls on day 1 was considered a measure of the increased ability of each mouse to become familiarized to the rod. Higher latency to fall was considered a measure of locomotor learning on day 2 during trial one to five and a measure of maximum locomotor ability during trial six.[244] Data for males and females were graphed separately for day 1 and 2 if there was an effect including sex on either day.

Light-dark box

The light-dark box test[246,247] was used to test anxiety-like behaviour using a modified protocol.[248,249] The light-dark box was built in-house using white acrylic on the light side and black acrylic on the dark side. The dimensions of the box were 27.5 cm high walls all around, 27.4 x 59.5 cm light side, and 27.4 x 15.2 cm dark side covered from light with black acrylic. An open hole in the barrier between the light and dark side was 3 x 4.2 cm. Corncob bedding (Teklad 7097, Envigo) and a plastic shelter were placed in the dark side. Mice were placed in the light side at the end farthest from the dark side with the light side brightly lit. Mice were provided five minutes to freely roam the apparatus while video recorded (C920, Logitech) and analyzed manually. The light side was cleaned with ethanol between mice. Anxiety-like behaviour can be difficult to dissociate from impulsivity.[250–253] Latency to enter the dark side the first time was considered a combination of impulsivity and anxiety-like behaviour whereas total time spent on dark side was considered a more reliable measure of anxiety-like behavior.[254] Mice

that never entered the dark side were excluded. Data from both measures of latency to enter the dark side and time in dark side were transformed logarithmically.

Spontaneously elicited object-based cognitive behaviours

The two spontaneously elicited objected-based cognitive behaviours used in this study include spontaneous object recognition (SOR) to test 24 hour long-term recognition memory based on a protocol adapted from others[96,255] and spontaneous location recognition (SLR) to test 4 or 6 hour short-term spatial memory based on a protocol adapted from others.[97,111,112] Mice were subjected to SOR prior to SLR at young and old age. Each mouse was familiarized to being handled by the experimenter for one minute per day for at least 14 days prior to testing. To encourage increased spontaneous exploratory behaviour, mice were food deprived down to 85-90% body weight for one week prior to testing and maintained at that weight during the SOR protocol. Moreover, mice were tested during the dark phase of their light cycle for both SOR and SLR also to increase exploratory behaviour. The SOR protocol was conducted using a white acrylic Y-shaped arena, 32.5 cm high walls and 6.5 cm width arms, under red light with one trial per mouse per day for five days. Mice were habituated to the empty SOR arena for 10 minutes each on day 1 to 3 and provided objects at the end of two arms of the Y during the 10 minute sample phase on day 4 and 5 minute choice phase on day 5, as depicted in Figure 6A. Two identical objects were used in the sample phase. In the choice phase, the familiar object was identical to that used in the sample phase and the novel object differed in shape and colour. Two separate sets of objects were used at each age tested (Figure S14A). The object type used in the sample phase and the left-right position of the novel object was counterbalanced within each group. 70% ethanol was used to clean objects between each mouse and clean the arena after any mouse had urinated or defecated. The SLR protocol was conducted over seven days using a circular arena, 33 cm high walls and 39 cm diameter, with corncob bedding (Teklad 7097, Envigo) coating the floor, different white spatial cues placed at a height of 48 cm on three of the four 122 cm high black walls positioned 5 cm outside the arena. Mice were habituated to the empty SLR arena for 10 minutes per day on day 1 to 5 and tested with objects in the arena during a 10 minute sample phase and 5 minute choice phase separated by a 4 or 6 hour delay on day 6 and 7 as depicted in Figure 6F. On the first day of habituation, the empty SLR arena functions as an open field in which thigmotaxis anxiety-like behaviour was measured as the time spent near the wall in the outer zone of the arena (Figure 5A) in a similar manner used by others in the past.[116,256] In the sample phases, three identical objects were placed in a triangular formation with their locations relative to the spatial cues and the distance between two of the three objects varied on day 6 and 7 to be either farther apart (dissimilar, dSLR) or closer together (similar, sSLR). In the choice phases, two objects, identical to those used in the sample phase, were placed such that one was in a novel location equidistant from the two object locations with variable distances apart in the sample phase prior and one in a familiar location that was identical to the third object in the sample phase prior. SLR was tested at two levels of difficulty. A higher requirement for pattern separation to distinguish between the novel and familiar location in the choice phase of sSLR compared to dSLR makes sSLR a more difficult task for mice than dSLR. Object type differed in dSLR and sSLR for each group of mice with the object type and order of testing for dSLR and sSLR counterbalanced. Different object types and locations relative to the spatial cues were used for testing at young and old age (Figure S14B). The corncob bedding was partially replenished, defecation pellets removed, and objects cleaned with 70% ethanol between each mouse. In SOR and SLR, mice were video recorded (C920, Logitech) and exploration of objects was manually scored with scorers blinded to the age, genotype, and sex of the mice. Objection exploration times were used to calculate a discrimination ratio for each mouse in the sample phase for SOR and SLR. To control for innate bias between locations in SLR and SOR, discrimination ratios were compared between sample and choice phases. SOR sample phase discrimination ratios were calculated by subtracting exploration time of the object on the side that will be the location of the familiar object in the choice phase for that mouse from exploration time of the object on the other side, with exploration time on each side normalized to total exploration time for that trial. SLR sample phase discrimination ratios were calculated by subtracting exploration time of the object in the location that will be the familiar location in the choice phase for that mouse on that day from the average exploration time of the two objects in locations that will be absent in the choice phase for that mouse on that day, with exploration time for each object normalized to total exploration time for that trial. SOR and SLR choice phase discrimination ratios were calculated by subtracting exploration of the novel object (SOR) or location (SLR) from exploration time of the familiar object (SOR) or location (SLR), with exploration time for each object normalized to total exploration time for that trial. The magnitude of increase in discrimination ratio for choice phase compared with sample phase was considered a measure of memory in both SOR and SLR. Data for males and females were analyzed and graphed separately if there were sex-specific statistical differences.

Morris Water Maze

The Morris Water Maze[257] was used to test spatial learning and long-term memory, as well as locomotor ability, as adapted from a previous protocol[258] depicted in Figure 7A. The testing area was arranged with a 120 cm diameter tank (San Diego Instruments) placed in the centre, different spatial cues on each of the four walls, and an adjacent holding area, out of site from inside the testing area. The tank was filled with water made opaque with white paint (SAR173696, Sargent Art Inc) and maintained at approximately 26°C for each of the 15 days in the protocol. A 15 cm diameter circular platform was placed approximately 1 cm below the surface of the water. On day one, all mice were habituated to the holding area for 1 hour remaining in their home cages. On day two, each mouse was placed on the platform in the centre of the tank and remained there for a continuous 15 seconds to become familiarized to the testing area, tank, and platform. On day three, each mouse was familiarized to swimming and escaping on an invisible platform by being placed in the water at edge of the tank and given 90 seconds to swim to the platform in the centre and remain there for a continuous 15 seconds. Days 4-7 were considered days 1-4 of training mice to find the platform in the correct target location. On every training day each mouse underwent four trials with 10 minute intertrial intervals. During

intertrial intervals, each mouse was kept alone in a holding cage on a heating pad. Training day trials each involved placing a mouse in the water at the edge of the tank with the starting location corresponding to a rotating cardinal direction each trial and each day. Once in the water for a training day trial, mice were given 90 seconds to swim to the platform in the centre of an unchanging target quadrant and remain there for a continuous 15 seconds. If a mouse jumped off the platform on day one or had not found the platform in 90 seconds on day two or any of the training day trials, then at that time the mouse was directed to the platform to ensure it remained there for a continuous 15 seconds. On day eight and day fifteen, each mouse underwent the 24 hour and 7 day probe trial, respectively. Probe trials involved placing each mouse in the water at the edge of the tank and letting them swim without the platform for 60 seconds. After the 7 day probe trial, each mouse underwent a flag trial whereby the mouse was placed in the water at the edge of the tank and given 90s to find the platform in the centre of the quadrant opposite the target quadrant with a flag on it to make it visible above the water. All data from mice that failed to find the platform during the flag trial were excluded. For every trial, mice that were not in the tank during that trial and the experimenter remained in the holding area. Mouse behaviour in the tank was video recorded (C920, Logitech) and tracked using automated software (RRID:SCR_014289, ANY-Maze, Stoelting). Lower average latency and distance travelled to find the platform were measures taken on each training day interpreted as learning. Higher percentage of time spent in the target quadrant and lower mean distance from the centre of the platform area in the target quadrant were measures taken on each probe trial interpreted as memory. Higher average swimming speed on training days and swimming speed and distance travelled in probe trials were measures interpreted as locomotor ability. Data for male and female mice were analyzed and graphed separately for training days if there was a sex difference identified in learning or locomotor ability during training and for probe trials if there was a sex difference identified in memory, learning, or locomotor ability during probe. Locomotor ability was measured as average swimming speed during training days and swimming speed and distance travelled during probe trials.

Puzzle box

The puzzle box test[98] was used to test various cognitive abilities, including problem solving ability, 3 minute short-term memory, and 24 hour long-term memory, according to an modified protocol[98,259] as depicted in Figure 8A. The puzzle box test was conducted using the same apparatus used for the light-dark box test. For each trial in the puzzle box, mice were placed in the light side at the end farthest from the dark side and video recorded (C920, Logitech) until successfully passing through blockage and entering the dark side through the hole in the barrier. Mice were subjected to nine trials in total with three trials in immediate succession per day for three consecutive days. Blocking material was omitted in trial 1. Trial 2 through 9 had the floor elevated such that mice needed to climb down through a 4.2 x 4.2 cm hole in the floor to pass through the hole in the barrier. Trial 2, 3, and 4 had nothing blocking the hole. Trial 5, 6, and 7 had corncob bedding (Teklad 7097, Envigo) filling the hole. Trial 8 and 9 had crinkle cut paper strands (CNK, The Andersons) filling the hole. Mice were kept alone in a holding cage between trials on each day. The apparatus was cleaned with 70% ethanol between trials (3 minutes) and between mice. Videos were analyzed manually for a latency to enter the dark side. Higher latency was considered worse performance on the trial. As depicted in Figure 8A, performance was considered habituation to the apparatus in trial 1; problem solving ability in trial 2, 5, and 8; 3 minute memory during trial 3, 6, and 9; and 24 hour memory in trial 4 and 7. Latency to enter the dark side was logarithm transformed. Data for males and females were analyzed and graphed separately if there were sex-specific statistical effects.

QUANTIFICATION AND STATISTICAL ANALYSIS

Data were analyzed statistically and visualized using GraphPad Prism version 9.3.1 (471) (RRID:SCR_002798). Statistical comparisons for figures are described in each figure legend. GCMS metabolomic data (peak area intensities) were analyzed using principal component analysis and partial least squares discriminant-analysis using MetaboAnalyst 5.0 (RRID:SCR_015539)[260,261] without filtering. Data were log transformed and auto scaled. For all figures, ns = $p>0.05$, * = $p<0.05$, ** = $p<0.01$, *** = $p<0.001$, and **** = $p<0.0001$. Data from males and females were consolidated wherever there were no sex differences detected.